Process Engineering
MSc Thesis
2022

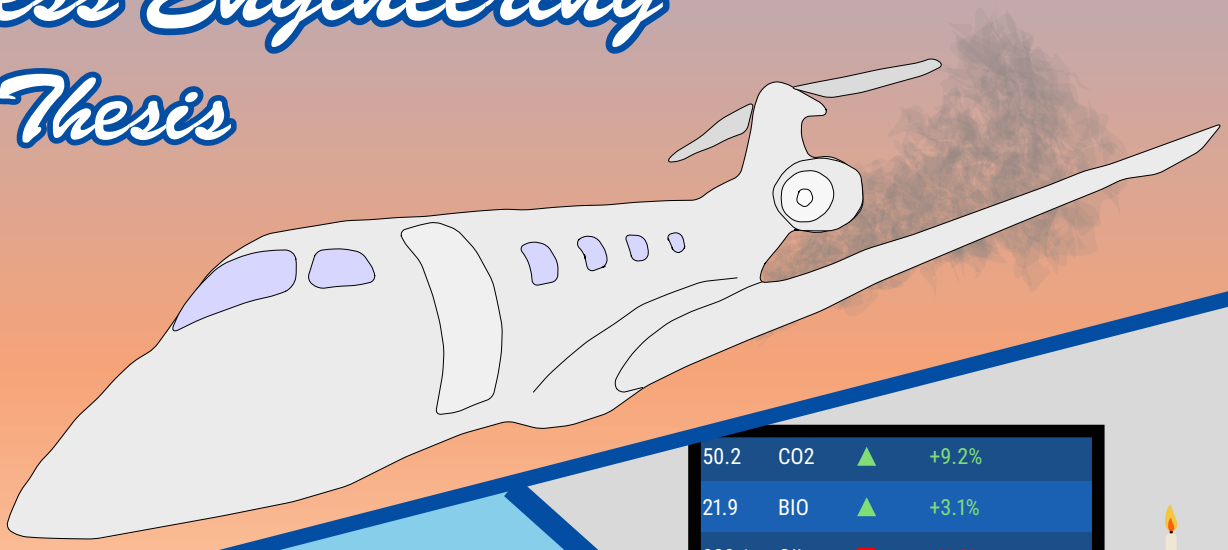

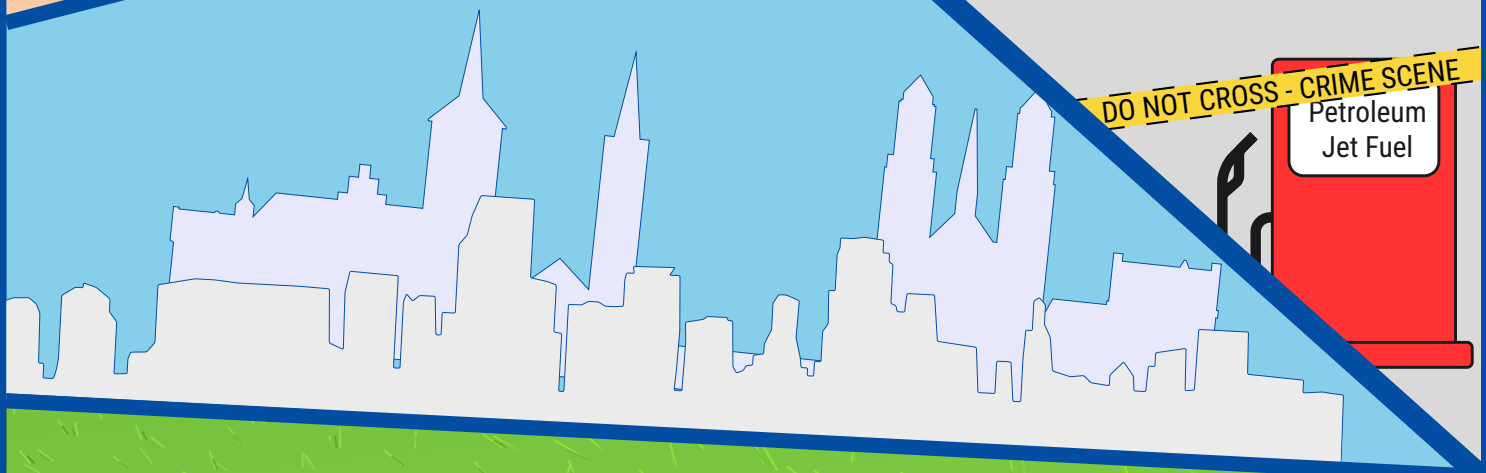

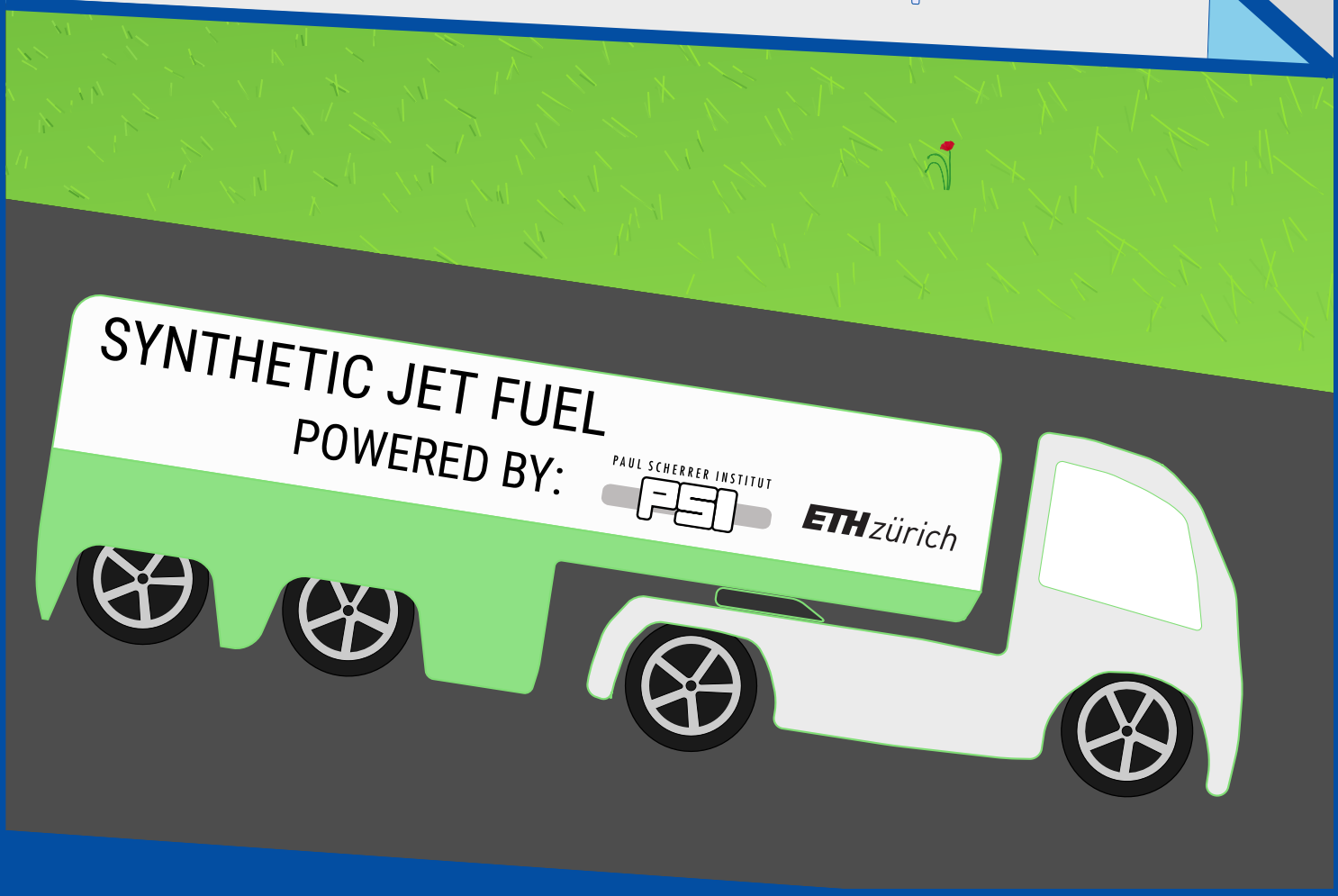

Synthetic Jet Fuel Production Processes - A Life Cycle Sustainability Assessment

by Dimitri M. Saad

in partial fulfillment of the requirements for the degree of
MSc in Process Engineering

at ETH Zürich, Switzerland
in collaboration with the Paul Scherrer Institute

Supervised by:

Mr. Christian Bauer
Dr. Romain Sacchi
Mr. David Shu
Prof. André Bardow

Submitted on the 12th of August, 2022

Abstract

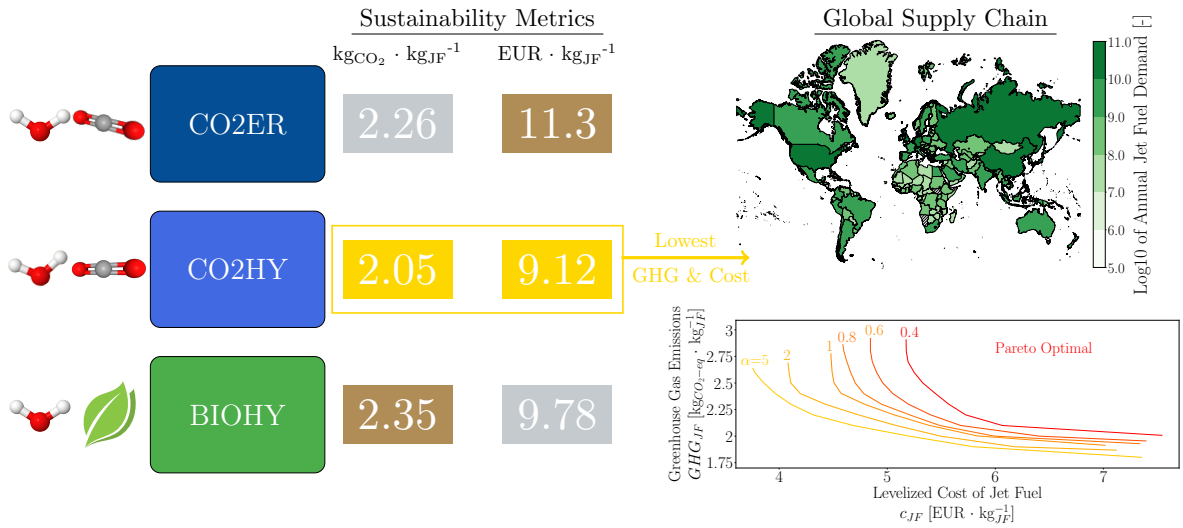

The aviation sector alone emits over 2% of the annual CO_2 emissions. As a result, synthetic jet fuels using biogenic feedstocks are emerging as promising pathways that reduce overall greenhouse gas emissions (GHG) relative to the petroleum-based jet fuel.

In this study, the decarbonization of the aviation sector is tackled via the technological assessment of 3 synthetic jet fuel production processes using environmental and economic metrics. These synthetic jet fuel processes convert feedstocks of water and CO_2 or biomass to jet fuel via methanol. This assessment includes a comprehensive process-based life cycle assessment (LCA) and costing (LCC) of the 3 processes, to determine the GHG emissions and the levelized cost of producing jet fuel in Switzerland. The results show that the process distinguished by the direct hydrogenation of CO_2 to methanol has the highest GHG emission reductions (33.8% reduction) and the lowest levelized cost (9.12 EUR/$kg_{JetFuel}$) if it is produced in Switzerland.

The model is extended to a global supply chain optimization including 140 countries. The supply chain optimization utilizes country-based inputs such as jet fuel demand, shipping routes, the electricity mixes and production capacity in 2050, as well as the determined GHG emission and cost quantities of the synthetic jet fuel production process via CO_2 electrochemical reduction. Three optimization problems are considered: (1) cost minimization, (2) GHG minimization, and (3) the trade-off between GHG and cost. The solution of these problems show that synthetic jet fuel costs can be relatively competitive with the petroleum-based fuels, but not simultaneously with low GHG emission reductions. The optimization solutions reveal an urgent need for a rapid expansion in global electricity production to shift to more sustainable jet fuels and energy systems. The need for high energy is attributed to capturing and converting the feedstocks, particularly due to high energy needed to capture CO_2 and to convert water to hydrogen, both of which contribute to the majority of the GHG emissions and jet fuel production costs. Furthermore, the results show that countries with high capacity to implement offshore wind farms are the favored countries to produce these synthetic fuels, provided the electricity is available for synthetic jet fuel production. Finally, the results emphasize the importance of accounting for transportation in minimizing the global emissions and costs associated with a well-to-tank jet fuel life cycle.

Preface

> “All models are wrong, but some are useful.”
>
> — George E. Box

Hopefully this thesis is useful enough to turn the wheel forward regarding decision making for a sustainable energy transition.

Acknowledgements

Who I am today and what I've achieved is in part a product of the contribution of a countless number of people. I am very grateful to all the people, friends, family, colleagues, and professors that have helped me become the researcher and human I am today. I cannot emphasize the extent of my gratitude, but I will try in this acknowledgements section.

It goes without saying that I would not be here at all without my family. I am indebted to my parents who sacrificed so much for my sister and me, and I am very thankful and blessed that they put our education and our welfare above anything. I hold these values very highly. So, thanks mom and dad.

In just 2 years at ETH, I learned so much as a result of the warm and enlightening interactions I've had with people here. I thank Prof. Maria Lukatskaya and Prof. Giovanni Sansavini for always finding the time for fruitful academic discussions. I am also grateful for the support of Prof. André Bardow as my tutor, mentor, and co-advisor of this thesis. Additionally, I want to specifically thank my semester project supervisors Dr. Georgios Kelesidis, Prof. Sotiris Pratsinis, and Dr. Christos Frouzakis, for an amazing introduction into soot particle dynamics and combustion, and for motivating me to push past my limits at every step along the way. Moreover, I owe a lot of gratitude to Dr. Michael Rawlence and the battery engineering team at FPT Motorenforschung AG, where I conducted my industrial internship.

Finally, a big warm appreciation goes to my Paul Scherrer Institute (PSI) family, especially my supervisors Christian Bauer and Dr. Romain Sacchi, who were superb advisors during my time at PSI. This project is part of the synfuel initiative, which consists of many collaborators in different fields across PSI and Empa. Therefore, I want to acknowledge and thank Matthieu André Dessiex, Jiyun Kwen, Dr. Juan Herranz Salañer, and Dr. Felix Büchi for their contribution and support in characterizing the electrochemical systems; Luca Maggiulli, Dr. Tilman Schildhauer, Dr. Emanuele Moioli, Dr. Florent Jules Dubray, and Dr. Davide Ferri for their help in selecting and evaluating thermochemical conversion of methanol to jet fuel; Dr. Hang Xiang, Dr. David Baudouin, and Dr. Frédéric Vogel for introducing us to biomass to jet fuel via hydrothermal processes; Dr. Blazhe Gjorgiev for helpful conversations on reliability assessment; Churchill Agutu for his help in exploring risk premiums; Dr. Viola Becattini and Daniel Pokras in supporting this work with everything related to direct air capture; and Dr. Carlos Gomez and Dr. Roland Hischier for fruitful life cycle assessment discussions. Special thanks go to the colleagues in the Laboratory for Energy Systems Analysis that supported me, namely Xiaojin Zhang, Dr. Thomas Heck, and of course Tom Terlouw, for their fruitful and insightful exchanges. At last, I want to sincerely thank David Shu for his supervision and support as part of the ETH oversight of this thesis.

When I will think of my time at ETH Zürich and PSI, I will recall these interactions with these people.

Thank you.

Contents

List of Figures

List of Tables

Nomenclature

A	Area
C	Cost
CF	Capacity Factor
D	Diameter
E	Energy
FR	Fractional Recovery
H	Height
J	Current Density
K	Load Factor
L	Length
$LCOJF$	Levelized Cost of Jet Fuel
$LMTD$	Logarithmic Mean Temperature Difference
M	Molar Mass
$MAINT$	Maintenance Costs
N	Number/Quantity
P	Power Rating
R	Gas Constant
REV	Revenue
S	Supply of Jet Fuel from a specific country
T	Temperature
V	Voltage
W	Work (Electrical)
X	Excess Factor
ΔE	Electricity Production Increase
ΔF	Flow
ΔG	Gibbs Free Energy
ΔT	Temperature Difference
$\dot{W}$	Rate of Work
$\underline{\underline{T}}$	
$\underline{\underline{T}}$	Environmental Intervention Matrix
$\forall$	Volume
WHSV	Weight Hourly Space Velocity
$\underline{f}$	Functional Unit Vector
$\underline{g}$	Intervention Vector
$\underline{s}$	Scale Vector
a'	Surface Area Per Unit Length
c	Cost Per Unit Mass
ch	Working Fluid Charge
f	Fraction
j	Uniform Series Present Worth Factor
k	Ratio of Specific Heats
n	Production and Supply Quantity
p	Pressure
q	Specific Heat/Heat Per Unit Mass
r	Rate
u	Velocity
w	Specific Work/Energy Per Unit Mass
y	Constant
z	Inlet Composition (Mass Fraction)
U	Overall Heat Transfer Coefficient
$\dot{Q}$	Heat Rate
$\dot{m}$	Mass Flowrate
Q	Heat Energy
m	Mass

Acronyms

CED	Cumulative Energy Demand
CoEly	Co-electrolyzer Unit
COP	Coefficient of Performance
DAC	Direct Air Capture Unit
Ely	Electrolyzer Unit
GHG	Greenhouse Gas Emissions
GWP	Global Warming Potential
HTHP	High Temperature Heat Pump
KERSN	Petroleum-based Jet Fuel Production Process
LCA	Life Cycle Assessment
LCC	Life Cycle Costing
LCIA	Life Cycle Impact Assessment
LCI	Life Cycle Inventory
LUO	Land Occupation
PEM	Proton Exchange Membrane
PGM	Platinum Group Metal
WDP	Water Depletion
BIOHY	Biomass-to-Jet Fuel process via hydrogenation

$CO2ER$	CO_2-to-Jet Fuel process via electrochemical reduction
$CO2HY$	CO_2-to-Jet Fuel process via direct hydrogenation

Global Supply Chain Indeces

i	Receiving Country
j	Supplying Country
k	Renewable Energy Technology

Greek Letters

α	Fraction of Available Electricity for Jet Fuel Production
β	Porosity Fraction
χ	Single-Pass Reaction Conversion
δ	Thickness
ℓ	Lifetime
ϵ	Purge Fraction
η	Efficiency
μ	Allocation Parameter
∂	Demand
ρ	Mass Density
σ	Stength
ς	Selectivity

Sets

C	Countries
RET	Renewable Energy Technologies
UP	Unit Processes

Superscripts

$=$	Alkane/Olefin
$capex$	Capital Investments
LB	Lower Bound
$opex$	Operating Costs
sc	Optimal Solution for Supply Chain
UB	Upper Bound

Subscripts

ℓ	Over Its Lifetime
AC	Absorption Chiller
C	Cooling
cat	Catalyst
cd	Condenser
cf	Cooling Fluid
$chiller$	Chiller
cmp	Compressor
$coely$	Co-electrolyzer
D	Distillate
d	Design
DAC	Direct Air Capture
dc	Distillation Column or Separator
DPE	Diphenyl Ether
ds	Discount
e	Electrical
el	Electricity
ely	Electrolyzer
eq	Equivalent
F	Faradaic
$feed$	Feed
$furnace$	Industrial Furnace
H	Heating
hf	Heating Fluid
HP	Heat Pump
hx	Heat Exchanger
i	Inlet
is	Isentropic
JF	Jet Fuel
l	Liquid
m	Mechanical
NG	Natural Gas
o	Outlet
$product$	Product of the Reaction
$pump$	Pump
rb	Reboiler
rec	Recycled
ref	Reference
$reflux$	Reflux
rx	Reactor
sep	Flow to be separated
$shell$	Shell in Shell and Tube Heat Exchanger
$steel$	Steel
$target$	Targeted Value
tpt	Transport
$trays$	Trays
$tubes$	Tubes in Shell and Tube Heat Exchanger
v	Vapor
$weld$	Welding
yr	Per Year

this page is intentionally left blank

1 Introduction

The continuously increasing atmospheric CO_2 concentration poses a significant threat to the Earth. These carbon emissions act as a driver for global warming, which results in a global increase in temperature [1], rise in sea level [2], and threatening the viability of ecosystems [3]. As a result of such concerns, the Paris Agreement was enacted in 2015 by nations to outline frameworks and develop strategies that can prevent climate disasters [4]. In particular, these strategies revolve around mitigating carbon emissions in various sectors.

The aviation sector is a key contributor to the global increase in atmospheric CO_2. Today, this industry is responsible for over 2% of the yearly global CO_2 emissions [5]. This notable contribution arises since aviation produces the highest carbon emissions per passenger amongst all modes of transport at 90 g_{CO_2} per passenger per kilometer [6]. This industry nevertheless plays a pivotal role in the global economy by promoting international trade, transportation, tourism, and social development [7]. Consequently, projections for this industry over the next few decades dictate that aviation will continue to drive globalization and exhibit a 115% increase in passenger number by 2037 relative to 2016 [8, 9]. Thus, aviation is expected to grow and is unlikely to be replaced by alternative modes of transport. The increasing environmental concerns caused by global warming then necessitate that the projected growth of the aviation sector is accompanied by its decarbonization [10].

The primary climate impact of aircraft operation relates to the fuel-associated emissions [11]. In addition to emissions due to its production, the combustion of 1 kg of jet fuel produces 3.16 kg of CO_2 [6]. As a result, the development and utilization of low-carbon jet fuels is paramount to ensure the sustainability of life on Earth without sacrificing economic and societal growth.

1.1. Aviation Fuels

Aviation fuels possess the highest contribution to the carbon emissions produced by the aviation industry [11]. These emissions are generated during fuel combustion and during its extraction and refinement [12]. Battery-powered vehicles can prove to be competitive and low-emission alternatives to fuels in automotive applications, but a similar shift cannot be completely enacted in aviation due to their low energy density compared to liquid fuels [13]. The focus herein is therefore strictly limited to liquid fuels.

There are 2 types of aviation fuels: (1) jet fuels, whose requirements are specified by various standards and are compatible with current aircrafts, and (2) alternative fuels, which differ in composition and whose utilization could require changes in the aviation infrastructure.

1.1.1. Jet Fuels

The conventional aviation fuel utilized today is derived from petroleum. Aviation fuels are commonly referred to as jet fuels, and are expected to meet specific property requirements. Jet fuel is typically composed of a mixture of C_8-C_{18} hydrocarbons, namely alkanes, iso-alkanes, and naphthenics [14]. Such a mixture enables the fuel to remain liquid at airplane altitudes. For this reason, standards such as the ASTM D1655 exist to govern jet fuel composition and properties for safe and optimal operation. These property specifications are reported in Table 1.1 [15].

Specification	Units	**ASTM D1655**	**MIL-T-5624**
Grade	-	Jet A	Jet B
Aromatics	%	25	25
Maximum Sulfur Mass Fraction	%	0.3	0.4
Minimum Flash Point	°C	38	-
Maximum Freezing Point	°C	-40	-51
Density, at 15 °C	$kg \cdot m^{-3}$	775-840	750-801
Maximum Viscosity, at -20 °C	$mm^2 \cdot s^{-1}$	8	-
Specific Energy	$MJ \cdot kg^{-1}$	42.8	42.8

Table 1.1. A sample of the specifications of the jet fuels named Jet A and B governed by ASTM D1655 and CGSB-3.22 respectively, which determine the recommended fuel composition and properties for safe aircaft operation [15].

The specifications in Table 1.1 show the specificity of the properties that are determined by the ASTM D1655 and CGSB-3.22 standards. Thus, sustainable fuels developed for aviation should conform to such standards. The current process to produce conventional jet fuels from crude oil, which satisfy the properties shown in Table 1.1, mainly centers on fractional distillation [16]. Sustainable jet fuels can thus satisfy the standards by exploring different routes and feedstocks to synthetically produce the same jet fuel via synthetic routes or determine alternative fuels that can still conform to the standards of Table 1.1.

The target of synthetic fuel production is to develop a fuel with nearly the same properties and composition as those of conventional jet fuels, but using a different production method. Synthetic jet fuel production processes produce synthetic jet fuels whose carbon footprint is significantly lower than their petroleum-based counterparts. The reduction in carbon footprint is not attributed to a change in combustion emissions, since the synthetic jet fuel is similarly combusted during operation. Instead, the emissions are reduced by using biogenic sources of CO_2, which remove CO_2 from the environment [17]. The removal of CO_2 from the environment negates the combustion emissions since the amount is the same. The net emissions from synthetic jet fuels are thus strictly attributed to its production emissions. For instance, biomass is created via CO_2 consumption. In summary, synthetic fuels are distinguished by their utilization of feedstocks that remove CO_2 from the environment.

Biogenic CO_2 feedstocks can include triglycerides-based feedstocks [18], lignin [19], camelina and soybean oils [20, 21], and sugar (which can produce alcohol or other hydrocarbons) [11, 22, 23]. The pathways to produce these jet fuels starting with such feedstocks are also various and include the hydrogenated esters and fatty acids (HEFA), catalytic hydrothermolysis (CH), hydrothermal liquefaction (HTL), and hydroprocessed depolymerized cellulosic jet (HDCJ) [11]. The Fischer-Tropsch (FT) process produces jet fuel from syngas (CO and H_2), if biomass generates syngas [11]. Pure CO_2 is also considered a biogenic source of CO_2, which classifies it

as another possible feedstock for synthetic jet fuels [24].

Regardless of the life cycle characteristics shown by these fuels and their pathways, the readiness of such technologies should be carefully considered. Some pathways remain restricted to laboratory scales and could face difficulties in scaling up, while others are already operational at commercial scales [11, 25].

1.1.2. Alternative Fuels

Unlike "drop-in" jet fuels, alternative fuels for aircraft usage are fuels that differ in composition and properties from the standard jet fuels shown in Table 1.1. However, such fuels are incompatible with current aircraft engines and instead require infrastructure modifications [26]. The prominent alternative fuels discussed herein are ethanol, liquefied natural gas (LNG), and hydrogen (H_2).

Ethanol proves to be a fuel source with relatively lower environmental footprint compared to jet fuels [27]. However, ethanol's low flashing point could pose a hazard to handle at airports, while its high volatility could cause problems during operation [14]. Apart from these safety concerns, the main issue with ethanol lies in the substantial costs required for retrofitting current engines and infrastructure to accommodate for it as a fuel [14]. This issue is replicated in the arguments against hydrogen and liquefied natural gas as aircraft fuels, despite their capacity to reduce carbon emissions as an aircraft fuel [28–30]. However, both fuels should be in the cryogenic state during operation, which would introduce further retrofitting complexities compared to liquid fuels at operating temperatures [14].

The aforementioned alternative fuels provide some advantages in their production processes, but so far remain complicated to implement due to infrastructure requirements. These complications would deter their adoption as sustainable fuels. As such, the fuels considered herein as part of the life cycle analysis study are restricted to jet fuels from Section 1.1.1.. These fuels would still consist of the same composition of Jet A for instance, but would consist of distinct production pathways whose life cycle emissions reduces greenhouse gas emissions compared to the petroleum-based fuel.

1.2. Life Cycle Sustainability of Synthetic Jet Fuel

Synthetic jet fuel can be produced using several feedstocks and via various conversion pathways. The production and adoption of these synthetic fuels relies on measures of their sustainability. A process is considered sustainable if it "meets the needs of the present generations without compromising the ability of future generations to meet their own needs" [31]. Such a definition implies that sustainable processes offer longevity for the future, while also meeting the demands of today. The implication of this definition for a jet fuel production plant is that the plant can sustain itself financially and generate profits. In addition, the production plant should not interfere with planetary boundaries and contribute to climate disasters [32]. In fact, the International Civil Aviation Organization (ICAO) [33, 34] defines a sustainable fuel as one that provides a minimum of 10% reduction in life cycle green house gas emissions (GHG) relative to the conventional kerosene jet fuel. By this definition, a sustainable fuel is a fuel whose life cycle greenhouse gas emissions does not exceed 3.17 $kg_{CO_2} \cdot kg_{JF}^{-1}$. This limit is not a suitable indicator for

sustainable fuels since it does not present significant reductions in GHG emissions. As for the jet fuel cost, there is no threshold that would render it sustainable. The current price of jet fuel is 1.15575 EUR · kg_{JF}^{-1} and serves as the benchmark for the cost [35].

The life cycle assessment studies of synthetic jet fuel processes have typically focused on the environmental impact due to on greenhouse gas emissions and land usage [36]. The emissions estimated for the life cycle of synthetic jet fuel depend on the pathway utilized and on the different potential feedstocks [36, 37]. The studies that evaluate synthetic jet fuels in the literature mainly consider 2 feedstocks: biomass derivatives [11, 20, 26, 37–40] and pure CO_2 [24, 41–43]. Processes using biomass as feedstocks presented synthetic jet fuels whose GHG emissions are significantly lower than the petroleum-based fuel [38, 39]. Morevoer, Staples et al. [38] conducted a pioneering life cycle assessment and costing of "drop-in" synthetic jet fuels from biomass feedstocks. They showed that synthetic jet fuel GHG was negative for one process, which is a rather unrealistic estimate of synthetic jet fuel production processes. This negative value shifted to a positive value upon using a different attribution method of allocation instead of displacement [38]. The variation in environmental impact results due to the utilized attribution methodology has been also shown by similar studies [37, 44]. As a result, this distinction in attribution method across the studies makes it more difficult to establish accurate life cycle comparisons [20, 26]. Furthermore, Neuling & Kaltschmitt [39] investigated both cost and GHG using biomass feedstocks converted via various pathways. The pathway using alcohol-to-jet using a wheat straw feedstock can reduce the GHG emissions by over 50%. Their work, however, did not extensively assess land usage metrics. The work of Staples et al. [38] portrayed that land usage influences and increases GHG emissions, which is an outcome that was similarly reiterated by Souza et al. [45].

In contrast, few studies explored the production emissions of synthetic "power-to-liquid" fuels that use CO_2 from direct air capture (DAC) and water as feedstocks. CO_2 to jet fuel via hydrogenation has been investigated via LCA. More recently, feeding CO_2 into a co-electrolysis unit rather than direct hydrogenation is gaining traction [46]. Meurer & Kern [47] investigated the technical performance of such electrochemical reduction of CO_2 to CO, so that the CO is in FT to produce jet fuel. However, their work does not quantify the environmental emissions associated with this alternate pathway [47]. Most of the assessed CO_2-to-jet fuel processes consist of a Fischer-Tropsch pathway [43, 48]. Treyer et al. [48] showed that Power-to-Liquid and Sun-to-Liquid processes can convert CO_2 to jet fuel, with 90% less GHG emissions. Other pathways propose the conversion CO_2 or CO to methanol, which is then converted to olefins that oligomerize to produce jet fuel. This process was developed by Mobil [49] back in 1988. Both CO_2 to jet fuel via methanol and FT were reviewed by Schmidt et al. [43]. They reported that the GHG of synthetic jet fuels using a CO_2 feedstock can range between 0.4 and 1.2 $kg_{CO_2} \cdot kg_{JF}^{-1}$ [43]. This range of GHG emissions corresponds to a renewable electricity mix purely formed of wind and photovoltaics (in Germany). Compared to processes starting with biomass feedstocks, the key benefit in such Power-to-Liquid processes is the lower land usage and competition with food and agriculture. However, this benefit is opposed by higher electricity requirements per unit of synthetic jet fuel [48].

Amongst the studies that conducted a life cycle assessment, only a few complemented their environmental assessment with a life cycle costing evaluation. The levelized costs of jet fuel shown in the literature differ notably based on the modeling assumptions and regions. For CO_2-to-Jet Fuel processes, Schmidt et al. [42] estimated the cost of synthetic jet fuel at 1-2 EUR ·

kg_{JF}^{-1} , while other studies [43] depicted higher costs at 3-4 EUR · kg_{JF}^{-1} . These aforementioned studies respectively used a cost of electricity of 0.04 [42] and 0.1 EUR · kWh^{-1} [43]. The difference in cost of electricity explains the doubling of the synthetic jet fuel cost. The work of Zhou et al. [41] emphasizes this dependence of synthetic jet fuel cost on the cost of electricity. Furthermore, Neuling & Kaltschmitt [39] estimated a very competitive (relative to petroleum-based jet fuels) levelized cost of synthetic jet fuels from biomass feedstocks at around 1 EUR · kWh^{-1}. Generally, the cost of electricity used in these studies is not exactly representative and is in most cases very optimistic. Additionally, Schmidt et al. [43] conducted sensitivity analysis that quantified the effect of electricity costs on the levelized cost of jet fuel, which is a beneficial analysis that is absent from most similar studies.

Besides the study of Neuling & Kaltschmitt [39], the life cycle costing studies rarely account for a process-based costing. In some cases, a generalized correlation (example: cost of FT process per unit energy of fuel produced) that covers several units together is utilized [24]. While such correlations are useful for order of magnitude estimates, they do not allow for a direct correspondence between the environmental and economic boundaries in the modeling of the unit processes [50].

Thus far, the aforementioned studies have not accounted for jet fuel production on the global scale. In particular, the variation in vital quantities, such as electricity prices and emissions, prevents the direct comparison of the synthetic jet fuel production processes. These quantities are dependent on the region in which they are utilized [51]. Similarly, the availability of biomass feedstock for instance can vary across countries [52]. For this reason, restricting the assessment to a single region with fixed quantities does not enable determining the locations with the lowest GHG emissions or costs of jet fuel. Therefore, it is imperative to explicitly account for geography when attributing these quantities, and to ensure that all the quantities refer to the same region. This reason serves the first argument for accounting for country-based synthetic jet fuel production. Furthermore, these studies have so far only considered the production and combustion of the synthetic jet fuel. However, a well-to-tank approach should include jet fuel transportation, where the synthetic jet fuel is delivered to the well following production. The inclusion of jet fuel transportation then begs the question: where is the synthetic jet fuel transported from? This question raises the second argument in favor of accounting for country-based synthetic jet fuel production. The production location of a commodity produced in hundreds of Mtons annually [53] would contribute to the overall environmental and economic impacts incurred if transportation is accounted for. Finally, very few studies have addressed mass production of synthetic jet fuel on a global scale that satisfies the global demand. Such an assessment on a global scale could present obstacles and constraints regarding available energy, thus potentially rendering some economically or environmentally attractive processes completely infeasible. Consequently, a global scale model combining synthetic jet fuel production and transportation is required to determine a more realistic cost and GHG emission values.

1.3. The Synfuel Initiative

The synfuel initiative targets the technological development and assessment of processes converting biogenic CO_2 sources to synthetic jet fuel. These processes aim to capitalize on the emergence of CO_2 [24] and biomass [54] as sustainable carbon sources for aviation fuels. Furthermore, the processes are divided into 2 stages: (1) CO_2/biomass to methanol

and (2) methanol to jet fuel. The 2nd stage is common for all 3 processes, and they are distinguished primarily by the 1st stage. The first process converts CO_2, captured by a direct air capture unit, to CO via electrochemical reduction. The produced CO is combined with H_2, which is generated by water electrolysis, to produce syngas. The resulting syngas then reacts to produce methanol. This process is referred to as *CO2ER*. The second process similarly uses CO_2 from a direct air capture unit and H_2 from a water electrolyzer. The key difference is that CO_2 is combined directly with H_2 to produce methanol. This reaction is known as CO_2 hydrogenation, and the process is referred to as *CO2HY*. The third process uses biogas generated from sewage sludge (waste biomass) waste treatment and water as the main feedstocks. Biogas contains both CO_2 and CH_4, and the CO_2 is reacted with H_2 from water electrolysis to produce methanol. This process is referred to as *BIOHY*. Unlike the *CO2ER* and *CO2HY*, which consists of both stages in the same chemical plant, the first stage of the *BIOHY* process takes place decentrally in the vicinity of a biogas production plant. The methanol mixture produced from this process is then transported to a centralized plant, which can receive methanol from various decentralized methanol reactors. The first stage of each process is depicted in Figure 1.1.

Figure 1.1 (a), (b), and (c) respectively portray the main units of the 1st stage of the *CO2ER*, *CO2HY*, and *BIOHY* processes. The *CO2ER* process in Figure 1.1 (a) requires more energy for the co-electrolysis unit to reduce CO_2 electrochemically to CO, but less energy for the water electrolysis unit. This energy reduction in the water electrolysis unit is attributed to the stoichiometry of the syngas-to-methanol reaction. Moreover, the reaction between CO and H_2 can produce almost pure methanol. In contrast, the direct hydrogenation of CO_2 in the *CO2HY* process forms both methanol and water as products. The water byproduct thus requires separation from methanol before methanol is used in the 2nd stage of the process. Thus, more separation units are required in the *CO2HY* process relative to the *CO2ER* process. Finally, the *BIOHY* process in Figure 1.1 (c) leverages a waste treatment plant to produce methanol in a decentral location. Compared to the other processes, the stages of the *BIOHY* process are spatially separated. However, this process assumes that the appropriate infrastructure and pipeline systems are available. This assumption could show practical limitations, such as low product output due to limited waste treatment and biogas production plants.

The 2nd stage of the 3 processes is identical. This stage begins with methanol, which then flows through a series of reactors to eventually produce jet fuel. The first reactor converts methanol to olefins and water. The second reactor consists of the oligomerization of the olefins to produce jet fuel-range alkenes. Finally, these alkenes are hydrogenated to produce the synthetic jet fuel. This 2nd stage is visualized in Figure 1.2.

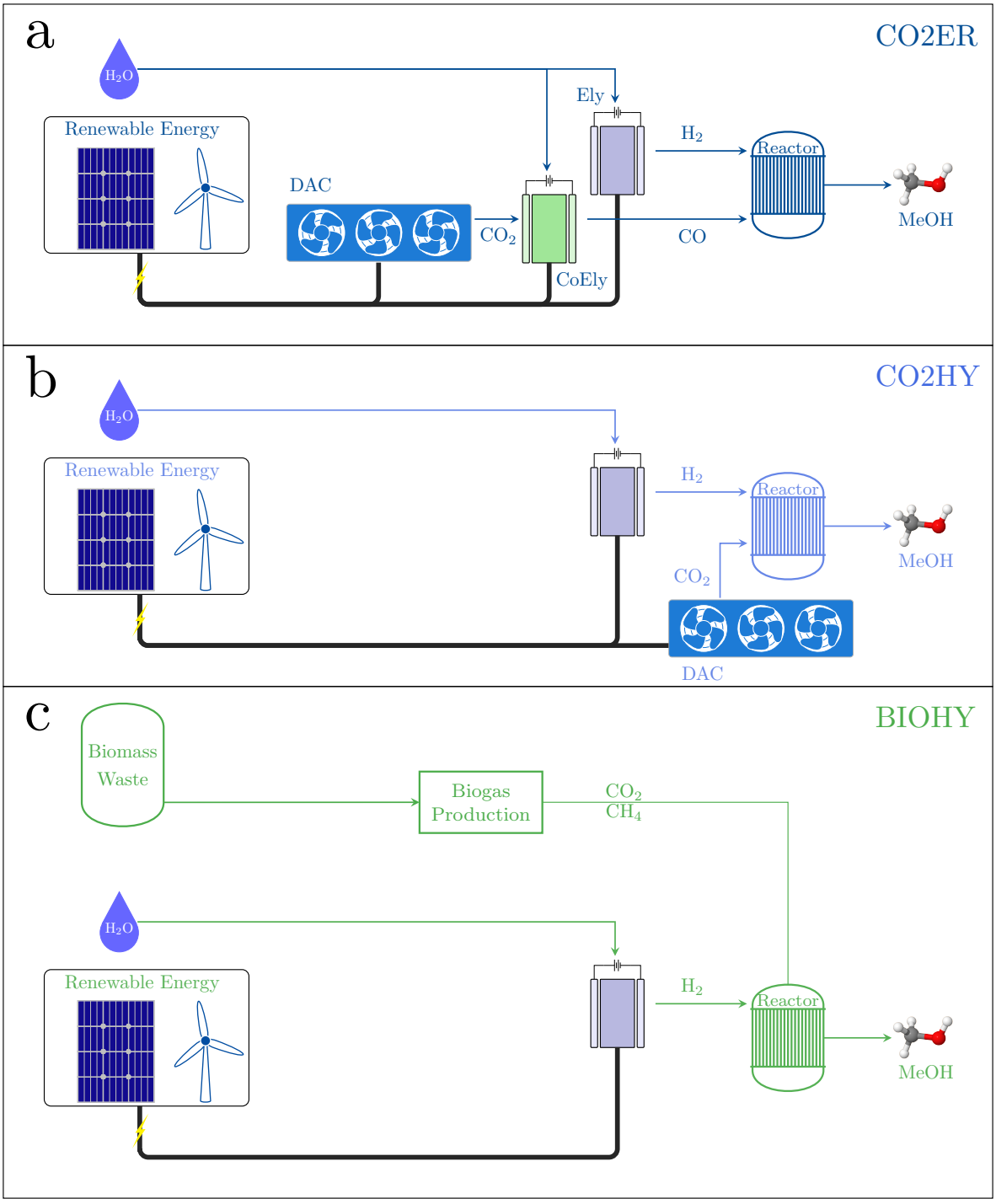

Figure 1.1. A schematic demonstrating the first stage of the 3 studied processes: *CO2ER* (a), *CO2HY* (b), and *BIOHY* (c). The first stage of each process uses a biogenic CO_2 source (*CO2ER*, *CO2HY*: CO_2 from direct air capture; *BIOHY*: biogas from waste treatment of sewage sludge) and water as a feedstock. The conversion pathways from feedstock to methanol (MeOH) include thermocatalytic (reactor) and electrochemical units (H_2O electrolyzer (Ely) and CO_2 electrolyzer (CoEly)) in addition to a direct air capture unit (DAC). Note that only the main units are included; i.e. no heat exchangers, compressors, and separators are shown this schematic.

1.4. Thesis Outline

In this thesis, novel jet fuel production processes are evaluated in terms of environmental and economic indicators. Three processes associated with the synfuel initiative are evaluated, whose feedstocks are one of the following: (1) carbon dioxide and water, (2) biomass waste and water.

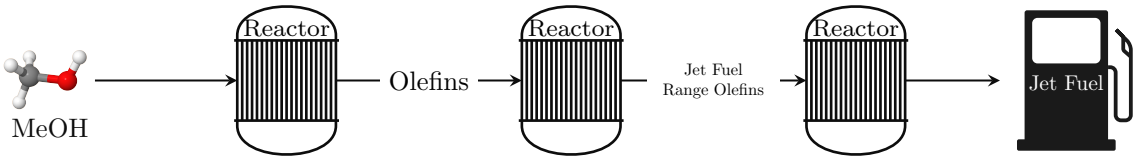

Figure 1.2. A schematic demonstrating the second stage of the 3 studied processes (*CO2ER*, *CO2HY*, and *BIOHY*). This second stage follows the conversion of methanol (MeOH) via a series of reactors to eventually produce jet fuel. The conversion pathway includes mainly thermocatalytic (such as the reactor) units. Similarly, only the main units are included; i.e. no heat exchangers, compressors, and separators are shown this schematic.

These feedstocks comprise biogenic CO_2. Upon utilizing biogenic CO_2, the carbon cycle is closed and the greenhouse gas emissions due to jet fuel combustion is negated by the utilization and removal of the biogenic CO_2 from the atmosphere.

The units necessary to produce synthetic jet fuels are integrated using a process design and flowsheeting approach. The energy and mass balances of the units are defined, such that the total energy and mass flows are modeled for the production of a unit of synthetic jet fuel. Based on these energy and mass balances, a life cycle inventory of each process is determined. Thus, a systematic life cycle methodology is developed to evaluate and compare the economic and environmental performance of the processes. The life cycle assessment methodology assesses the processes using their units' inventories to determine environmental impact categories, such as those of climate change, land usage, water depletion, and cumulative energy demand. The life cycle costing methodology determines the levelized cost of jet fuel by accounting for capital and operating costs, which are determined by the units' energy and mass balances. Similarly, the units are sized and their cost is determined via an approach that factors economies of scale. The units evaluated in the various processes included energy sources (high temperature heat pump, grid electricity, absorption chiller, and fired furnace), electrochemical units (water electrolyzer and CO_2 electrolyzer), a direct air capture unit, and conventional chemical units (distillation columns, separators, compressors, reactors, and heat exchangers). This methodology aims to output impact categories and costs per unit of synthetic jet fuel produced via each of the 3 processes.

The greenhouse gas emissions and levelized cost are calculated for only one process in varying countries in a global supply chain optimization. The target of the supply chain optimization is to determine the optimal jet fuel production locations. The model factors the environmental and economic burden of production and transportation of synthetic jet fuel, in addition to several datasets that help in modeling the production capacities and the supply chain. Thus, the algorithm determines the optimal locations to produce synthetic jet fuel and establishes optimized shipping routes, based on minimizing the global life cycle emissions or life cycle cost of jet fuel.

The thesis concludes by highlighting the key takeaways from the results and offers recommendations for further studies to build on the current work and help pave the way for a sustainable aviation industry.

2 Life Cycle Assessment

The life cycle assessment (LCA) of synthetic jet fuel production processes establishes the methodology used by defining phases: the study's goal and scope, its life cycle inventory, and life cycle impact assessment. Based on this methodology, the results are presented and discussed. Certain phases of the methodology were iterated and refined based on the feedback from different phases, such that the overall study's objectives are met and delivered with minimal uncertainty.

This study complies with the life cycle assessment methodology guidelines (ISO 14040) [55], which were developed by the international organization for standardization (ISO).

2.1. Goal & Scope

The goal of this study is to assess the environmental impact of 3 novel synthetic jet fuel production processes. Aviation forms an essential aspect of modern economies, thus makes minimizing its environmental footprint of interest within the scope of climate change. A study using a LCA approach is essential in a comparative assessment of these different process pathways that produce synthetic jet fuel.

The study aims to inform policy and decision makers at governmental and industrial levels, and is part of the synfuel initiative. The potential and role of producing synthetic aviation fuel in low-carbon economies are evaluated, accounting for their contributions to the Swiss target of reaching net-zero greenhouse gas emissions.

Following up on the work of Treyer et al. [48], the production of synthetic fuels for aviation is evaluated using a process-centered life cycle approach.

The geographical scope of this study is limited to Switzerland. Electricity prices and emissions are those corresponding to Switzerland. Life cycle inventory datasets utilize the Swiss datasets (CH) when possible, or European ones (RER) as a close approximation. Remaining literature data is assumed to be general and valid irrespective of geographical location.

The temporal scope ranges from today till the near future (20 years into the future). This temporal projection is established by setting the synthetic jet fuel production plant lifetime to 20 years. The disposal of the studied plants was excluded from the study, since end-of-life or circular handling of infrastructure in 20-40 years exhibits high uncertainties.

2.1.1. Processes & System Boundary

The boundary of the evaluated processes covers the units directly involved in the production of synthetic jet fuel using a well-to-tank approach. This includes the equipment needed to build the

chemical plant, the material and energy flows needed on a continuous basis (such as catalysts and electricity), in addition to extraction of feedstock from the environment. The disposal of the chemical plant is not covered. This boundary applies for both life cycle assessment and costing.

The exact units utilized in the modeling of the processes are shown in Figure 2.1.

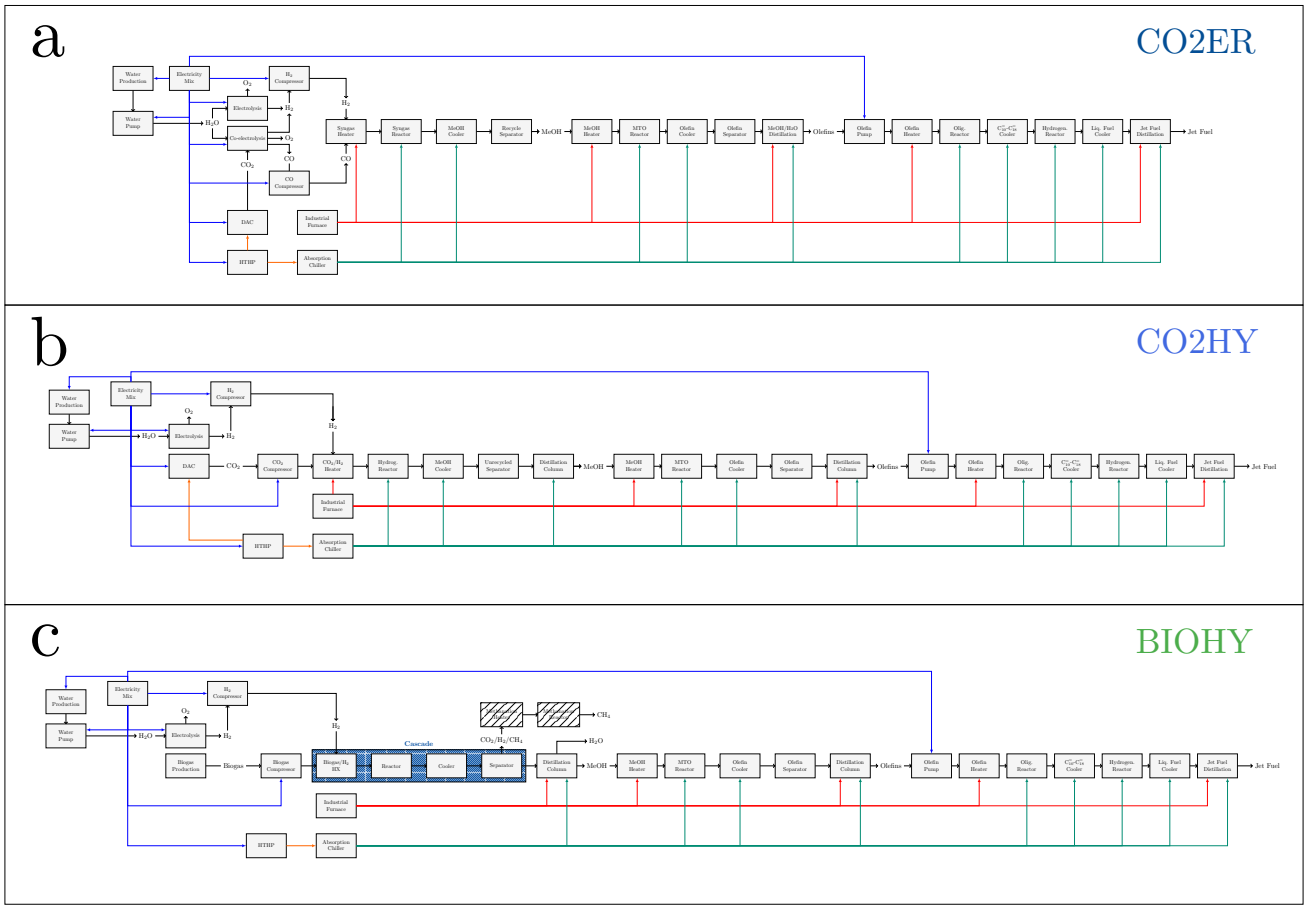

Figure 2.1. The modeled unit processes within the system boundaries of each of the *CO2ER* (a), *CO2HY* (b), and *BIOHY* (c) processes. The diagram shows the connected units via mass and energy. The energy sources utilized are the electricity mix, absorption chiller, high temperature heat pump (HTHP), and industrial furnace, whose energy flows are denoted by the thick lines. The mass flows are denoted by the thin black lines. Key components are methanol (MeOH), C10-C18 olefins ($C^{=}_{10}$-$C^{=}_{18}$). Key units are the direct air capture (DAC) unit, methanol to olefin (MTO) reactor, oligomerization reactor (olig. reactor), liquid fuel cooler (liq. fuel), and hydrogenation reactors (hydrogen.). The cascaded region highlights the repetition of the same blocks from left to right several times. Hatched blocks are only included to highlight the remainder of the process that was not included in the life cycle modeling.

As stated in Section 1.3., each process consists of its own unqiue pathway that converts the feedstocks to methanol. From methanol to jet fuel, the pathway is identical for the 3 processes. Heaters and coolers are utilized to change the temperature to the desired reaction or separation (before separators or distillation columns) temperature, while the compressors and pumps are employed to increase the pressure of a fluid. Due to the presence of reactions that do not go to complete conversion, some separation is typically required to separate the reactants from the unreacted chemicals, which is returned to the reactor via a recycle stream. The cascaded region in Figure 2.1 (c) implies that the units in this region are repeated in the specified order several times to achieve a desired methanol yield. Since this is a synthetic fuel, the energy demand of the modeled energy sources were accounted for in the foreground, thus allowing direct quantification of the energy demand per unit of synthetic jet fuel.

For both *CO2ER* and *CO2HY*, the processes consist of an electrolyzer that scales nonlinearly

with its power rating, which leads to reduced costs due to economies of scale. However, this is not the case for the *BIOHY* process, which depends on a nearby biogas production plant for its operations. The biogas production plants typically produce 200 m^3 of biogas per hour [56]. Thus, it is assumed that this portion is diverted in its entirety to the decentral methanol production plant. Thus, the costing here is conducted as follows: (1) sizing the electrolyzer corresponding to the stoichiometric hydrogen flowrate needed for 200 $m^3 \cdot h^{-1}$, and (2) scaling this cost linearly, thus representing the incorporation of the same plant and its capacity, each in the vicinity of an identical biogas production plant. Note that the stoichiometric ratios also account for the CH_4 production via CO_2 methanation, which is beyond the defined system boundaries. This approach is accounted for in both the inventory analysis for the life cycle assessment and the costing in the life cycle costing.

2.1.2. Functional Unit

The definition of a functional unit is critical since this functional unit serves as the reference unit for all environmental and economic metrics. Utilizing an energy functional unit of MJ of jet fuel (based on its lower heating value) is useful when comparing processes that could produce varying jet fuel compositions that still conform to the specifications shown in Table 1.1. However, the evaluated processes utilize the same MeOH-Jet Fuel production pathway, so the comparison per unit mass (i.e. kilogram) could suffice.

Thus, the functional unit is defined as "1 kg of Jet Fuel produced and consumed". The consumption only accounts for the CO_2 emissions (3.16 $kg_{CO_2} \cdot kg_{JF}^{-1}$ [6]), and does not incorporate other effects. This is applicable for Chapters 2 and 3. In Chapter 4, the functional unit is defined as "1 kg of Jet Fuel produced, transported, and consumed". This definition achieves a proper well-to-tank definition.

2.1.3. Reference System

The reference system that will benchmark the LCA results of the production pathways is the conventional petroleum-to-jet fuel process. The petroleum-based jet fuel production process is referred to as *KERSN* throughout this study. The production of petroleum-based jet fuel generates 0.36 $kg_{CO_2} \cdot kg_{JF}^{-1}$ [51], while its combustion emits 3.16 $kg_{CO_2} \cdot kg_{JF}^{-1}$ [6]. The ecoinvent activity used to refer to petroleum-based jet fuel production is "kerosene, petroleum refinery operation (CH)". Moreover, the production emissions derived from this activity is conducted by economic allocation [57], which could lead to some variation in the life cycle emissions of petroleum-based jet fuel. This variation originates due to differing economic parameters used in allocating its emissions. This ecoinvent dataset is nevertheless used as the activity generating the benchmark environmental impacts.

Thus, the total greenhouse gas emissions amount to 3.52 $kg_{CO_2} \cdot kg_{JF}^{-1}$, while the remaining impact categories will use the emissions associated with the ecoinvent activity depicting kerosene production.

2.1.4. Life Cycle Inventory

The life cycle inventory (LCI) combines datasets developed in ecoinvent and literature studies. For the background unit processes, the LCI is based on ecoinvent (version 3.8), using the "Allocation, cut-off by classification" system model [51]. Unless stated otherwise, European and/or Swiss datasets from ecoinvent were used when possible. The inventory of foreground unit processes relies on attributed flows derived from the literature studies or direct experimental measurements from collaborators of the synfuel initiative. These flows are expressed as ecoinvent activities when possible; otherwise, a flow is approximated by another proxy activity. Furthermore, the transportation of equipment is not included in the inventory, with the exception of the mass transported from the decentralized methanol production to the centralized plant (Section 2.1.1.). The utilized LCI for each unit process is explained in Section 2.2., and the inventory values are tabulated in detail in Table A.1. The mass and energy balances are similarly derived and shown in Section 2.2., such that total inventory is documented transparently and explicitly.

2.1.5. Multi-functional Units

Economic allocation is used to attribute contributions of byproducts in multi-functional units. This allocation approach was selected to establish a consistent comparison with the reference system [57] (Section 2.1.3.).

As a result, the contributions of three units are allocated economically. These units are the electrolyzer, co-electrolyzer, and a separator. The electrolyzer is used in every process that was evaluated (*CO2ER*, *CO2HY*, and *BIOHY*), while the co-electrolyzer (*CO2ER*) and the separator unit *BIOHY* are used in specific processes. For the electrolyzer unit, the same allocation parameters are consistently used for each process. Other than the specific separator of the *BIOHY* process, separators distillation columns were not allocated since the byproduct was either water that was recirculated within the process (for electrolysis) or produced negligible byproducts. This design decision implies that the heavy petroleum distillate (generated with jet fuel) and lower order olefins (generated with the other olefins) are not attributed emission burdens. The allocation parameter, μ_A, utilized to divide the emission contributions is expressed as:

$$\mu_A = \frac{m_\mathrm{A} \cdot c_\mathrm{A}}{\sum_i m_i \cdot c_i} \tag{2.1}$$

In Equation 2.1, m_i and m_A represents the output mass of products i and A respectively, c_i and c_A represents the unit cost of products i and A respectively. The product A refers to the product whose allocation factor, μ_A, is desired. Furthermore, the values of m_i for all products correspond to the same functional unit.

The mass parameters are those highlighted in Section 2.2., while the cost values are derived from the literature or market prices. These quantities and the resulting allocation parameters are tabulated in Table 2.1. The results of the allocation parameters shown in Table 2.1 strongly depend on the cost values used. The utilization of costs following market crashes or fluctuations of the unit cost of a chemical could lead to misguided results. Therefore, the costs utilized herein are chosen conservatively when possible. For instance, the cost of H_2 (the desired product in water electrolysis) depends on its production method, and could range between 1.5 USD $\cdot$ kg^{-1} to 10 USD $\cdot$ kg^{-1} [58]. It is set herein to 1.5 USD $\cdot$ kg^{-1} , which reflects the market price more accurately. Similarly, the cost of O_2 exhibits great variations. It could range from 0.04 USD $\cdot$

Table 2.1. The documentation of the attribution of multi-functional units via economic allocation. The allocated units were the electrolyzer unit (all processes) that co-produces O_2 and H_2 from H_2O, the co-electrolyzer unit (*CO2ER* process) that co-produces O_2, H_2, and CO from CO_2 and H_2O, and a separator unit (*BIOHY* process) that separates a mixture of unreacted CO_2, H_2, CH_4 from CH_3OH and H_2O following the hydrogenation of CO_2 in biogas to CH_3OH. The relative masses are documented for each unit process in Section 2.2., the costs are derived from the literature, and the allocation parameter is estimated by using the mass and costs in Equation 2.1. The desired product is marked in its row by a right triangle symbol (▹).

Multi-functional Unit	Desired Product	Chemical	Mass [kg]	Cost [EUR · kg^{-1}]	μ [-]
Electrolyzer	▹	H_2	1	1.5	0.824
		O_2	8	0.04	0.176
Co-electrolyzer	▹	H_2	0.0092	1.5	0.0218
		O_2	0.49084	0.04	0.031
	▹	CO	1	0.04	0.9472
Separator	▹	CH_3OH	0.45	1.5	0.710
		CH_4	1.2526	0.147	0.290

kg^{-1} [59] to 3 EUR · kg^{-1} [60, 61] refer to the H_2 and O_2 market prices respectively. According to this formulation, the allocation parameter of oxygen μ_{O_2} amounts to 0.18, which implies that the contribution of O_2 should not be overlooked from an economic perspective. Such a high cost can be supported due to the need for medical oxygen in hospitals. Maggio et al. [60] claimed that hospitals could find it appealing to purchase oxygen at a cost of 3.3 EUR · kg^{-1} . Several other studies estimated oxygen could cost around 0.1 EUR · kg^{-1} around based on techno-economic analyses. The conservative option is chosen herein, at $c_{O_2} = 0.04$ USD · kg^{-1} . Treyer et al. [48] avoided any allocation or system expansion of the unit process and modeled O_2 as a waste flow to the air. Van Der Giesen et al. [62], however, argue that O_2's economic value should not be overlooked, since it could reduce the overall cost of H_2 if this byproduct is sold. More recently, Zhou et al. [41] included the cost of oxygen in their economic assessment. Thus, allocation due to oxygen was utilized.

The same approach and reasoning were used for the co-electrolyzer. The co-electrolzyer produces 3 products, and 2 of these products are desired products. H_2 is not the target product of the co-electrolysis unit, but it is nevertheless chosen as a desired product since this H_2 is used with CO (the target product of co-electrolysis). In this case, the process would need slightly less H_2 produced via water electrolysis, since a portion of the required H_2 is supplied via co-electrolysis. As a result, the contributions of H_2 produced by co-electrolysis are included since the produced H_2 byproduct is used with CO in the syngas reactor.

Finally, the separator in the *BIOHY* process separates the unreacted gas constituents (CO_2, H_2, and CH_4) of the inlet stream from the liquid constituents (CH_3OH and H_2O). The BIOHY process dictates that the gas outlet is further processed, where the remaining CO_2 and H_2 are transformed into CH_4. The additional H_2 needed for the higher stoichiometry for the CO_2 methanation is accounted for in the process. This processing, however, is not included within the boundary of the life cycle assessment (Section 2.1.1.). Thus, economic allocation is conducted, but only accounting for the existing CH_4 in the gas outlet stream exiting the separator, and not the total CH_4 that would have been produced following CO_2 methanation. This allocation is hence conservative to avoid exaggerated attributions to the methane co-production part of the overall process.

2.2. Energy and Mass Balances of Unit Processes

The energy and mass flows connecting the unit processes are essential in the formation of the technosphere matrix, $\underline{\underline{T}}$, which would in turn affect the total process emissions. The scale of a unit process, s_i is defined as the magnitude of increase required by a unit process to satisfy the need of the other unit processes, subject to a functional unit, $\underline{f}$. Thus, the scale vector is determined by:

$$\underline{s} = \underline{\underline{T}}^{-1} \cdot \underline{f} \tag{2.2}$$

The scale vector expressed in Equation 2.2 determines the relative scale of each unit process based on the need of the the considered unit process in the overall process. This scale factor applies to the mass and energy of the unit processes, and determines how much of the energy and mass inputs of a unit process is required to achieve a desired functional unit of the overall process. By accounting for the process scales, the intervention vector, $\underline{g}$, quantifies the total emissions generated by each process based on their scale using:

$$\underline{g} = \underline{\underline{B}} \cdot \underline{s} \tag{2.3}$$

In Equation 2.3, $\underline{\underline{B}}$ is the environmental intervention matrix that quantifies emissions associated with each unit process, which are generated based on their defined inventory. As a result, the emission flows are combined to form $\underline{g}$, and it is utilized to quantify the life cycle impact assessment metrics.

Thus, it is essential to accurately model the unit process material and energy flows. Only technosphere flows are shown in the processes. The unit processes are modeled so as to ensure one unique output flow per unit process.

The environmental emissions of units' equipment scale linearly with the increase in capacity since the capacity scales directly with the mass in a linear fashion, or indirectly via volume or flowrate, which in turn linearly affects mass based on its corresponding sizing equation.

To quantify the total emissions, it is essential to accurately determine the energy and mass balances of the processes, which will in turn determine the scale and then the emissions.

2.2.1. Electricity Mix

The electricity mixes modeled herein is the low voltage grid electricity produced in Switzerland. The Swiss electricity mix is amongst the mixes with the lowest emissions, due to its formation of several renewable energy technologies [63]. The constituents of the Swiss grid electricity mix is portrayed in Figure 2.2.

As shown in Figure 2.2, 98% of the electricity mix relies on renewable energy technologies or technologies with low emissions (nuclear). Hence, the resulting carbon intensity of the Swiss electricity (low voltage) is 0.045 $kg_{CO_2} \cdot kWh^{-1}$.

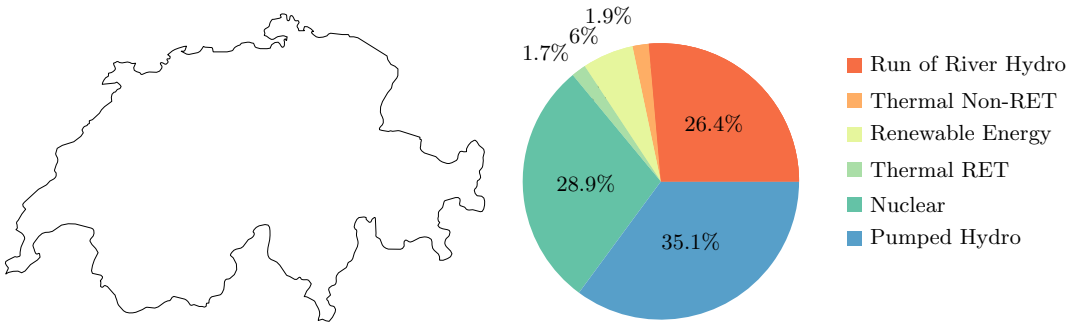

Figure 2.2. The distribution of energy sources that form the Swiss electricity mix based on renewable energy technologies (RET) and non-renewable energy technologies [63].

The mass and energy flows across the unit process of the Swiss electricity mix can be visualized in Figure 2.3.

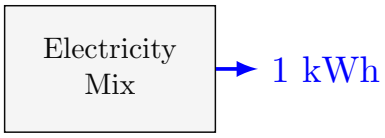

Figure 2.3. The unit process for the electricity mix of the Swiss grid, which displays the model energy and mass flows across the unit.

The life cycle inventory associated with the production of the functional unit of the unit process, which is 1 kWh, is derived from ecoinvent [51] using the "market for electricity production, low voltage". Using the grid electricity avoids the added complexities of dealing with the intermittency exhibited by pure solar or wind electricity mixes and storage issues. An electricity mix formed of privately built RET could, however, decrease electricity costs and potentially emissions, which is an option that should be explored to assess alternative scenarios.

2.2.2. Industrial Furnace

Heat is typically transferred in chemical plants via steam. The modeling of the energy and mass flows associated with heating via steam as the circulating fluid in a heat exchanger would thus be straightforward, with 1 kg of steam capable of releasing 2.257 MJ as latent heat [64]. However, the range of temperatures required in chemical plants could exceed that of the highest steam supply (high pressure steam: 250°C and 40 bar, critical temperature 400°C [65]). While it is possible to generate steam directly via solar parabolic-trough collectors and reach 400°C, the technology is not commercial [66, 67]. For this reason, diphenyl ether is instead used as circulating fluid, due its high temperature range (critical temperature = 493°C [68]).

The life cycle inventory for a fired heater using natural gas mainly requires a heat production system and the circulating fluid, which is diphenyl ether. The heat production system (ecoinvent activity: “heat production, natural gas, at industrial furnace low-NOx >100kW”) accounts for the usage of natural gas and for the industrial furnace unit itself to generate 1 MJ in heat. This

activity forms part of the life cycle inventory of the fired heater, and this is scaled by unity to obtain 1 MJ of heat, which is the functional unit of this unit process.

In addition to the heat production system, the working fluid is accounted for via a mass of diphenyl ether that can transfer 1 MJ. This value of this mass would be the reciprocal of the total heat (in MJ) that 1 kg of diphenyl ether can transfer during its lifetime. Because the production of diphenyl ether is highly polluting (8 $kg_{CO_2} \cdot kg^{-1}_{\text{diphenyl ether}}$), a closed loop fired heater is necessary to maintain the working fluid [69]. However, there is a lack of data describing the working fluid in a closed loop heater. Because this gap, it is assumed that 1 kg is able to roughly handle the one entire heat needed for one year, after which it is replenished on a yearly basis. The total energy that can be transferred by 1 kg of diphenyl ether, $E_{hf,\ell}$, is thus:

$$E_{hf,\ell} = \ell_{hf} \cdot m_{JF,yr} \cdot q_H \tag{2.4}$$

In Equation 2.4, ℓ_{hf} represents the heating fluid lifetime (assumed to be 1 year), $m_{JF,yr}$ is the total jet fuel output per year (assumed to be 10 Mega tons per year), and q_H is the specific heat needed to produce 1 kg of synthetic fuel (assumed to be 11 MJ based on Section 2.4.2.; prior to heat integration). Due to the very limited data quantifying this closed loop heater using diphenyl ether, many assumptions were made and the uncertainty regarding this variable is rather high. The final LCI of the industrial furnace is shown in Table A.5 of the Appendix.

Furthermore, Figure 2.4 highlights the energy and mass balances that are modeled as part of the furnace that can be exchanged with the remaining unit processes.

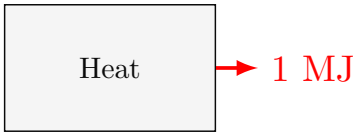

Figure 2.4. The unit process for the industrial furnace, which displays the model's energy and mass flows across the unit.

2.2.3. Heat Pump

The high temperature heat pump (HTHP) is a key unit primarily in the supply of heat to the direct air capture unit, which requires heat to be supplied at roughly 100°C [70, 71]. While this heat demand could be supplied via the industrial furnace, the relatively high emissions of its heat supplied to a comparatively lower temperature target could warrants finding a heat source with lower emissions that can still reach 100°C. Such heat pumps can provide heat using a heat sink at a temperature above 100°C [72], rendering them suitable for delivering heat to DAC units. Furthermore, they are capable of installation and operation at heating capacities in the range of megawatts, which enables their utilization in high capacity and large scale chemical plants [73]. The HTHP heat can also satisfy the heating demand for the absorption chiller, which renders the HTHP a fundamental energy source that can support the decarbonization of chemical processes when the temperature range is suitable [74].

The LCI of the heat pump consists of a brine-water heat pump. The working fluid in the heat pump cycle is thus a brine-water mixture, which is not accounted for in the inventory since this mixture in a closed loop cycle would have negligible emission contributions. Instead, only the heat pump unit is accounted for. The energy output of a single HTHP unit over its lifetime is expressed as:

$$E_{HP,\ell} = \ell_{HP} \cdot P_{HP} \tag{2.5}$$

In Equation 2.5, $E_{HTHP,\ell}$ denotes the lifetime energy output of the HTHP unit, P_{HP} is the power rating of the HTHP (10kW using the ecoinvent entry), ℓ_{HP} is the heat pump lifetime in hours (assumed to be 20 years). The number of units required to produce 1 MJ of HTHP heating is similarly the reciprocal of the $E_{HP,\ell}$.

The energy and mass balance of the HTHP depends on the value for the coefficient of performance, COP. Based on the work of Deutz & Bardow [71], the COP was estimated to be 2.51. Terlouw et al. [70], however, chose a COP value of 2.9 as a conservative assumption. Both values appropriately lie within the range COPs high temperature heat pumps can be implemented in large capacities, as demonstrated by Arpagaus et al. [73]. Thus, the energy and mass flows of the HTHP are visualized in Figure 2.5.

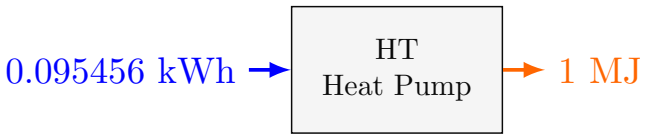

Figure 2.5. The unit process for the high temperature heat pump (HTHP), which displays the model's energy and mass flows across the unit.

In this study, the COP is chosen to be 2.9, which is in line with the work of Terlouw et al. [70] and is on the more conservative side of the range presented by Arpagaus et al. [73].

2.2.4. Absorption Chiller

The absorption chiller is utilized to deliver a cooling load via a circulating fluid. In typical applications, water is used in the form of lake water or from absorption chillers. Due to the need for cooling at subzero temperatures due to cryogenic distillation, ammonia is instead utilized as the cooling fluid. At atmospheric conditions, NH_3 evaporates at -33°C, which is suitable for the conditions herein.

The LCI of the chiller is modeled per MJ of cooling load delivered using a scaled absorption chiller unit, 0.02 kWh of electricity, and a mass of the circulating cooling fluid. Similar to the industrial furnace, the LCI of the circulating fluid is determined by accounting for the total energy that 1 kg of fluid can provide, and then using its inverse. which is modeled using:

$$E_{cf,\ell} = \frac{\ell_{cf}}{ch_{\mathrm{NH_3}}} \tag{2.6}$$

In Equation 2.6, ℓ_{cf} is the lifetime of the ammonia and ch_{NH_3} refers to the refrigerant charge of the ammonia chiller. The charge of the chiller determines the mass of ammonia as a function of the power rating of a closed loop absorption chiller. Unlike the case of the fired heater, a closed loop evaluation of the charge is available, with a common value of 0.6 kg·kW^{-1} [75]. The lifetime ℓ_{cf} is established in years, assuming the plant operates continuously (8760 hours). The circulating fluid herein is conservatively modeled due to uncertainties regarding its leakage and replenishment. Thus, it is modeled using a yearly replenishment rate, which implies that $\ell_{cf} = 1$ year (8760 hours). Consequently, the LCI of the absorption chiller unit is evaluated based on:

$$E_{chiller,\ell} = \ell_{chiller} \cdot P_{chiller} \tag{2.7}$$

Equation 2.7 quantifies the amount of energy assumed to be produced by a single unit of absorption chiller, $E_{chiller,\ell}$, with a rating of $P_{chiller}$, over its lifetime, $\ell_{chiller}$. The reciprocal of $E_{chiller,\ell}$ is used as the LCI of the unit.

To extract 1 MJ of cooling from the ammonia, the absorption chiller must be supplied with energy. Ammonia chiller systems are usually characterized by a COP of 0.5-0.6 [74–76]. The utilized COP is conservatively selected to be 0.5, which implies that the heat input needed is twice the cooling output. This energy can be supplied by a 85-100°C heat source [74]. This temperature range for heat flow would output chilled water at 6°C, which is higher than the subzero target temperature of ammonia. Thus, a higher temperature range might be required in practice, but it will be assumed as sufficient herein. As a result, rather than use the natural gas powered furnace, the HTHP can supply the required heat at lower GHG emissions. In the ecoinvent database, the absorption chiller dataset utilizes this input heat from a combined heat and power plant, and thus the proposed configuration reduced overall GHG emissions [74]. Therefore, the energy and mass flows of the absorption chiller is shown Figure 2.6.

Figure 2.6. The unit process for the absorption chiller unit, which displays the model's energy and mass flows across the unit.

2.2.5. Electrolyzer

A water electrolyzer unit (Ely) splits H_2O electrochemically to H_2 and O_2. H_2 is an essential intermediate chemical in the production of synthetic fuels, which renders the electrolysis unit modeling quite significant [77]. The power requirement to produce 1 kg of H_2 using a proton exchange membrane (PEM) water electrolyzer is today rated at 47.7 kWh [78]. The production of O_2, however, is a byproduct in water electrolysis. The anode outlet is assumed to be fully O_2, requiring no flash separation with unreacted H_2O if any exists. This allocation is more clearly visualized in Figure 2.7.

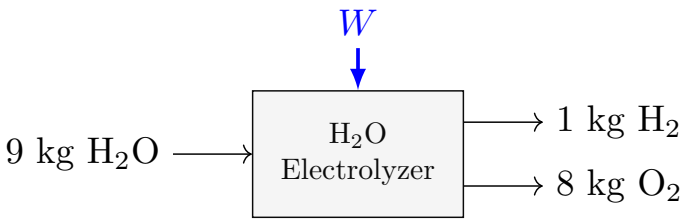

Figure 2.7. The unit process for a water electrolysis unit, which displays the model's energy and mass flows across the unit. The unit process requires electricity to split water into its constituents: O_2 and H_2.

The LCI of this unit predominantly consists of the emissions generated in manufacturing the electrolyzer unit, in addition to the complementary components required to maintain its operation (balance of plant). These emissions are modeled by combining the LCI of the materials needed for the electrolyzer, which are modeled in [find author name] [79]: The exact required masses of the aforementioned materials can be found in Table A.8. The LCI of all these materials can be found in the utilized ecoinvent database, with the exception of Iridium. Iridium is a Platinum Group Metal (PGM), which denotes that it is typically mined as a byproduct of Platinum mining. Thus, the emissions associated with Iridium mining are modeled as a fraction of those generated by Platinum mining, based on a mass allocation. The study of Nuss & Eckelman [80] identifies multiple proportions of Iridium and Platinum yields based on various mining locations. In this study, a proportion of 1.8-51.1 of Ir-Pt yield is utilized, and this mass proportion is used to estimate the emissions associated with Iridium [81].

The materials required to build a 1 MW rated Ely unit are thus presented in Table of the A.8. To calculate the life cycle emissions of the materials and the total of the unit, the amount of CO that is formed over the unit's lifetime, $m_{CO,\ell}$, is calculated using:

$$m_{H_2,\ell} = \frac{\ell_{ely} \cdot P_{ely}}{w_{ely}} \tag{2.8}$$

In Equation 2.8, ℓ_{ely} is the lifetime of the Ely unit, P_{ely} is the power rating used (1 MW) as a reference for the inventory materials, and w_{ely} is the specific energy needed to produce 1 kg of H_2, which is 47.7 kWh · kg^{-1} [78]. The result of this equation yields the total amount of H_2 produced based at a capacity of 1 MW over its lifetime. The electrolyzer lifetime is quite extensive, spanning up to 80000 h [82]. This relatively high lifetime enables a higher mass of H_2 produced over the lifetime per Ely unit. Inversely, the amount of units required to produce 1 kg of H_2 using a 1 MW rated Ely unit is the reciprocal of Equation 2.8. The materials in Table A.8 are scaled by this resulting value, since the original masses in [79] correspond to the amount required for a 1 MW Ely unit. Therefore, a high lifetime is particularly beneficial in decreasing the amount of noble metals required over its lifetime since the frequency of catalyst replenishing would be less.

2.2.6. Co-Electrolyzer

The co-electrolyzer (CoEly) is utilized to reduce CO_2 to CO and bypasses the production of water during methanol synthesis. The electrochemical reduction occurs by transforming H_2O and CO_2 into H_2, CO, and O_2, according to the half reactions in Table 2.2.

Cathode Reactions

$$XCO_2 + 2\,\eta_{F,CO}\,H^+ + 2\,\eta_{F,CO}\,e^- \longrightarrow \eta_{F,CO}\,CO + \eta_{F,CO}\,H_2O + [\,(X-1) + (1\text{-}\eta_{F,CO})\,]\,CO_2 \quad \text{(R.1)}$$

$$2\,(1\text{-}\eta_{F,CO})\,H^+ + 2\,(1\text{-}\eta_{F,CO})\,e^- \longrightarrow (1\text{-}\eta_{F,CO})\,H_2 \quad \text{(R.2)}$$

Anode Reactions

$$X_{H_2O}\,H_2O \longrightarrow (X_{H_2O} - 1)\,H_2O + \tfrac{1}{2}\,O_2 + 2\,H^+ + 2\,e^- \quad \text{(R.3)}$$

Table 2.2. The half-reactions of the co-electrolyzer unit. The reaction yields depend on the Faradaic efficiency, $\eta_{F,CO}$, and the excess factors, X, for CO_2 and water (w).

In Equations R.1, R.2, and R.3, $\eta_{F,CO}$ represents the Faradaic efficiency and X represents the excess factor for CO_2 entering the cathode of the CoEly unit. The goal of this unit is to output CO to be utilized as the carbon source to produce methanol. However, minor traces of H_2 are produced as a byproduct [46], as shown in Equation R.2 at the cathode. In addition, similar to the case of the water electrolyzer, O_2 is produced at the anode side (Equation R.3). The overall unit process flows are therefore highlighted in Figure 2.8.

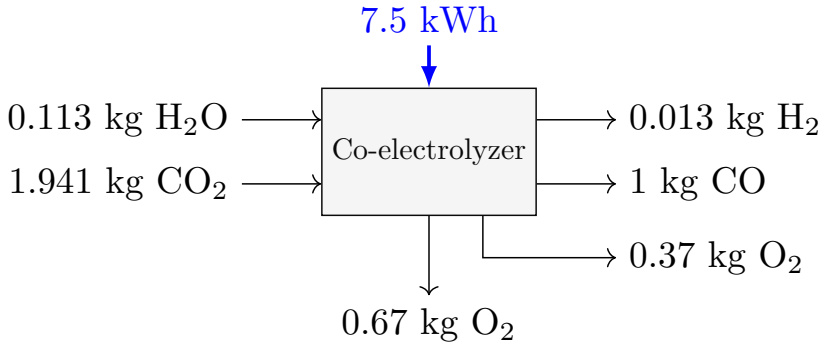

Figure 2.8. The unit process for a co-electrolysis unit, which displays the model's energy and mass flows across the unit. The unit process requires electricity, CO_2, and H_2O as inputs, while the outlet products are CO and O_2, with minor amounts of H_2. The half reactions are combined to facilitate the expression of the net mass balance of the system.

The unreacted CO_2 and produced CO and H_2 exit the CoEly unit from the cathode (Equations R.1 and R.2), while O_2 exits with the excess H_2O from the anode. The spatial separation of the products across the electrodes helps in avoiding separation of O_2 from the other gases, all of which are useful for the syngas reactor. This indicates that there is no need for further separation of the gases, which would prove to be rather difficult.

The inventory utilized for the CoEly unit is similar to that of the Ely unit, and it is tabulated in Table A.9 based on the results of the author of [79]. The variations between the Ely and CoEly unit are predominantly that on the cathode, where silver nanoparticles are used instead of Pt, which would present a significant reduction in GHG emissions due to Pt mining. Another difference is in the membrane material. The bipolar membrane is modeled as being half Nafion and polysulfone, which is commonly used for alkaline membranes [83, 84]. The materials are thus presented in Table A.9 for 1 MW. To calculate the life cycle emissions of the materials and the total of the unit, the amount of CO that is formed over the unit's lifetime, $m_{CO,\ell}$, is calculated

using:

$$m_{\mathrm{CO},\ell} = \frac{\ell_{coely} \cdot P_{coely}}{w_{coely}} \tag{2.9}$$

In Equation 2.9, ℓ_{coely} is the lifetime of the CoEly unit, P_{coely} is the power rating used (1 MW) as a reference for the inventory materials, and w_{coely} is the specific energy needed to produce 1 kg of CO, which is 7.5 kWh · kg^{-1} (derived in Section VII). The result of this equation yields the total amount of CO produced based at a capacity of 1 MW over its lifetime. However, a great deal of uncertainty exist with the lifetime of this unit, and it is in fact unstable. Nevertheless, studies have shown that CoEly units can be developed to last up to 3000 hours before deactivating, which explains the usage of this value as the lifetime [85–87].

Similar to the previous LCI expressions, the reciprocal of Equation 2.9 would serve as the fraction of a 1 MW unit required to generate 1 kg of CO. Applying the value of the reciprocal as a further scale to the amount of materials needed would yield the mass of materials needed for the production of 1 kg of CO, thus forming the inventory of the co-electrolysis unit.

2.2.7. Direct Air Capture

The direct air capture unit (DAC) can provide a carbon source for processes. This unit is particularly important for the processes using CO_2 as a feedstock. Furthermore, the utilized LCI for the DAC unit is based on solid sorbent technology and accounts for the amine sorbent life cycle emissions, which was provided by Terlouw et al. [70].

To extract 1 kg of CO_2 from air, significant quantities of electric energy and heat are required. These mass and energy flows are visualized in Figure 2.9.

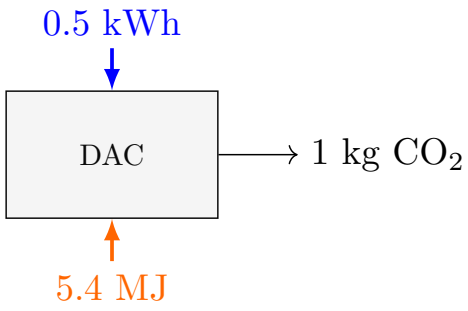

Figure 2.9. The unit process for a direct air capture unit, which displays the model's energy and mass flows across the unit. The unit process requires heat and electricity as inputs, while the outlet is captured CO_2. The air returned to the atmosphere is not considered in the mass balance.

There is some variation in literature studies regarding the exact magnitude of the heat and electricity (Figure 2.9) required by the DAC unit. A sample of energy requirements from different studies [70, 71, 88, 89] are reported in Table 2.3.
The heat values highlighted in Table 2.3 show slight disagreement in the ranges. The required heat presented by Fasihi et al. [88] and Sutter et al. [89] are similar to those of Terlouw et al. [70] and Deutz & Bardow [71]; however, the data for electric energy that they utilized are rather optimistic. The energy flows implemented herein are those based on the work of Terlouw et al. [70], which assessed an expected near-future upscaled DAC unit with reduced energy

Table 2.3. The reported heat (q) and electrical work (w) requirements necessary to capture 1 kg of CO_2 based on various studies [70, 71, 88, 89]. This data is representative of the solid sorbent-based DAC unit (without compression).

q [MJ · $kg_{CO_2}^{-1}$]	w [kWh · $kg_{CO_2}^{-1}$]	Reference
5.4	0.5	Terlouw et al. [70]
5.4-7.2	0.2-0.3	Fasihi et al. [88]
4.7	0.7	Deutz & Bardow [71]
6.3	0.25	Sutter et al. [89]

requirements. However, the DAC unit inventory already accounts for the energy flows. For this reason, these energy flows are removed from the DAC inventory and instead implemented in the model as energy inputs, to prevent double counting of energy flows (both electricity and heat). This decoupling also allows the assessment of environmental burdens due to DAC energy requirements in any country, not just those modeled in the inventory.

The DAC unit consists of high energy inputs, which motivates the research in the direction of lowering heat requirements to decrease the environmental footprint associated with heating [90]. The energy required, however, represents data for the near-future. Consequently, a low-emissions mode of heating at 100°C should be used to minimize the overall envrionmental burdens [24]. The studies in the literature show that waste heat could be used for DAC purposes, thus reducing alternative heat inputs to a minimum [70]. The assumption that heat input is supplied via waste heat is not a very reasonable assumption to produce on-demand synthetic jet fuel due to availability limitations. Using waste heat could contribute to the lowest GHG compared to other heating methods [70], but it could pose as a barrier against the scale up of synthetic jet fuel production using CO_2 supplied by DAC. Moreover, the environmental life cycle assessment presented by Terlouw et al. [70] shows that, for low carbon electricity, heat pumps can be competitive with other heat sources, thus validating heat pumps as the choice of heating.

2.2.8. Compressor

The compressor is required to compress H_2 to reduce storage volume of the storage tank. While some studies have approximated the LCI of a gas compressor using that of an air compressor on Ecoinvent [91], the LCI data for a compressor is derived from the work of Peng et al. [92]. Their LCA study quantifies the material masses required to build a centrifugal compressor whose power rating was 18404 kW. While a lot of metal waste is generated, it will also be assumed that complete recycling is done and the waste metal can be retained.

Herein, the emissions that the modeled compressor contributes will be scaled according to the given power rating of Peng et al. [92]. In addition, their study provided the energy needed to convert the materials required into the key components (spindle, impeller, plates, nuts, etc.). This energy data on energy thus enables a more accurate representation of the environmental footprint required to manufacture such units.

The lifetime of one compressor unit is similarly based on the mass of compressed flows over its lifetime:

$$m_{cmp,\ell} = \frac{\ell_{cmp} \cdot P_{cmp}}{w_{cmp}} \tag{2.10}$$

In Equation 2.10, $m_{cmp,\ell}$ refers to the total mass compressed to a desired pressure using a power rating of 18404 kW over its lifetime, while ℓ_{cmp} refers to the compressor lifetime (assumed to be the same as the plant lifetime), P_{cmp} is the compressor power rating used for the inventory (18404 kW), and w_{cmp} is the compressor specific work. The reciprocal of the lifetime compressed mass determines the amount of compressor units needed to compress 1 kg of a given gas, which would then be used a scale factor for the inventory of materials (Table A.10 in the Appendix) to determine the amount of materials needed for 1 kg of compressed fluid.

Moreover, the compressor unit process and its energy/mass flows are portrayed in Figure 2.10.

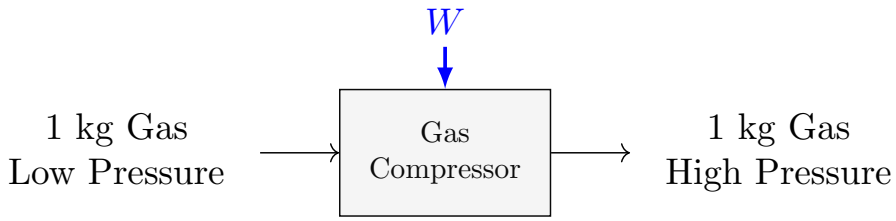

Figure 2.10. The unit process for a compressor unit, which displays the model's energy and mass flows across the unit. The unit process requires electricity to increase the pressure of a given gas. The magnitude of the energy needed depends on the gas being compressed and the final pressure.

The value of the compressor specific work, which is the energy required to compress 1 kg of a flow depends on the final pressure and the fluid properties. This dependence is encapsulated in the following equation [93]:

$$\dot{W}_{cmp} = \frac{\dot{m}_{H_2} \cdot w_{is,cmp}}{\eta_{is,cmp} \cdot \eta_m \cdot \eta_e} \tag{2.11}$$

where $w_{is,cmp}$ is the specific work of the unit, $\eta_{is,cmp}$ is the isentropic efficiency (80%), η_m is the mechanical efficiency (98%), and η_e is the electric generator efficiency (96%). The isentropic specific work of the compressor unit, $w_{is,cmp}$, is determined using [93]:

$$w_{is,cmp} = \frac{k}{k-1} \cdot R \cdot T_i \left[\frac{p_i}{p_o}^{\frac{k-1}{k}} - 1 \right] \tag{2.12}$$

In Equation 2.12, k is the ratio of specific heats of the gas [94], R is the gas constant, T_i is the inlet temperature, and p_i and p_o are the inlet and outlet pressures respectively. The specific work for the modeled compressors are tabulated in Table 2.4.

Table 2.4. The estimated specific work required to compress fluids from an inlet pressure, p_i to a higher outlet pressure, p_o. The specific work values are estimated using efficiencies of Minutillo et al. [93] based on Equation Equations 2.11 and 2.12.

Process	Gas Mixture	T_i [°C]	p_i [MPa]	p_o [MPa]	w_{cmp} [kWh · kg_{inlet}^{-1}]
CO2ER	H_2	27	0.1	5	2.4729
CO2ER	CO	27	0.1	3	0.08556
CO2HY	CO_2	27	0.1	5	0.18831
CO2HY, BIOHY	H_2	27	0.1	3	1.9739
BIOHY	Biogas	27	0.1	3	0.1671

2.2.9. Heat Exchanger

The heat exchanger units encompass coolers and heaters. It is modeled as a tube and shell heat exchanger, in which the heating/cooling fluid is diphenyl ether/ammonia. The flows across the unit process are visualized in Figure 2.11.

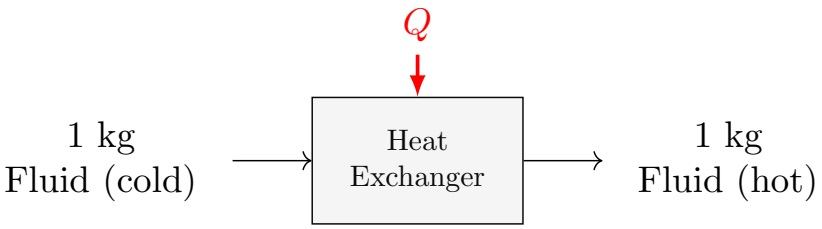

Figure 2.11. The unit process for a heat exchanger unit, which displays the model's energy and mass flows across the unit. The unit process requires heat/cooling, supplied by a circulating hot/cold fluid, to increase/decrease the temperature of a fluid. The amount of heating or cooling load required depends on the final temperature and the properties of the fluid.

Determining the amount of heat depends on many factors such as the heat exchanger topography, the exchanging fluids, and flowrates. An initial iteration was conducted using an elaborate methodology [95] to determine the overall heat transfer coefficient, U, such that the heat exchanger area, A is estimated. The heat exchanger area helps in calculating the length of the heat exchanger and thus the total mass of a heat exchanger (using standardized tube and shell diameters [95]). The analysis begins with determining the heat needed, which is done using Aspen HYSYS, but is based on Q, which is the heat energy required to reach the final temperature for 1 kg of the inlet. Based on the amount of mass to be heated in one year, which is determined from the process functional unit and the scale factors, the energy quantity Q is transformed into the heat rate, $\dot{Q}$. The area of the heat exchanger, A_{hx}, is a fundamental parameter in the determination of the heat exchanger inventory, which is expressed as:

$$A_{hx} = \frac{\dot{Q}}{U \cdot LMTD} \tag{2.13}$$

In Equation 2.13, LMTD refers to the logarithmic mean temperature difference, determined by:

$$LMTD = \frac{\Delta T_i - \Delta T_o}{\ln\left(\frac{\Delta T_i}{\Delta T_o}\right)} \tag{2.14}$$

In Equation 2.14, ΔT_i and ΔT_o denote the temperature difference at the inlet and outlet respectively. Thus, the difference is across the different streams.

The heat transfer coefficient, U, is assumed constant for the different heat exchangers based on the fluids in the shell, tube, and whether phase change is included. Table 2.5 summarizes the values based on data enlisted by Ulrich [96]. While Luyben [97] provides a general value of 568 W m^{-2} K^{-1} used for hydrocarbons, we use the values of Ulrich in an attempt to be more specific when possible regarding the flows exchanging heat.
Furthermore, the environmental emissions of the heat exchanger equipment is scarce in the literature. While there are some data that accounts for HX emissions via its stainless steel materials [79, 98], some of it is either outdated or targeting specific applications, which questions

Table 2.5. The overall heat transfer coefficients (U) and the logarithmic mean temperature difference ($LMTD$) for the modeled heat exchangers. The fluids in the tube/shell are approximated by the available dataset presented by Ulrich [96], with the lower bound typically selected. The heat exchangers are sized conservatively by using the exchange with oil, such as diphenyl ether, since it has a lower U value, despite the fact that some streams exchange heat within one another via heat integration. s/l refers to the type of heat transfer: sensible or latent; h/c refers to the heating or cooling that is supplied by the chemical plant.

			Stream Fluids			
Stream Name	h/c	s/l	Shell	Tube	U [W m^{-2} K^{-1}]	$LMTD$ [°C]
Syngas pre reaction	heating	sensible	Air, nitrogen, (compressed)	water/brine	230	206
CO_2-H_2 pre reaction	heating	sensible	Air, nitrogen, (compressed)	water/brine	230	206
Syngas Reactor Outlet	cooling	both	Hydrocarbon vapors (partial condensers)	oil	140	159
CO_2-H_2 Reactor Outlet	cooling	both	Hydrocarbon vapors (partial condensers)	oil	140	159
MeOH pre reaction	heating	both	Alcohol vapor	water	570	1.63
Liquid Fuel Range Olefins after reaction	cooling	both	Kerosene	Oil	110	237
Liquid Fuel pre Distillation	cooling	both	Kerosene	Oil	110	142
Olefin pre reaction	heating	both	Hydrocarbon vapors (partial condensers)	Oil	140	246
MTO Reactor Outlet	cooling	both	Hydrocarbon vapors (partial condensers)	Oil	140	133
H_2-Biogas	heating	sensible	Hydrogen-containing natural gas mixtures	Water	450	150
Biogas/MeOH Reactor Outlet	heating	both	Hydrogen-containing natural gas mixtures	Water	450	150

the data's validity. Nevertheless, a conservative approach is used, coupled with thorough design principles [95, 99]. A shell-and-tube heat exchanger is considered with tube OD of 1 inch and shell ID of 25 inches, with 2 passes, thus leading to a number of tubes, N_{tubes}, of 252 [99]. The mass of the heat exchanger is thus:

$$m_{hx} = m_{hx,tubes} + m_{hx,shell} \tag{2.15}$$

In Equation 2.15, $m_{hx,tubes}$ and $m_{hx,shell}$ refer to the mass of the tubes and shell respectively. The equations for these quantities are respectively expressed in Equations 2.16 and 2.17 [95]:

$$m_{hx,tubes} = N_{tubes} \cdot \rho_{tube} \cdot \delta_{tube} \cdot L \cdot D_{tube} \tag{2.16}$$

$$m_{hx,shell} = \rho_{shell} \cdot \delta_{shell} \cdot L \cdot D_{shell} \tag{2.17}$$

In Equations 2.16 and 2.17, ρ_{tubes} and ρ_{shell} are the tube and shell material density, δ_{tubes} and δ_{shell} is the tube and shell thickness, D_{tubes} and D_{shell} is the tube and shell diameters, and L denotes the heat exchanger length, estimated using [95]:

$$L = \frac{A_{hx}}{N_{tubes} \cdot a'} \tag{2.18}$$

In Equation 2.18, a' is the surface area per unit length. The specific values of these quantities are listed in Section VIII.

The mass estimated using Equation 2.15 estimates the mass of the heat exchanger equipment, whose lifetime could be many years. In this case, it is assumed herein to equal the plant lifetime. Thus, the heat exchanger mass is normalized by the total mass of a fluid it heats up its lifetime, where its LCI is determined by:

$$m_{hx,\ell} = \frac{m_{hx}}{\dot{m}_{hx} \cdot \ell_{hx}} \tag{2.19}$$

In Equation 2.19, $m_{hx,\ell}$ is the mass of heat exchanger required to generate 1 kg of product output, while ℓ_{hx} is the reactor lifetime in years. Similar to the reactor, the data supplied herein by Gerloff [79] only supplies data for the inventory of the equipment, without identifying mass quantities and relating to a capacity of the heat exchanger/reactor. For this reason, the mass required per unit kg heated is determined via this normalization conducted in Equation 2.19.

Some heat integration is conducted so that the heat load is minimized. This reduces the quantities of heat needed, but does not affect the sizing of the reactor. The methodology by which heat exchanger was conducted is outlined in Table A.11.

2.2.10. Reactor

Thermocatalytic reactors are essential stages in the processing and conversion of the starting feedstock to jet fuel. While the focus of this study does not extend to optimization of reaction networks, it nonetheless examines and screens several reactions and determines the reaction sequence that maximizes jet fuel yield.

The LCI of a reactor is modeled by the mass of steel that forms the reactor and the catalysts within the reactor. The mass of the reactor is correlated with the reactor volume and uses chromium steel [79] as a function of the required mass. The reactor mass depends on the desired rate of production of the products in the reaction outlet, denoted by $\dot{m}^R$. High yields are ensured by implementing recycling stream is established to achieve an overall complete conversion. In this case, the unconverted reactants are fed again to reactor. The total mass entering the reactant is thus [100]:

$$\dot{m}_{rx,rec} = \frac{\dot{m}_{rx}}{\chi + \epsilon - \chi\epsilon} \tag{2.20}$$

In Equation 2.20, $\dot{m}_{rx,rec}$ refers to the mass flowrate following entering the reactor the recycling, $\dot{m}$ to the mass flowrate pre-recycling loop, χ is the single-pass reaction conversion, and ϵ is the purge fraction. The purge fraction is considered to be 0.01, and it is implemented to ensure no reactor overload [100]. Naturally, in doing so the reactor volume increases, which would increase the reactor cost, but would ensure overall conversion of the reactants.

The modeling of the LCI begins by extracting the reaction data, which is covered by the reactor empty volume, $\forall_{rx}$, which is determined by:

$$\forall_{rx} = \frac{\dot{m}_{rx,rec}}{\beta \cdot \rho_{cat} \cdot WHSV} \tag{2.21}$$

In Equation 2.21, β is the porosity fraction (assumed to be 0.4 [100, 101]) and ρ_{cat} is the catalyst density (Table A.16), and $WHSV$ is the weighted hourly space velocity. The WHSV quantifies the mass flowrate that can be catalyzed by a unit mass of catalyst. Equation 2.21 is central to the LCI since it incorporates the reaction data with the desired output.

However, this reactor volume represents the total volume, and not the volume of the steel manufactured, as shown in:

$$\forall_{rx,steel} = \delta_{rx} \cdot \frac{\pi}{4}\left(D_{rx} \cdot L_{rx} + \frac{1}{2}D_{rx}^2\right) \tag{2.22}$$

In Equation 2.25, L_{rx} is the reactor length, D_{rx} is the reactor diameter, and δ_{rx} is the reactor thickness. This equation assumes the reactor to be cylindrical. The length is modeled to be 4 times the diameter ($L_{rx} = 4 \cdot D_{rx}$) [100, 101], which leads to:

$$D_{rx} = \sqrt[3]{\frac{\forall_{rx}}{\pi}} \tag{2.23}$$

The thickness, in turn, is determined according to whatever his name was [102], and is a function of pressure:

$$\delta_{rx} = \frac{p_d \cdot D_{rx}}{2 \cdot \sigma \cdot \eta_{weld} - 1.2 \cdot p_d} \tag{2.24}$$

Assuming a welding efficiency, $\eta_{weld} = 1$, $\sigma = 10800$ psi (designed conservatively for worst temperature), and $p_d = 1.1p$ (10% increase from operating pressure) [102]. Using the resulting volume from Equation 2.22, the steel mass needed to build the reactor, $m_{rx,steel}$, is expressed as:

$$m_{rx,steel} = \rho_{steel} \cdot \forall_{rx} \tag{2.25}$$

In Equation 2.25, ρ_{steel} is the density of chromium steel. The magnitude of $m_{rx,steel}$ represents the mass of the reactor needed to generate products from reactants entering the reactor at a rate of $\dot{m}_{rx,rec}$. However, the lifetime of the reactor extends to several years, and thus this mass is normalized by the total amount of products generated over its lifetime, where its LCI is determined by:

$$m_{rx,\ell} = \frac{m_{rx}}{\dot{m}_{rx,rec} \cdot \ell_{rx}} \tag{2.26}$$

In Equation 2.26, $m_{rx,\ell}$ is the mass of reactor needed to generate 1 kg of product output, while ℓ_{rx} is the reactor lifetime in years. Everything is linear since D is a function of 1/3 of reactor volume and since the others are expressed through D, we get Vsteel as a function of D to the 3 which is Vreac. This mass quantity represented by $m_{rx,\ell}$ is thus attributed to chromium steel, and 31% of this value is added as electricity needed in manufacturing [79]. These are tabulated in Table A.12.

The production of catalysts is considered as background contributions within the reactor contributions. A detailed breakdown of how the individual catalyst inventories were modeled is shown in Tables A.14 and A.16. The LCI of the catalyst is expressed as a function of the amount of products it can catalyze over its lifetime, $m_{product,\ell}$, as:

$$m_{product,\ell} = \ell_{cat} \cdot WHSV \tag{2.27}$$

In Equation 2.27, ℓ_{cat} is the lifetime of the catalyst. The reciprocal of $m_{product,\ell}$ models the amount of catalyst needed to produce 1 kg of product. Moreover, the quantification of a ℓ_{cat} is accompanied by high uncertainty, since most studies do not consider stability over thousands of operating hours. Some studies say minimum of 5 years, others have regeneration cycles following deactivation [103]. Thus, it is modeled herein to be replenished every year, and their environmental emissions is included by scaling their contribution by the amount of times the catalyst is replenished.

The life cycle emissions of the catalyst contribution are thus strictly due to the materials used, and does not take into account the energy required to manufacture such nanoparticles. The review of Salieri et al. [104] provides a thorough analysis of nanoparticle and catalyst LCA studies, but does not contain such studies for catalysts involved in the methanol to jet fuel pathway due to the field's infancy. In addition, the quality of data and the extent of information reported varies significantly between the studies. For instance, Griffiths et al. [105] assessed the environmental impacts of various catalysts, including their source material and manufacturing energy requirements, the data for the required manufacturing energy is not reported. In contrast, Caramazana-González et al. [106] provided a detailed life cycle assessment of delivering 1 kilogram of nano TiO_2, providing a complete inventory including energy inputs

required for nanoparticle stirring, heating, and cooling. However, these energy requirements varied drastically amongst the selected nanoparticles, which renders it difficult to derive a general correlation for energy input for nanoparticle synthesis. Thus, the synthesis energy for catalysis will be neglected due to lack of reliable and representative data for the utilized catalysts.

A sample of the energy and mass flows of a reactor unit process is shown in Figure 2.12.

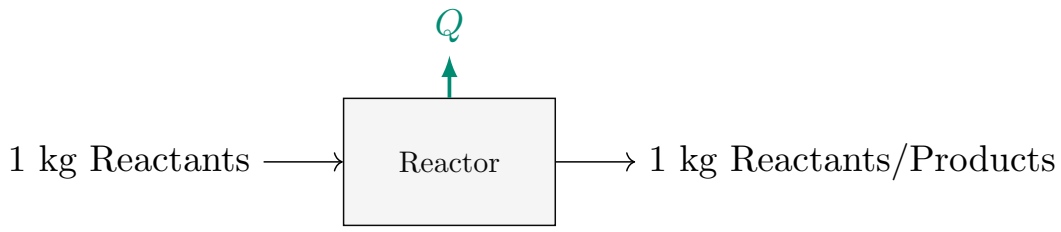

Figure 2.12. The unit process for a reactor, which displays the model's energy and mass flows across the unit. The inlet of the unit process comprises of the reactants, while the outlets are the products and heat (extracted as cooling). The boundary of the unit process includes the reactor and the recycling stream, such that the overall conversion is 100% when the single-pass conversion is less than 100%.

Each process consists of at least 4 reactions. The products and reactants of each reaction, which would slot in Figure 2.12, are summarized in Table 2.6.

Table 2.6. The various reactions considered for the 3 processes (*CO2ER*, *CO2HY*, *BIOHY*; ALL refers to the reaction/reactor present in the 3 processes). The table highlights the reaction equation, in addition to reaction yields such as selectivity (ς), conversion (χ), based on the reaction conditions such as temperature (T), pressure (p), weight hourly space velocity (WHSV), and the utilized catalyst. For the methanol to olefins step, C4, C5, and C6 olefins are produced, but C6 is represented in the olefin oligomerization reaction where jet fuel is represented as an average of C12 alkane. The selectivity value does not include byproduct of water and only models the hydrocarbon selectivity. The term FER refers to ferrierite zeolite.

			Yield		Conditions				
Process	**Reaction**	**Target Product**	**ς [%]**	**χ [%]**	**WHSV [h^{-1}]**	**T [°C]**	**p [MPa]**	**Catalyst**	**Reference**
CO2ER	$CO + 2\,H_2 \longrightarrow CH_3OH$	CH_3OH	96	37.57	10	230	5	CuZnAl	[107]
CO2HY	$CO_2 + 3\,H_2 \longrightarrow CH_3OH + H_2O$	CH_3OH	100	7.7	4.2	220	3	$PdZn/CeO_2$	[108]
BIOHY	$CO_2 + 3\,H_2 \longrightarrow CH_3OH + H_2O$	CH_3OH	100	28	N/A	250	3	CuZnAl	[109–111]
ALL	$CH_3OH \longrightarrow H_2O + \frac{1}{n} C_nH_{2n}$	C_4H_8,C_5H_{10},C_6H_{12}	86	100	1.2	400	0.1	CeO_2-FER	[112]
ALL	$2\,C_6H_{12} \longrightarrow C_{12}H_{24}$	$C_{12}H_{24}$ (~ JF range)	98	50	3	140	10	Al-SBA-15	[113]
ALL	$C_{12}H_{24} + H_2 \longrightarrow C_{12}H_{26}$	$C_{12}H_{26}$ (~ JF)	100	100	3	140	1.135	Pd/Al	[114]

The production of methanol from syngas is a well developed process. Dieterich et al. [115] provided a comprehensive overview of commercial syngas to methanol technologies. The reaction that was chosen was that which was developed by BASF [107]. This reaction was selected not only due to its high selectivity but also since its input matched the outlet of the CoEly unit, where there were still some unreacted CO_2 which can be used in the reaction.

Olefin production is a vital intermediate step in the production of jet fuel. For jet fuel production, the olefin precursor is usually alcohols, such as methanol [103, 116–122] or ethanol [123, 124], or syngas via Fischer-Tropsch [125]. Because methanol is more easily produced from

syngas, it is chosen herein as the olefin precursor. Tian et al. [103] demonstrated the scale-up of MTO from micro reactors to industrial ones. The catalyst suffers from periodic deactivation, which thus necessitates its regeneration every few hours [119, 126, 127]. However, the scaleup shown by Tian et al. [103] shows that regeneration cycles can be implemented to maintain product output over thousands of operating hours.

The process of converting methanol into olefins is based on the work of Park et al. [112]. In their study, the comprehensive data availability and high efficiency and showed a higher lifetime (>20 hours). In particular, this process maximizes C_4-C_6 olefins, which is the required precursor for the olefin oligomerisation reaction [113]. By nature of the stoichiometry, 1 kg of methanol produces 0.5625 kg of water, with the balance is the mass of hydrocarbons. This sets an upper limit of hydrocarbon production, which could encourage the investigation of other process such as Fischer-Tropsch [48].

The recovered C4-C6 olefins are thus oligomerized to jet fuel range alkenes. Several jet fuel production pathways have been developed and evaluated [128–131]. Mobil was the first company to demonstrate the commercial feasibility of such a process in 1988, by coupling methanol-to-olefin and olefin-to-gasoline distillate units, with both processes using a ZSM-5 catalyst [49, 132]. A more recent study by Saavedra Lopez et al. [123] depicted high yields of jet fuel-range olefins. However, their reactions consisted of mainly C2-C3 olefins. In this study, some units were constrained to incorporate the work of collaborators in the Synfuel Initiative. As a result, the modeled olefin oligomerization reaction was that which was developed by Dubray et al. [113]. Their reaction shows high selectivity (98%) towards jet fuel range alkenes (C10-C18 olefins), even at a conversion as high as 50%. While the results presented in their work are based on the conversion of C5-C6 olefins, C4 olefins are expected to yield the same range of C10-C18 due to the higher reactivity of C4 olefins compared to C5-6 [113]. This reaction produces 98% of jet fuel, with the remaining 2% corresponding to heavies. The final step lies in hydrogenating the jet fuel-range alkenes to alkanes. The jet fuel hydrogenation process typically utilizes Pt catalysts [21, 133–135]. The best one [133] utilizes (0.5%) Pt on Alumina, 10% excess H_2 at 11.35 bar and 150°C, and WHSV=3 h^{-1}. These conditions lead to almost a 100% hydrogenation conversion. Thus, following this reaction pathway, 0.37 kg of jet fuel are converted from 1 kg of methanol.

For the *CO2HY* process, the selected catalyst ensures 100% methanol selectivity, which eliminates the need for further separation of carbon sources [108]. The hydrogenation reaction of CO_2 in biogas (process *BIOHY*) is done in a cascade, where the reacting flow undergoes separation of MeOH/water via simple condensation, so that the remaining unreacted flows can react again. The first heat exchanger consists of 3 sets of reactors, heaters, coolers, and separators, as highlighted in Figure 2.1. Compared to the first cascade reactor, the 2nd reactor and 3rd reactor are smaller in size, since there is less reactants to react. The first cascade contains the entire flow, while the 2nd contains 28% less and the 3rd contain 47.3% less flow. The sizing is based on these reductions in flows, and is applied for the reactors, condensers, coolers, and heaters.

2.2.11. Distillation Column & Separator

The distillation column LCI is based on the work of Brondani et al. [136]. Their study focused on the environmental impact of the required materials. Thus, the height and diameter of the column largely influence the amount of materials utilized. In addition to the aforementioned

environmental footprint, the heating is included herein via the energy flows, which was not considered in their study since the reboilers and condensers necessary in the separation process were not accounted for.

In the study of Brondani et al. [136], the environmental assessment of a distillation column was limited to the manufacturing of the column and not its operations and potential inefficiencies. This evaluation was conducted using a functional unit of a range of ethanol output (15-30 L/h). Such a functional unit is in fact not comprehensive, as it does not allow generalization or scaling to account for different distillation column sizes. For instance, if the output flow of the desired product is used as the functional unit, the effect of the internal flow (inlet flow), pressure conditions, and the separation difficulty (number of stages, outlet compositions) are not accurately accounted for. Thus, the functional unit utilized herein corresponds to the mass of the distillation column, sized via the required weight of the stainless steel and not the total column weight. This metric quantifies the sizing much more accurately, and is in fact more consistent with the costing analysis.

In summary, the life cycle emissions of the manufacturing of the column are estimated based on the data supplied by Brondani et al. [136], but scaled via the determined mass of the designed distillation column, which is expressed as:

$$m_{dc,steel} = \rho_{steel} \cdot \frac{\pi}{4} \cdot H_{dc} \left((D_{dc} + \delta_{dc})^2 - D_{dc}^2 \right) \tag{2.28}$$

In Equation 2.28, D_{dc} represents the diameter of the column, Δ_{dc} the column thickness, and H_{dc} the column height. The column's design typically involves several degrees of freedom, which renders it a relatively open problem with several potential solutions depending on the design choices. The design herein, however, will utilize a standardized but conservative methodology to unify the model of the multiple columns in the different processes considered. These methodologies are based on well-established heuristics and guidelines proposed by Wankat [137] and Seider et al. [99].

$$m_{dc,\ell} = \frac{m_{dc,steel}}{\dot{m}_{sep} \cdot \ell_R} \tag{2.29}$$

Sizing a distillation column determines the column diameter and height. The column diameter is determined by the internal fluid flow, while the height is determined by the relative volatility and desired final compositions. The values of both quantities must be appropriate for a column, which requires several iterations would be required to ensure designing a practical column. For instance, a common heuristic states that the column height should not exceed 20 times its diameter [99]. The distillation unit herein is simply modeled by a single feed stream entering the unit, with 2 outlet streams (distillate and bottoms; no side-stream). Thus, the column diameter is determined via the following [137]:

$$D_{dc} = \sqrt{\frac{4F_v}{\pi \cdot \rho_v \cdot u_v}} \tag{2.30}$$

In Equation 2.30, D refers to the column diameter, F_v to the vapor flowrate within the column, ρ_v to the vapor density, and u_v to the allowable flooding velocity. F_v is a function of the desired outlet compositions, and is determined via [137]:

$$F_v = F_D(1 + r_{reflux}) \tag{2.31}$$

In Equation 2.31, F_D refers to the distillate flow rate and r_{reflux} denotes the reflux ratio. The reflux ratio is determined via the results from Aspen HYSYS. The equation for the distillate flowrate, however, is determined by:

$$F_D = \sum_i F_{feed} \cdot z_{feed,i} \cdot FR_{D,i} \tag{2.32}$$

In Equation 2.32, $z_{feed,i}$ is the mass fraction of component i in the feed, F_{feed} is the feed flowrate, and $FR_{D,i}$ refers to the fractional recovery of component i in the distillate, which is set to 0.995 to achieve a high recovery. Moreover, the flooding velocity is determined using the Souders-Brown equation [137]:

$$u_v = K_v \sqrt{\frac{\rho_l - \rho_v}{\rho_v}} \tag{2.33}$$

In Equation 2.33, ρ_l is the liquid density and K_v is the vapor load factor, whose value varies as a function of the tray spacing, $h_{tray} = 36$ inches. A conservative choice of $K_v = 0.03$ m/s is chosen. The values of ρ_l and ρ_v are determined using Aspen HYSYS.

Moreover, the distillation column height is calculated as:

$$H = N_{trays} \cdot d_{trays} \tag{2.34}$$

In Equation 2.34, N_{trays} is the number of trays required in the column, and d_{trays} is the distance between the trays. N_{trays} is approximated for all distillation columns as 20 and 5 for separators, while d_{trays} is the maximum allowable distance at 36 inches. N_{trays} is also scaled by 2.5 to ensure sufficient separation trays are modeled [137].

Due to lack of any more representative distillation capacity data, the distillation column mass is modeled based on the flow and then correlated with the remaining unit materials. Similar to the reactor and heat exchanger, the mass is normalized by the total mass of distilled products over its lifetime, where the lifetime is assumed to be the same as that of the plant lifetime.

The materials utilized from Brondani et al. [136] are tabulated with their respective masses in Table A.13. Additional inventory is included to account for the reboilers and condensers. These units are essentially heat exchangers, and thus incorporate the heat exchanger inventory demonstrated in Section 2.2.9..

The distillation column and separators were modeled using the flows shown in Figure 2.13.

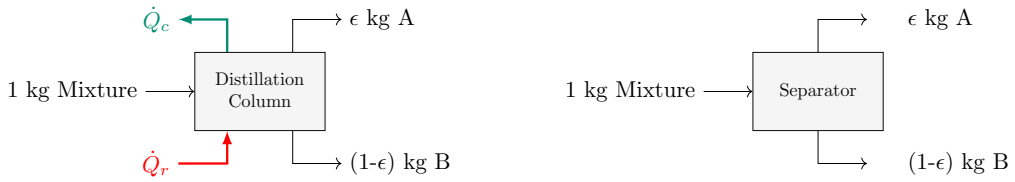

Figure 2.13. The unit process for the distillation column(left) and the separator (right) units, which displays the model's energy and mass flows across the unit. Note that the separator (right) does not include the heat streams since the inlet flow is cooled/heated in a heat exchanger prior to entering.

The separations that occurred are reported in Table 2.7 by identifying the separation streams, the product of interest in the process, and heat and cooling loads for the reboiler and condenser

Table 2.7. The various separations considered for the 3 processes (*CO2ER*, *CO2HY*, *BIOHY*; ALL refers to the reaction/reactor present in the 3 processes). The table highlights the separation units with their key products, heat/cooling input, column reflux ratios, and temperatures when possible. Empty entries (-) denote the separation is conducted in a separator and not a distillation column. Separation recovery is almost 100% to maximize jet fuel output. The key products denote the contents of the 2 outlet streams, with the content in each stream separated by the backslash (/).

Process	Key Products	Target Product	r_{reflux}	q_{cd} [MJ · kg_{inlet}^{-1}]	q_{rb} [MJ · kg_{inlet}^{-1}]	p [MPa]
CO2ER	Uncreacted CO – H_2/CH_3OH	CH_3OH	-	-	-	5
CO2HY	Uncreacted CO_2 – H_2/CH_3OH – H_2O	CH_3OH – H_2O	-	-	-	5
BIOHY	Uncreacted Biogas/CH_3OH – H_2O	CH_3OH – H_2O	-	-	-	3
CO2HY, *BIOHY*	CH_3OH/H_2O	CH_3OH	1.43	0.7028	1.708	0.1
ALL	$C_3^=$/$C_{4+}^=$ Olefin	$C_{4+}^=$ Olefin	-	-	-	0.1
ALL	Olefin/Water	Olefin	7.713	1.935	1.824	0.1
ALL	Jet Fuel/Heavies	Jet Fuel	0.04	0.3256	0.3058	0.1

when possible. These units are incorporated partially in the heat integration. The heating data is generated at a fractional recovery of 99.5%. A separator was used when the separation difficulty was low and the units could be flashed and separated directly.

The decentral nature of methanol production in the the *BIOHY* process, necessitates the transportation of this flow to the centralized plant following separation. This transportation of MeOH/H_2O to be further refined to jet fuel in the central plant is modeled herein. A transportation distance of 200 km is assumed, and the ecoinvent activity associated with this transportation is "transport, freight, lorry 16-32 metric ton, EURO5, RER". The unit of this activity is in ton · km, and the mass scales with the increase of the functional unit of the separator.

2.2.12. Water Production

Water is an essential feedstock in the production of synthetic fuels. Its utilization in the scope of a life cycle assessment necessitates accounting for the life cycle emissions associated with its production. Thus, while water is purchased as an operating expense, its life cycle models its production prior to utilization in the chemical plant. The resulting water is in fact deionized. The schematic for this unit process is shown in Figure 2.14. The power required is 0.0000265 kWh, and

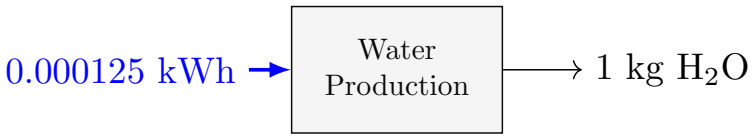

Figure 2.14. The unit process for water production, which displays the model's energy and mass flows across the unit.

is retrieved from the ecoinvent dataset of this activity [51]. Similar to the DAC unit assessment, the electricity input is decoupled from the inventory dataset to avoid double counting. Instead, the electricity flow is considered in the energy balance of this unit process, such that the overall electricity dependence can be examined.

2.2.13. Pump

Pumps are needed to supply compress and transport liquid flows in the chemical plant. For water, the pump would help circulate it as a feedstock to the required units, which is in the case the co-electrolysis and electrolysis units. In particular, a high water pressure at the electrode inlet could provide benefits in reducing the energy needed to reduce the cost of H_2 compression [138]; however, high pressure is not implemented by the experimental collaborators. As for the olefins, the pump enables increasing the pressure to a setpoint that represents an improved reaction pathway and yield [113].

The LCI of the pump utilizes the ecoinvent dataset for a water pump. While this very suitable for the water pump, it might not be the most representative for pumping olefins. Nevertheless, due to lack of better datasets, it is assumed that the pump lifetime is not affected by the olefin fluid properties relative to those of water. Moreover, the unit process energy and mass flows are highlighted in Figure 2.15.

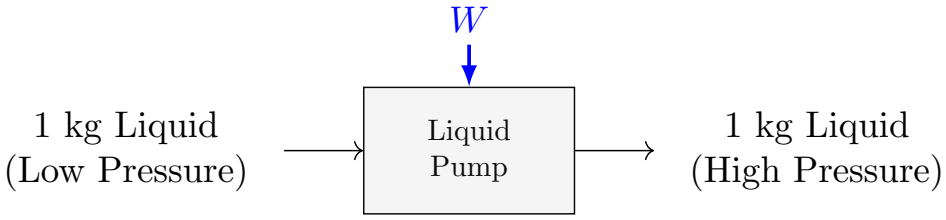

Figure 2.15. The unit process for a pump, which displays the model's energy and mass flows across the unit. This unit is used for pumping water and liquid olefins.

$$\dot{W}_{pump} = \frac{\dot{m} \cdot (p_o - p_i)}{\rho_{fl} \cdot \eta_{pump}} \tag{2.35}$$

In Equation 2.35, $\dot{W}_{pump}$ refers to the calculated pump power, p_o is the outlet pressure determined by the electrolyzer water input, p_i is the inlet pressure, ρ_{fl} is the fluid density, $\dot{m}$ is the mass flowrate across the pump, and η_{pump} is the pump efficiency.

The inventory and mass/energy balances highlighted are applicable for both water and olefins. The amount of pumping power distinguishes both units since they are determined by the target final pressure and fluid properties. These properties are tabulated in Table 2.8. The target

Fluid	p_o [bar]	w_{pump} [kWh · kg^{-1}]
Water	0.5	0.00013843
Olefin	60	0.0032278

Table 2.8. The target pressure and energy inputs required by the 2 modeled pumps, whose liquids are water and mixture of $C_4^=$, $C_5^=$, and $C_6^=$ respectively. The water specific work is calculated using Equation2.35, while that of the olefin mixture is calculated using Aspen HYSYS.

pressure in Table 2.8 is assumed as 5 times the ambient pressure, such that water circulation around the chemical plant is ensured.

2.2.14. Biogas Production

Biogas is the feedstock in the *BIOHY* process. Its production is modeled using ecoinvent's biogas production using sewage sludge, which is common in Switzerland. The resulting biogas composition is thus 67% CH_4, 32.3% CO_2, and 0.7% of N_2 [139]. The process model, however, developed by Moioli et al. [56] utilizes a composition of 60% CH_4-40% CO_2. Due to lack of more representative data, the utilized biomass composition will be assumed to have the same conversion performance as in the process model.

The energy and mass balance of the biogas production with respect to the system boundary is thus shown in Figure 2.16.

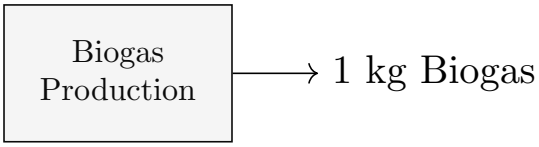

Figure 2.16. The unit process for biogas production via sewage sludge waste treatment, which displays the model's energy and mass flows across the unit.

The ecoinvent database models the biogas production as a byproduct of sewage sludge treatment, and thus comprises no emissions since the burden is attributed to the waste treatment process, which generates emission-free biogas [51]. Such a property can enhance the overall GHG of synthetic jet fuel by avoiding feedstock emissions.

2.3. Life Cycle Impact Assessment

The life cycle impact assessment (LCIA) metrics to be examined are: (1) the climate change impact, (2) cumulative energy demand, (3) land occupation, and (4) water usage. The final values corresponding to these metrics, in addition to up to 50 contributing flows, were quantified as part of this analysis. They are summarized in Table 2.9.

Impact Categories	Symbol	Unit
Climate Change Impact	GHG	$kg_{CO_2\text{-eq}}$
Cumulative Energy Demand	CED	MJ-eq
Land Occupation	LUO	$m^2 \cdot yr$
Water Depletion	WDP	m^3

Table 2.9. Summary of life cycle impact categories considered in the comparative assessment of synthetic jet fuel processes. These categories include the climate change impact defined by the IPCC in 2013 using a 100 year horizon for global warming potential (GWP), cumulative energy demand (including that of biomass, fossil, geothermal, nuclear, primary forest, solar, water/hydro, and wind energy), land usage and occupation, and water depletion metrics [51].

The impact category names, shown in Table 2.9 as used in ecoinvent [51], are outlined in greater detail the Table A.1. These metrics are quantified per kilogram of jet fuel.

2.3.1. Climate Change Impact

The climate change impact metric is quantified by the calculated greenhouse gas (GHG) emissions, which measures the equivalent CO_2 emissions emitted by the synthetic jet fuel production process. This metric is particularly important since the life cycle carbon footprint of conventional jet fuel is 3.52 $kg_{CO_2\text{-}eq} \cdot kg_{JF}^{-1}$ [6, 51]. In this study, biogenic CO_2 is used as a feedstock, either directly through DAC units or biomass, and the same amount of CO_2 is later released following jet fuel combustion. For this reason, the CO_2 footprint should be assessed. Its unit is $kg_{CO_2\text{-}eq}$, which includes the contributions by 211 chemicals that, like CO_2, trap heat in the environment. The impact of heat trapping is evaluated over a 100 year horizon (GWP 100a), and summed together as an equivalent mass of CO_2 having the same heat trapping effect. Consequently, the GHG emission units CO_2-eq and CO_2 are used interchangeably as subscripts to simply the notation. While effects in the upper atmosphere due to contrails could contribute to more equivalent CO_2 emissions [140], these effects are not accounted for herein. The environmental impact due to contrails are presumed to be the same between conventional and synthetic jet fuels [14], although recent studies show that soot reductions via combustion of jet fuels with less aromatics could reduce contrail cloudiness [141]. Nevertheless, they are not accounted for herein.

2.3.2. Cumulative Energy Demand

The cumulative energy demand (CED) is key in assessing the total energy required to produce one unit of the desired product. This metric accounts for inefficiencies by quantifying the energy required to deliver the energy flows required by the jet fuel production process. The CED of each process is thus estimated by adding the various types of cumulative energy demands (renewable: biomass, geothermal, solar, hydro, wind; non-renewable: fossil, nuclear, primary forest) in ecoinvent [51, 142], and utilizes a unit of MJ-eq.

2.3.3. Land Usage Occupation

Land usage and occupation (LUO) is an essential metric to examine in light of the high land usage of processes utilizing biomass feedstocks. This metric could lead to synthetic fuels using CO_2 feedstocks to be more attractive than those using biomass feedstocks. Its unit is $m^2 \cdot yr$, which refers to the effective amount the area occupied over the duration of a year.

2.3.4. Water Depletion

Water depletion (WDP) is a also key metric due to the prominent utilization of water as a feedstock to produce H_2 via water electrolysis. Its unit is m^3 of water, which quantifies the volume of water consumed.

2.4. Results & Discussion

The results of the life cycle assessment of the 3 considered processes are presented using the life cycle impact assessment categories. These environmental metrics are further examined by assessing the energy utilization of the processes, and the derived GHG metric of each process is benchmarked with respect to similar literature studies. Finally, the processes are assessed in a sensitivity analysis based on parameters that have high levels of uncertainty or lack sufficient data.

2.4.1. Impact Categories

The selected impact categories by which the processes are assessed and compared are: (1) the climate change impact, (2) cumulative energy demand, (3) land utilization and occupation, and (4) water depletion. These metrics are shown in Figure 2.17.

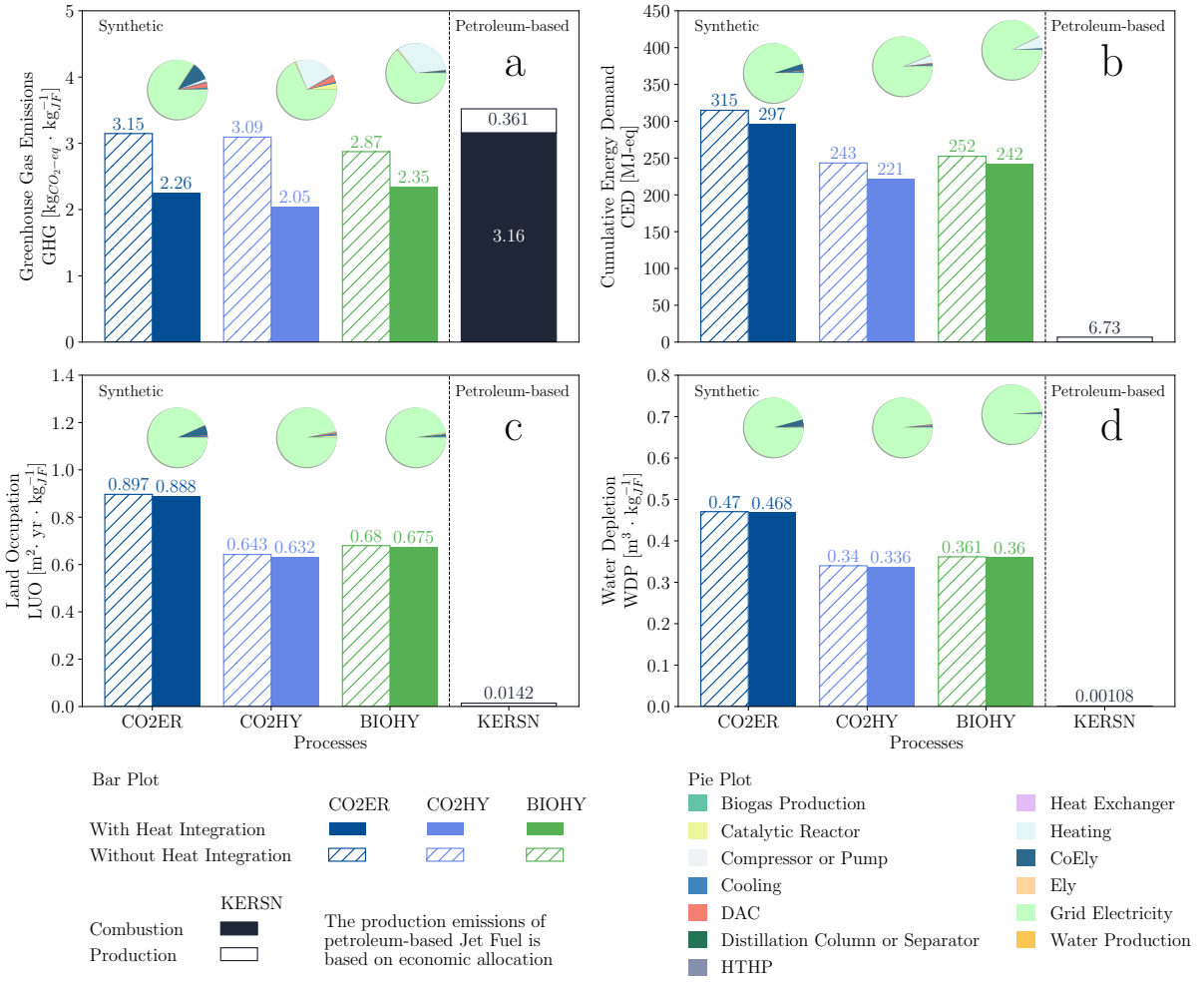

Figure 2.17. The variation in the climate change impact, *GHG* (a), cumulative energy demand, *CED* (b), land utilization and occupation, *LUO* (c), and water water depletion, *WDP* (d), produced by the considered synthetic jet fuel production processes (*CO2ER*, *CO2HY*, *BIOHY*). The impact categories are shown for each process without and with heat integration, highlighting the significant reduction when recovering heat in these processes. These synthetic processes are compared to the conventional petroleum-based jet fuel via the aforementioned metrics. The petroleum-based jet fuel metrics are divided into contributions via production and combustion. A decomposition of the units contributing to the emissions of the heat integrated synthetic processes is highlighted for each process using the pie charts. Grid electricity proves to be the highest contributor to all metrics assessing the 3 synthetic jet fuel production processes.

Figures 2.17 (a), (b), (c), and (d) portrays the climate change impact, the cumulative energy demand, the land usage, and the freshwater depletion metrics respectively for the 3 synthetic production processes and the petroleum-based jet fuel. The metrics of the 3 synthetic production processes are shown with and without heat integration. All 4 environmental metrics of the 3 processes exhibit reductions upon implementing heat integration. The greatest emission reduction due to heat integration is highlighted by the climate change impact in Figure 2.17 (a). Particularly, the *CO2ER* and *CO2HY* exhibit notable GHG reductions by 28.3% and 33.8%. The *BIOHY* process shows less reductions due to heat integration (18.3%), since this process is spatially separated and thus there is less potential for heat recovery. The 3 processes nevertheless show promising GHG reductions compared to the conventional petroleum-based jet fuel. Thus, the synthetic production of jet fuel via *CO2ER*, *CO2HY*, and *BIOHY* can reduce the carbon footprint of 1 kg of jet fuel (relative to the petroleum-based fuel utilized today) by 35.9%, 41.9%, and 33.3% respectively. These lower GHG values of the synthetic processes include production, combustion, and uptake due in the biogenic CO_2 feedstock. However, the usage of a biogenic source of carbon leads to a negative emission value and negates the combustion emissions. This negation implies that these GHG values are purely due to production, which is significantly higher than that of the petroleum-based fuel (0.361 $kg_{CO_2\text{-eq}} \cdot kg_{JF}^{-1}$ due to production) and consequently emphasizes the optimization of the production as a means to minimize these emissions. This deviation in production GHG emissions between the synthetic jet fuel processes and the petroleum-based process can be explained by the emission contributions highlighted by the pie plots in Figure 2.17 (a). For the *CO2ER* process, 83.8% of the GHG emissions is attributed to electricity emissions, while the balance is divided similarly between the co-electrolyzer (9.8%), electrolyzer (0.4%), DAC (2.46%), heating (1.5%), and cooling units (0.95%). It is worth noting that the co-electrolyzer has higher contributions than the electrolyzer unit, which is explained by the lower lifetime of the CoEly, despite the lower noble metal content. However, this is assuming the co-electrolyzer unit operates as modeled. Even under such optimistic circumstances, the CO2ER process shows higher emissions than the CO2HY. For the *CO2HY* process, the GHG emissions are mainly divided between electricity (68.2%), heating (22.8%), DAC (3.31%), and reactors (3.47%). The contribution of the reactor is particularly dominated by the CO_2 hydrogenation reactor, which is modeled to use a catalyst using Palladium, which is a noble metal. Finally, the *BIOHY* GHG emissions are distributed amongst the electricity (63.8%) and heating (33.8%). Thus, by evaluating the processes based on only the GHG, the *CO2HY* process is the most attractive from an environmental perspective, with a GHG that can be potentially reduced to 2.05 $kg_{CO_2\text{-eq}} \cdot kg_{JF}^{-1}$ via heat integration.

The cumulative energy demand highlighted in Figure 2.17 (b) show stark differences between the synthetic and petroleum-based jet fuel. The CED of the synthetic processes before heat integration ranges between 243 and 315 MJ-eq, while the range decreases to 221 to 297 MJ-eq following heat integration. This reduction is owed to the decrease in heating and cooling demand as a result of heat recovery. Nevertheless, the CED even after heat integration remains significantly higher than the energy demand of the petroleum-based jet fuel, which is approximately 7 MJ-eq. This value represents the energy demand to extract 1 kg of petroleum-based jet fuel via fractional distillation, and is determined via economic allocation. The contribution to the CED (visualized by the pie plots) are predominantly owed to the usage of the Swiss grid electricity (*CO2ER*: 94.9%, *CO2HY*: 93.82%, *BIOHY*: 92.45%). This high value could signify that either the processes require a lot of electricity or that an output of 1 MJ of electricity requires a higher primary energy value as input due to inefficiencies. The synthetic nature of these fuels justifies the former. A detailed breakdown of the usage electricity and

heat transfer is conducted in Section 2.4.2. to investigate the high contributions due to electricity.

Figures 2.17 (c) and (d) show that the land usage and water depletion of the CO2HY and BIOHY processes are similar, while that of CO2ER is notably higher. The similarity in the WDP values across all the processes is a result of the similar electrical energy required by the CO2HY and BIOHY the electrochemical units to produce 1 kg of jet fuel, while CoEly contribution in the CO2ER process adds more electricity reuiqrements. These metrics exhibit very minor reductions due to heat integration. In a similar manner to the GHG and CED, both LUO and WDP metrics are predominantly formed by land usage and water depletion due to the grid electricity. In the case of LUO, the contribution of electricity is around 90% (*CO2ER*: 93.2%, *CO2HY*: 96.6%, *BIOHY*: 97.3%,), while the electricity contribution in WDP is also around 90% (*CO2ER*: 95.65%, *CO2HY*: 98.1%, *BIOHY*: 98.65%,). The balance in LUO for the *CO2ER* process is attributed to units containing noble metals, which are respectively the CoEly unit. The same is true for WDP, where the balance is due to the CoEly unit (*CO2ER*). However, compared to the petroleum-based jet fuel, the synthetic jet fuel LUO and WDP metrics are over 2 orders of magnitude. In particular, the LUO of the synthetic processes is on average 5000% higher, while their WDP is on average 35000% higher.

The 3 synthetic processes generally have similar environmental impacts, which can be explained by the fact that the second half of each pathway (MeOH-to-Jet Fuel) is the same across the 3 processes. The inclusion of the co-electrolyzer unit, however, proves to provide a notable GHG increase in the *CO2ER* process metrics compared to the *CO2HY* and *BIOHY* processes. The increase in GHG is particularly highlighted by the reduction of CO_2 into CO which requires more electricity to do so. While the heating contribution is less in the *CO2ER* process due to the bypassing of an additional distillation column, the GHG values remain high compared to that of the *CO2HY* process. The *BIOHY*, on the other hand, capitalizes on biogas production from waste treatment, and thus uses a feedstock with zero emissions. However, this process suffers from its dependence on biogas production plants, and could encounter a multitude of logistical issues due to the spatial separation. It proves to be an interesting emission reducing pathway, but could face difficulties in scaling up. By examining all metrics combined, it can be established that *CO2HY* is generally more efficient than the other processes. The *BIOHY* process is also competitive in terms of GHG emissions, but could face practical issues in implementation. Besides electricity emissions, the emissions due to noble metals is evident, which also a target that must be reduced for the sustainable production of such commodity chemicals.

2.4.2. Energy Utilization

The decoupling of the energy required by the unit processes from their emissions necessitates a further examination of the various forms of energy required per kg of jet fuel and a breakdown of the unit processes that require this energy. This breakdown is particularly useful to ascertain the distribution of electricity demand across the units, which would help explain the high emissions due to electricity. This is shown in Figure 2.18.

Figure 2.18 (a) and (b) highlight the demand of electrical energy and heat via HTHP needed to produce 1 kg of synthetic jet fuel for each of the 3 considered processes (following heat integration). The electrical energy demand for the hydrogenation processes is roughly the same, ranging between 31 and 33 kWh $\cdot\ kg_{JF}^{-1}$, as shown in Figure 2.18 (a), while that of the *CO2ER* process is significantly higher at 42 kWh $\cdot\ kg_{JF}^{-1}$. The similarity between *BIOHY* and *CO2HY* process rather fortuitous due to the economic allocation (at the MeOH/methane separator)

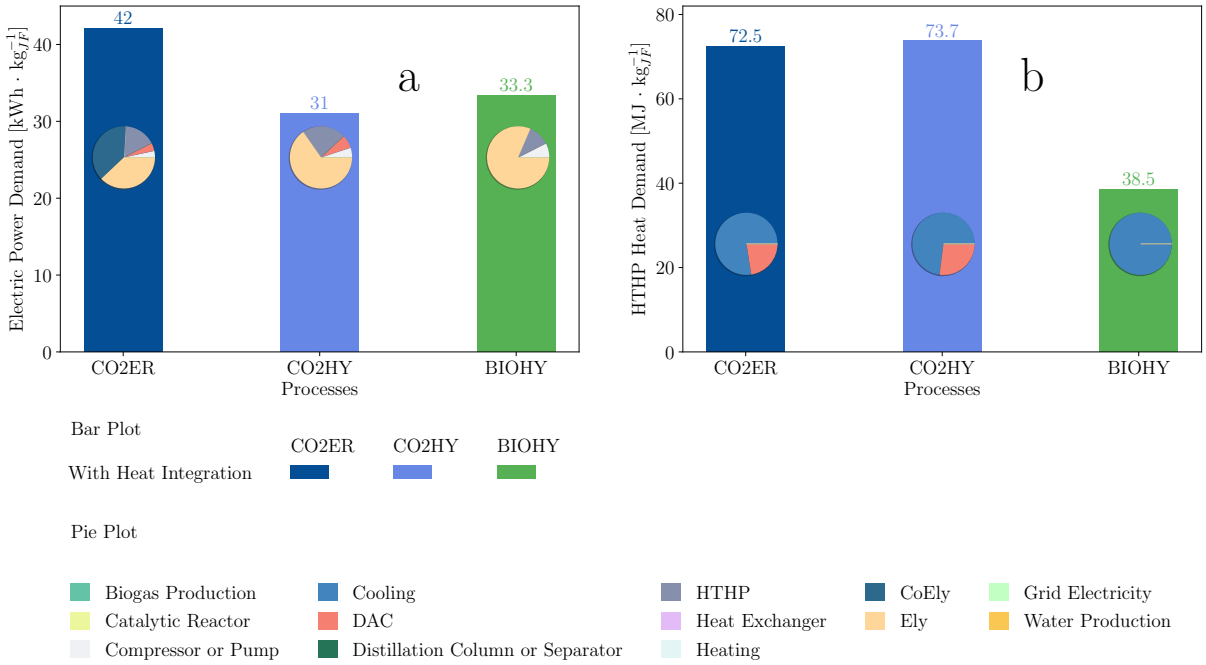

Figure 2.18. The variation in the electrical energy (a), and heat via high temperature heat pump (b) required per kg of synthetic jet fuel for the 3 production processes (*CO2ER*, *CO2HY*, *BIOHY*). The electrical energy and HTHP heat demands are shown only following heat integration. The pie charts show a breakdown of the units that require the shown energy flows. Heating refers to the industrial furnace heating.

conducted to quantify the methanol contributions. In contrast, the reason behind the high *CO2ER* process electric demand is owed to more electricity requirements by the CoEly unit. The distribution of electrical energy amongst the unit processes (pie plots) signifies that a majority of electrical energy is dedicated to the electrolyzer unit (Ely). The electrolyzer unit utilizes 37.9%, 65.3%, and 81.4% of the electrical energy in the *CO2ER*, *CO2HY*, and *BIOHY* processes respectively. While the electrolyzer percent contribution to electric power demand in *CO2ER* process is less than the remaining processes, this is owed to the added CoEly contribution at 38%. Moreover, the higher electrical input to the Ely unit in the *BIOHY* process is attributed to the higher input needed due convert the unreacted CO_2 to CH_4 (the methanation reaction occurs beyond the process boundary). The DAC unit also requires a notable portion of the electricity in the CO_2-based processes, with the *CO2ER* and *CO2HY* processes requiring 4.2% and 6.87%. Additional electricity inputs are needed by the high temperature heat pump (*CO2ER*: 16.5%, *CO2HY*: 22.7%, *BIOHY*: 11%) and compressors/pumps (*CO2ER*: 3.4%, *CO2HY*: 5.1%, *BIOHY*: 7.5%). Whether for CO_2 or H_2O electrolysis, the energy requirement to generate a unit of CO or H_2 remains quite high. The satisfaction of sustainability targets could depend on such energy requirements; at the moment, around at around 20 kWh is demanded by the Ely unit of the *CO2HY* per kg_{JF}. If this energy requirement is only considered as the power requirement (ignoring heating/cooling), the energy input (equivalent of 72 MJ) is nearly double the energy content of 1 kg of jet fuel (43 MJ). While the projections for this energy requirement for water electrolysis is expected to decrease by 2050 ($\sim$ 40 kWh · kg^{-1}) [78], this decrease is only a 16% reduction relative to today's quantity. This low energy efficiency could require the investigation of alternative H_2 production pathways.

In contrast, the HTHP heat demand shown in Figure 2.18 (b) shows more variation across the synthetic processes. The HTHP of the CO_2-based processes is similar at around 73 MJ · kg_{JF}^{-1} , while the biomass-based process requires 38.5 MJ · kg_{JF}^{-1} . These heat values are high, but are acceptable since the HTHP produces less emissions, even at a value of $COP = 2.9$. The

key difference in the HTHP heat demand lies in the dedication of the HTHP to heating of the DAC unit, where 22.5% and 27% of HTHP heat required by the DAC unit. Consequently, the majority of the HTHP demand is thus utilized for cooling (*CO2ER*: 77.5%, *CO2HY*: 73%, *BIOHY*: 100%), with variations in cooling demand due to the varying heat integration configurations. A closeup on the heating and cooling demands is thus shown in Figure 2.19.

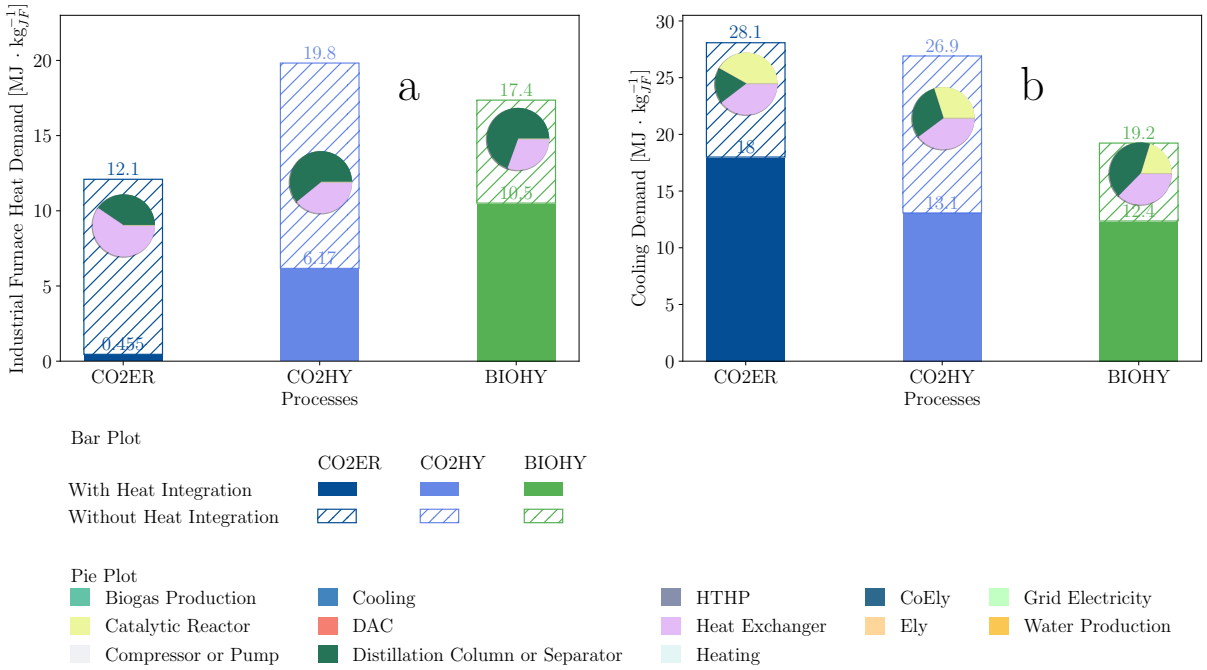

Figure 2.19. The variation in the heating via furnace (a), and cooling (via an absorption chiller) (b) required per kg of synthetic jet fuel for the 3 production processes (*CO2ER*, *CO2HY*, *BIOHY*). The heating and cooling demands are shown before and after implementing heat integration. The pie charts decompose the distribution of energy flows for the units' combined heating and cooling demand prior to heat integration. Heating refers to the industrial furnace heating.

Figure 2.19 (a) and (b) display the heating (via industrial furnace) and cooling demand (via absorption chiller) for the evaluated processes respectively prior to and after recovering heat. The heating demand per kg of synthetic jet fuel prior to heat integration is varies between 12.1 to 19.8 MJ, with the *CO2ER* requiring the lowest heat input. Following heat recovery, the *CO2ER* heat demand can be reduced by 96% to 0.455 MJ · kg_{JF}^{-1} . The *CO2HY* process, in contrast, exhibits a similar reduction to reach 6.17 MJ of heating demand. Compared to the *CO2ER* process that bypasses the MeOH/H_2O separation, the *CO2HY*'s inclusion of this separation step increases the heat demand due to the reboiler of the distillation column. This significant increase in heat demand due to the addition of a distillation column shows the importance of developing highly selective catalysts/reactions that can avoid extensive separations. The distillation heating requirements are visualized in the pie charts of Figure 2.19 (a), where the *CO2ER* process has a heat exchanger-distillation split of 59.5%-40.5%, while the distribution for the *CO2HY* process is 39.2%-60.8%. Finally, the *BIOHY* process is initially 17.4 MJ without heat integration, but can be decreased to nearly 11 MJ. The energy reduction due to heat integration is the lowest for the *BIOHY* process since the process is spatially separated, and thus heat cannot be recovered as efficiently as in the CO_2-based processes. The heating demand for this process is also distributed between the heat exchanger and distillation columns (30.5%-69.5%), with similarly high separation requirements due to the inevitable MeOH/H_2O separation.

The cooling demand in Figure 2.19 (b) is generally higher for each process than that of the

heating demand, which is attributed to the subzero separation of olefins. The reductions in the cooling demand due to heat integration, however, is naturally the same as the difference highlighted in Figure 2.19 (a). The cooling demand varies not only due to condensers for the distillation column and heat exchangers, but also as a function of the exothermicity of the considered reactions. The distribution of cooling requirements is thus distributed between reactors (*CO2ER*: 41.8%, *CO2HY*: 29.9%, *BIOHY*: 20.2%), heat exchangers (*CO2ER*: 39.6%, *CO2HY*: 39.7%, *BIOHY*: 37.3%), and distillation columns (*CO2ER*: 18.5%, *CO2HY*: 30.2%, *BIOHY*: 42.3%). Heat integration thus shows to be effective and necessary in emission reduction.

The overall energy efficiency can be assessed by relating the jet fuel energy output ($\sim$ 43 $MJ \cdot kg^{-1}$ [15]) to the overall energy input. The energy input assessed herein will be limited to the electricity and heating via industrial furnace to avoid double counting. The cooling system is not counted since the energy it outputs is based on inputs from the high temperature heat pump, whose output relies on electricity as input. From the results of Figures 2.18 and 2.19, the *CO2HY* process is the most energy efficient process and requires 111.6 MJ from electricity and 6.17 MJ of heat (after heat integration) to produce 1 kg of synthetic jet fuel. Thus, 118 MJ are needed to generate 43 MJ in jet fuel lower heating value output, which amounts to an energy efficiency of 36.4%. This efficiency is relatively close to the 42% efficiency of a process similarly using a methanol pathway, H_2 production via low temperature electrolysis, and CO_2 from direct air capture [42]. The difference, however, is their methanol to olefin path targets ethylene (C_2H_4), which is a mature process developed by Mobil [128]. The target of the synfuel initiative, however, is to develop an alternative methanol-to-jet fuel pathway by passing through higher order olefins as intermediates. At this stage of this initiative, not all reactions are developed completely nor coupled together, which would in that case promise higher jet fuel yields and lower energy expenditure. Thus, the efficiency is expected to increase and potentially reach that of the established processes.

2.4.3. Carbon Intensity of Electricity

The analysis conducted based on Figures 2.17 (a) and Figures 2.18 (a) highlight the high contribution of the electricity mix on the resulting GHG of the synthetic jet fuel. This contribution is sensible since these synthetic fuels are synonymous with electricity-based fuels. Nevertheless, the carbon intensity of electricity is highly location-dependent. The GHG of the 3 processes are less than that of the petroleum-based jet fuel (Figure 2.17 (a)), but this low GHG should acknowledge the low carbon intensity of the utilized Swiss grid, at 0.045 $kg_{CO_2\text{-eq}} \cdot kg_{JF}^{-1}$ (low voltage market production). Consequently, assessing the GHG of synthetic jet fuel should be examined beyond the production in Switzerland, which has hitherto been evaluated, such that the processes are properly benchmarked relative to other production pathways. The geographic assessment is examined in Figure 2.20.

Figure 2.20 portrays the dependence of the climate change potential of synthetic jet fuel, GHG_{JF}, on the carbon intensity of electricity, GHG_{el}. The carbon intensity of electricity is synonymous with the greenhouse gas emissions of electricity. This relationship is established for each of the 3 processes. The vertical dashed lines represent what the carbon intensity of electricity is in various countries. As a result, the intersection of a specific dashed lines with the solid process lines represent what the GHG processes would be in that specific country. The lowest carbon intensity of grid electricity is that of Switzerland, with the intersection of the dashed line and the solid lines replicating the values shown in Figure 2.17 (a). The only

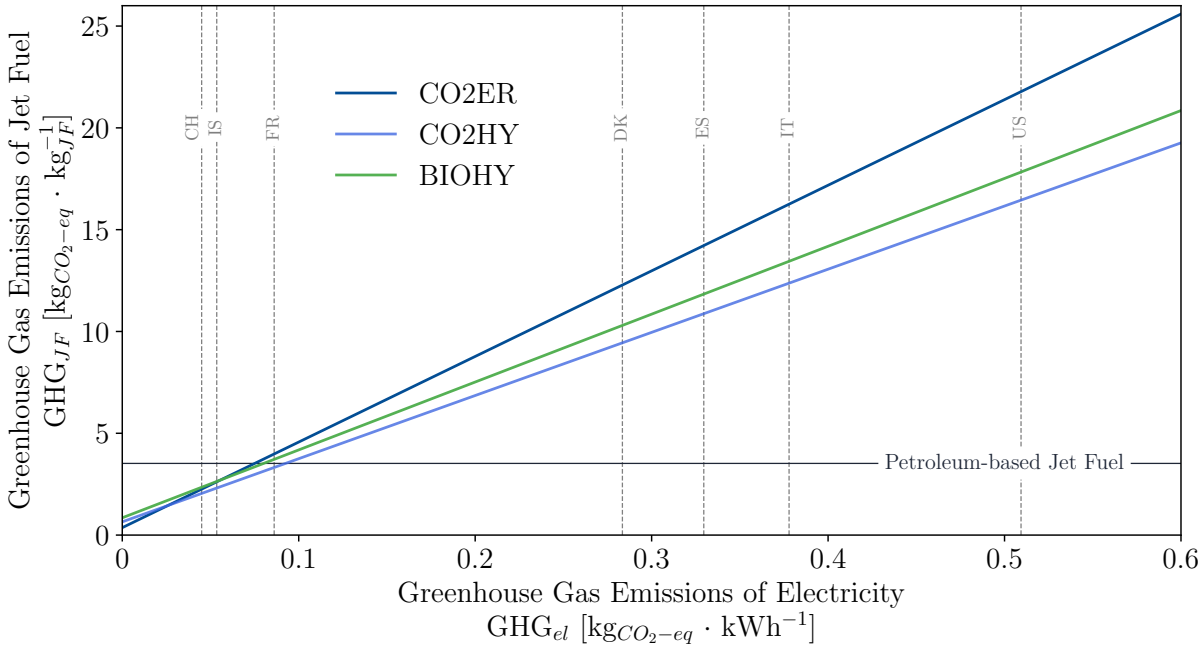

Figure 2.20. The evolution of the climate change impact of synthetic jet fuel, GHG_{JF}, as a function of the carbon intensity of electricity, GHG_{el}, for the 3 production processes (*CO2ER*, *CO2HY*, *BIOHY*). The value is referenced to the petroleum-based jet fuel, denoted by the horizontal line, whose GHG is 3.52 $kg_{CO_2\text{-eq}} \cdot kg_{JF}^{-1}$. The dashed lines represent low-voltage electricity production of selected countries such as: Switzerland (CH; without DE imports), France (FR), Germany (DE), Italy (IT), Spain (ES), Denmark (DK), and Iceland (IS).

other electricity mixes that can produce jet fuel whose GHG is less than the (horizontal line) petroleum-based jet fuel are those of Iceland and France. In particular, a carbon intensity less than 0.1 $kg_{CO_2} \cdot kWh^{-1}$ can produce synthetic jet fuel with nearly identical GHG emissions to that of the petroleum-based one. Such a carbon intensity can then be considered an upper limit to targets for carbon intensity, which is well below the current European and US averages.

At very low values of carbon intensity of electricity, the *CO2ER* process is the process producing the lowest GHG emissions per kg of jet fuel. This result highlights the main benefit of utilizing the *CO2ER* process, which is to bypass methanol/water separation by producing methanol only via syngas. The benefits incurred by the lower heating requirements are captured at low electricity intensity, where the high electricity demand of *CO2ER* would have negligible synthetic jet fuel GHG contributions. The *CO2ER* forfeit its lowest GHG rank at around 0.025 $kg_{CO_2} \cdot kWh^{-1}$, after which the CO2HY becomes the process generating lowest synthetic jet fuel GHG emissions. The GHG emissions of the *CO2ER* continues to increase and diverges as a result of high electricity utilization. This indication shows that from a static perspective, the optimal process depends on the carbon intensity of electricity, which implies that different processes can be optimal in different countries.

The remaining European countries whose carbon intensity was marked by dashed lines can generate synthetic jet fuel with a GHG between 8 and 15 $kg_{CO_2\text{-eq}} \cdot kg_{JF}^{-1}$, which is significantly higher than that of the petroleum-based. Synthetic jet fuel production in the US is similarly impractical. However, these values represent the carbon intensity of electricity of today [143]. Thus, the incorporation of these synthetic fuels should be accompanied by the utilization of low-emission grid electricity or dedicated private renewable energy systems to achieve GHG emissions that can reduce the overall carbon footprint relative to the petroleum-based equivalents.

3 | €

Life Cycle Costing

The life cycle costing (LCC) of the individual synthetic jet fuel processes accounts for all expenses incurred during the production of jet fuel, within the system boundaries defined in Chapter 2. These expenses include capital investments in equipment and machinery, in addition to operating costs, both of which are considered to determine the price per unit kg of jet fuel.

The flows and ratings associated with the units processes from in Chapter 2, such as mass flows, energy flows, and installed capacities, are transformed into costs.

3.1. Techno-economic Modeling of Unit Processes

Each process model consists of unit processes, which are identical to those evaluated in the LCA section. The goal of techno-economic modeling is to evaluate the cost of components as accurately as possible, using the energy and mass balances from Chapter 2. Thus, these unit processes are sized and priced based on their technical characteristics and performance. The costs associated with the units could be operating costs for purchased material/energy, equipment and capital costs (with maintenance), or both operating and initial capital costs. Unless otherwise stated, yearly maintenance costs are accounted for as 3.5% of CAPEX [144, 145]. Operating costs arising from energy requirements of units are decoupled, and instead accounted for by costing through the unit processes of the energy sources (electricity, heat, cooling) based on the total process energy demand. For the units whose cost is determined using the costing equations of Towler & Sinnott [65], the cost is scaled by a ratio of the Chemical Engineering Plant Cost Index (CEPCI). This ratio is the CEPCI of year 2021 ($CEPCI_{2021} = 708$ [146]) divided by that of 2010 ($CEPCI_{2010} = 532.9$ [65]), which is 1.328.

3.1.1. Electricity Mix

The electricity mix is representative of the Swiss grid electricity, which consists of a mix of several energy sources that are renewable and non-renewable (Figure 2.2).

The cost of electricity is thus an operating cost that is purchased per kWh. The Swiss utility rate for households is priced at 0.195 CHF · kWh^{-1} [147, 148]. This price is assumed not to change as a function of the increase in demand.

3.1.2. Industrial Furnace

The industrial furnace is modeled to complement the life cycle environmental burdens associated with the utilization of an industrial natural gas furnace to provide heat to the heating fluid. Thus, the investment cost (in EUR) associated with the natural gas furnace is expressed as [149]:

$$C_{furnace} = 250 \cdot \dot{Q}_H \tag{3.1}$$

In Equation 3.1, $C_{furnace}$ refers to the furnace capital cost as a function of the $\dot{Q}_H$, which is the associated heat rating required. Furthermore, the variable natural gas cost is expressed as [149]:

$$C_{furnace}^{opex} = 7.2 \cdot Q_H + c_{NG} \cdot Q_H + c_{DPE} \cdot m_{DPE} \tag{3.2}$$

In Equation 3.2, $C_{furnace}^{opex}$ denotes the operating expenses, which are a function of the heat energy generated, Q_H, the cost of natural gas, c_{NG}, which is 36 EUR· MWh^{-1} [149], and c_{DPE} the cost of the diphenyl ether (DPE), priced at 84 CHF · kg^{-1} [150]. DPE is used as the heating fluid due to its high temperature range as a gas before reaching its critial state [68]. A fixed maintenance cost is used as 4% of the CAPEX.

3.1.3. Heat Pump

The heat pump is sized and designed for the sole purpose of supporting the DAC unit with the required heating. The capital cost of the electrical compression heat pump, C_{HTHP}^{capex}, is evaluated using [88]:

$$C_{HTHP}^{capex} = 660 \cdot \dot{Q}_{HTHP} \tag{3.3}$$

In Equation 3.3, $\dot{Q}_{HTHP}$ refers to the rated capacity of the HTHP unit. Similarly, the operating cost of the HTHP, C_{HTHP}^{opex}, is expressed as:

$$C_{HTHP}^{opex} = 2 \cdot \dot{Q}_{HTHP} + 0.00180 \cdot Q_{HTHP} \tag{3.4}$$

In Equation 3.3, Q_{HTHP} refers to the heat energy supplied by the HTHP.

According to Fasihi et al. [88], the economic assessment of heat pumps is capital intensive and would increase the cost associated with DAC units. Nevertheless, heat supplied by a HTHP generates lower emissions compared to steam or heat via a furnace, which necessitates its incorporation in process design when waste heat is unavailable (Section 2).

3.1.4. Absorption Chiller

The absorption chiller (AC) is economically evaluated based on its capacity and cooling energy supplied, in addition to the cost of ammonia as its working fluid. Its capital cost, C_{AC}^{capex}, is evaluated using [151]:

$$C_{AC}^{capex} = 2500 \cdot \dot{Q}_C \tag{3.5}$$

In Equation 3.5, $\dot{Q}_C$ refers to the rated capacity of the AC unit. The operating cost associated with the absorption chiller is restricted to the cost of ammonia as the working fluid, since the electricity costs are decoupled and instead accounted for in the electricity mix section. Thus, the operating cost of the absorption chiller is expressed as:

$$C_{AC}^{opex} = c_{NH_3} \cdot m_{NH_3} \tag{3.6}$$

In Equation 3.6, m_{NH_3} refers to the mass of ammonia in the closed loop absorption chiller system, while c_{NH_3} is the cost of ammonia (0.6 EUR · kg^{-1} [152]). As stated in Section 2.2.4., the ammonia is replenished every year, so it is accounted for as a yearly operating cost.

3.1.5. Electrolyzer

The electrolyzer is unit is typically rated in terms of its power capacity. The common assessment of the capital cost associated with electrolyzers in literature studies [82, 93] expresses the cost is stated as a normalized specific cost (cost of cost per unit power). However, such a cost expression is in fact misleading if the capacity is not specified, since this a normalized cost refers to an electrolyzer of a specific size and capacity. This quantity is thus a normalized cost and does not accurately extrapolate to varying installed capacities. Instead, due to economies of scale, the electrolyzer cost is a nonlinear function of its capacity [153], which is shown in Figure 3.1.

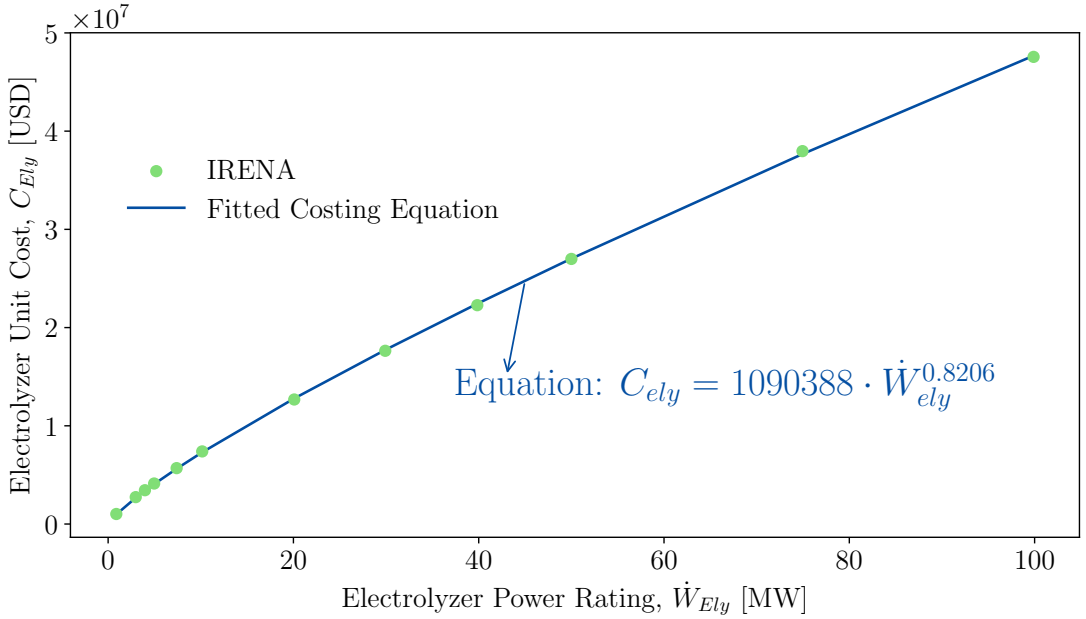

Figure 3.1. The capital investment cost of the electrolyzer unit as a function of its power rating. The data was generated by the International Renewable Energy Agency [153], and fitted to generate the cosing equation of: $C_{ely} = 1090388 \cdot \dot{W}_{ely}^{0.8206}$

Thus, according to the fit from Figure 3.1, the electrolyzer cost, C_{ely}, as a function of power is expressed as:

$$C_{ely} = 1090388 \cdot \dot{W}_{ely}^{0.8206} \tag{3.7}$$

In Equation 3.7, $\dot{W}_{ely}$ refers to the power rating of the electrolyzer. This rating is typically a function of the electrolyzer area and its operating conditions, and is determined using:

$$\dot{W}_{ely} = A_{ely} \cdot J \cdot V \tag{3.8}$$

In Equation 3.8, A_{ely} is the electrolyzer area, J is the current density, and V is the nominal electrolyzer voltage. ased on the electrochemical characteristics of the Ely unit, the current density and voltage are set to 1.6 A $\cdot$ cm^{-2} and 2 V respectively [154]. These quantities define the Ely operating point and help in determining A_{ely}, which quantifies the amount of catalysts needed. It is assumed that the costing equation based on the data of IRENA [153] covers all costs, including catalysts and noble metals, and thus the electrochemical catalysts are not accounted for separately to avoid double counting. This fitted costing equation has a similar equation form to that proposed by Dincer et al. [155], whose equation contains both a slightly higher base (1500000) coefficient and exponent (0.85).

The PEM electrolyzer has a lifetime of 80000 hours [82]. This is accounted for as the

stacks are purchased and put again, but at a cost of 40% of the total capital cost [82].

3.1.6. Co-Electrolyzer

The CoEly unit cost is conducted in a similar manner to that of the Ely unit but accounts for the variation in the materials and electrochemical performance. For instance, the same form of Equation 3.7 is used, but scaled by a multiple of 1.0368. This multiple is determined by comparing the specific costs and masses of the various components of both Ely and CoEly units. The ratio of total cost of the CoEly unit to that of the Ely unit is determined to be 1.0368.

Furthermore, the operating point of the CoEly unit is set to 0.1 A · cm^{-2} and 3.35 V to achieve a 0.85 Faradaic efficiency [156]. This also impacts the amount and thus cost of catalysts needed at the anode and cathode.

3.1.7. Direct Air Capture

The direct air capture (DAC) unit captures CO_2 directly from air. This method of CO_2 capture is more difficult since the CO_2 in the air exists at a low concentration. DAC system costs should account for capital investment, energy costs, and maintenance expenses [157]. The total system cost to capture 1 kg of CO_2 is estimated to be 0.578 EUR · $kg^{-1}_{CO_2}$ [24, 157]. This cost value however incorporates operation costs due to electricity and heat, both of which units are decoupled in the model herein. Thus, to avoid double counting, the DAC system CAPEX is used instead, while electricity and heat are included and priced separately.

Very few studies report CAPEX costs associated with the DAC unit in the literature due to confidentiality purposes. Amongst the few studies that do is that of Fasihi et al. [88], whose work presented the CAPEX costing for DAC plants as 730 EUR · $t_{CO_2}^{-1}$ · yr. This costing format allows for the decoupling of the DAC plant cost from the electricity and heat operating costs, whose emissions and cost vary as a function of geographical location. However, the resulting levelized cost per ton of CO_2 that Fasihi et al. [88] generated is a very optimistic estimate, hovering around 150 EUR/t_{CO_2} in 2019 [88, 90]. Instead, the utilized costing method is that proposed by Young et al. [158], which estimates the total cost of for the Climeworks Hinwil plant. Even though this method is more accurate, its limitation is that it models a very low capacity of CO_2 capture, which could result in inaccuracies scaling. Nevertheless, such inaccuracies would overestimate the cost of CO_2 capture, which remains consistent with the conservative approach utilized hitherto. Thus, the DAC CAPEX cost, C_{DAC}^{capex}, in EUR (using the conversions of Section 3.2.3.) is determined linearly using:

$$C_{DAC}^{capex} = 6.0931 \cdot \dot{m}_{DAC} \tag{3.9}$$

In Equation 3.9, $\dot{m}_{DAC}$ denotes the amount of carbon captured using a solid-sorbent DAC unit per year. This conservative costing equation forgoes the reduction of cost with economies of scale, which would thus lead to an overall higher cost of synthetic jet fuel. DAC units are expected to significantly decrease in cost over the years as the production capacity increases [24, 88]. The replenishment of amine sorbents is not modeled herein, and are assumed to last over the lifetime of the plant.

3.1.8. Compressor

The compressor cost is based on its power rating, $\dot{W}_{cmp}$, derived in Section 2.2.8. [65]:

$$C_{cmp} = 580000 + 20000 \cdot \dot{W}_{cmp}^{0.6} \tag{3.10}$$

In Equation 3.10, C_{cmp} is the capital investment cost of the compressor. The modeling equation used herein is applicable for a certain range of compressor power ratings. These ranges were not considered in this study. The equation shows that there is a high capital investment even if the power rating is zero, which is why the utilization of low production scales have been avoided in the modeling. This modeling decision enables more representative costing that does not risk unreasonable specific costs of units.

3.1.9. Heat Exchanger

The heat exchanger is sized according to Kern's methodology for a shell and tube heat exchanger [95]. The costing of such a heat exchanger would thus depend on its area, as shown in [65]:

$$C_{hx} = 28000 + 54 \cdot A_{hx}^{1.2} \tag{3.11}$$

In Eq. 3.11, C_{hx} refers to the heat exchanger cost while A_{hx} denotes its exchange surface area, which is determined in Section 2.2.9..

3.1.10. Reactor

The costing of the reactor is a function of its volume [65], as shown in:

$$C_{rx}^{capex} = 61500 + 32500 \cdot \forall_{rx}^{0.8} \tag{3.12}$$

In Equation 3.12, C_{rx}^{capex} refers to the reactor capital investment cost, while $\forall_{rx}$ is the reactor volume derived in Section 2.2.10..

The costing of the reactor includes its catalyst constituents, and are costed as the reactor opex as:

$$C_{rx}^{opex} = c_{cat} \cdot \frac{\dot{m}_{rx,rec}}{WHSV} \tag{3.13}$$

In Equation 3.13, C_{rx}^{opex} refers to the reactor operating cost due to catalyst purchases and c_{cat} denotes the specific catalyst cost, while $\dot{m}^R$ is the mass flowrate (in kg·h^{-1}) of the reactants and $WHSV$ is the weight hourly space velocity (in h^{-1}). The fraction of the reactants' mass flowrate to the weight hourly space velocity determines the catalyst mass. The catalysts are supposed to be classified as recurring costs; i.e. these costs are repeated on a non-yearly basis. However, because the catalysts are replenished every year, then they are included in the operating costs. The catalysts' costs that were gathered are tabulated in Table A.16.

3.1.11. Distillation Column & Separator

The distillation column is an intricate unit whose sizing and costing should be executed meticulously due its large size and intensive energy demand.

Initially, a more technical model for determining the aforementioned metrics was adopted (Section VIII). Upon further iteration, the model was simplified and a number of stages was set as 5 for separators and 20 for distillation columns, which showed negligible differences in both costing and LCIA metrics.

Following the determination of the column diameter and height in Section 2.2.11., the costing Equation used is [97, 159]:

$$C_{dc}^{capex} = 17640 \cdot D_{dc}^{1.066} \cdot H_{dc}^{0.802} \tag{3.14}$$

3.1.12. Water Production

Water is purchased at a process water cost of 0.2 USD $\cdot$ m^{-3}, which is around $2 \cdot 10^{-4}$ USD $\cdot$ kg^{-1} [99]. Compared to the other feedstocks, such as CO_2 or biogas/biomass, the cost of water is relatively inexpensive.

3.1.13. Pump

Water is transported from somewhere. We use a pump to transport it within the plant using pipes. We assume no pressure drop due to lack of data regarding distances or pipe lengths. The following equation sizes the water pump [65]:

$$C_{pump}^{capex} = -1100 + 2100 \cdot \dot{W}_{pump}^{0.6} \tag{3.15}$$

In Equation 3.15, C_{pump}^{capex} is the capital cost of the pump and $\dot{W}_{pump}$ is the pump power rating which is determined in Section 2.2.13.. By nature of the costing equation, C_{pump}^{capex} could be negative if it is not within its validity range. However, the pump cost is inexpensive relative to the remaining units, so a deviation due to a negative cost of pump leads to negligible changes in the overall estimation of the jet fuel cost.

3.1.14. Biogas Production

Biogas is purchased herein, and thus the only costs associated with it are operating costs. The cost of biogas utilized is 0.06 EUR $\cdot$ kWh^{-1} [160]. In addition, the biogas produced from sewage sludge possesses a heating value that ranges between 5.8-6.4 kWh $\cdot$ m^{-3} [161]. The upper limit will be considered so as to utilize a higher cost limit. Finally, the biogas density is considered to be 1.15 kg $\cdot$ m^{-3} [162]. These values yield a biogas cost of 0.3339 EUR $\cdot$ kg^{-1}.

3.2. Process Economics

Following the expression of the various costs incurred by a process, these values of capital and operational expenses are transformed and expressed using the same temporal attribute. In this case, the economic formulation of the jet fuel production plant is expressed in terms of a net present value, such that the plant's levelized cost is estimated.

3.2.1. Capital Investment

Capital investments are paid for in year 0, prior to when the plant begins its operation. These capital costs, $CAPEX$, are expressed based on the unit processes as:

$$CAPEX = \sum_{i \in UP} C_i^{capex} \tag{3.16}$$

In Equation 3.16, C_i^{capex} represents the yearly material and energy costs of unit i in the set of unit processes (UP).

3.2.2. Operating Expenses

The total operational costs, $OPEX$, are expressed as:.

$$OPEX = \sum_{i \in UP} \left[C_i^{opex} + MAINT_i - REV_i \right] \tag{3.17}$$

In Equation 3.17, C_i^{opex} represents the yearly material and energy costs of unit i in the set of unit processes (UP), $MAINT_i$ is the yearly maintenance costs of unit i, and REV_i is any potential revenue received during the year of unit i. These costs are calculated for one year as a function of the total jet fuel output per year. Such costs are also approximated to be fixed for each year of operation during the plant's lifetime. Unless specified, the maintenance costs are approximated as 3.5% of the CAPEX cost. It is 4% in the cases of the direct air capture unit [88] and the industrial furnace [149]. Revenues are considered as negative costs, and are only present in selected units, which are tabulated in Table 3.1.

Process	Unit Process	Product	Relative Mass Output		Market Price
ALL	Electrolyzer	O_2	8	$kg_{O_2} \cdot kg^{-1}{}_{H_2}$	0.04 EUR $\cdot$ kg^{-1}
CO2ER	Co-electrolyzer	O_2	0.49084	$kg_{O_2} \cdot kg^{-1}{}_{CO}$	0.04 EUR $\cdot$ kg^{-1}
BIOHY	MeOH/CH_4 Separator	CH_4	1.2526	$kg_{CH_4} \cdot kg^{-1}{}_{MeOH}$	0.147 EUR $\cdot$ kg^{-1}

Table 3.1. The unit processes that generate revenue due to selling a byproduct: the electrolyzer, co-electrolyzer, and the methanol-methane separator of the BIOHY process. The relative mass is expressed as output mass of selling product per functional unit of the respective unit, in addition to the costs (Section 2.1.5.).

3.2.3. Currency Conversions

The unit costing equations in the literature and material and energy costs are expressed by various sources in 3 different currencies: US Dollars (USD), Euro (EUR), and Swiss Francs (CHF). The EUR is the selected currency that will be used to express costs in this study. As a result, a conversion rate

from USD and CHF to EUR is based on the averaged 2021 average exchange rate from the European Central Bank [163]. As a result, 1 CHF is converted to 0.9234 EUR and 1 USD is converted to 0.8433 EUR. Although fluctuations in the conversion rates could change the relative cost of equipment or material, it is assumed that these conversions will have negligible impact over the overall levelized cost of jet fuel and unit process cost contributions.

3.2.4. Time-value of Money

The total lifetime cost of the synthetic jet fuel plant is expressed as a net present cost. In other words, all annual operating costs (OPEX) or revenues will be converted to their equivalent present values. This conversion is expressed using the uniform series present-worth factor, j, which is defined by:

$$j = \frac{(1 + r_{ds})^{N_{yr}} - 1}{r_{ds}(1 + r_{ds})^{N_{yr}}} \tag{3.18}$$

In Equation 3.18, r_{ds} is defined as the annual discount rate (or weighted cost of capital [164]), and N_{yr} is the plant's number of operational years. Thus, j converts the annual OPEX costs to their present value equivalent. Literature values of the discount rate vary between 8-10% [144, 165]. For renewable energy projects in Switzerland, an discount rate of 5% is commonly used [166, 167]. As a result, a value of 5% will be utilized in the Equation 3.18 since this project is part of the synfuel initiative.

3.2.5. Levelized Cost of Jet Fuel

The cost of an energy product could be estimated by various ways. The levelized cost is a commonly used metric to cost energy. However, this metric exhibits several limitations associated with the discounted costs over time, which could render the estimate unrealistic [168]. The cost of jet fuel referred to herein is defined as the minimum selling price of jet fuel that is required to generate a net present value of zero [169]. The expression of the levelized cost of jet fuel, c_{JF}, is thus:

$$c_{JF} = \frac{CAPEX + j(OPEX)}{m_{JF,yr} \cdot j} \tag{3.19}$$

In Equation 3.19, $m_{JF,yearly}$ refers to the yearly jet fuel output generated by the synthetic jet fuel production plant. The output capacity and the discount rate (expressed through j) can influence the eventual cost quite significantly, which necessitates their explicit definition, espeically for comparison and validation purposes.

3.3. Results & Discussion

The levelized cost of synthetic jet fuel of the 3 considered processes are compared with the petroleum-based jet fuel and then further evaluated as a function of cost of electricity.

3.3.1. Cost Analysis

The levelized cost of synthetic jet fuel represents a key factor in the decision making regarding a transition towards sustainable jet fuels. The cost of the synthetic jet fuel produced of the 3 processes and their breakdown is visualized in Figure 3.2.

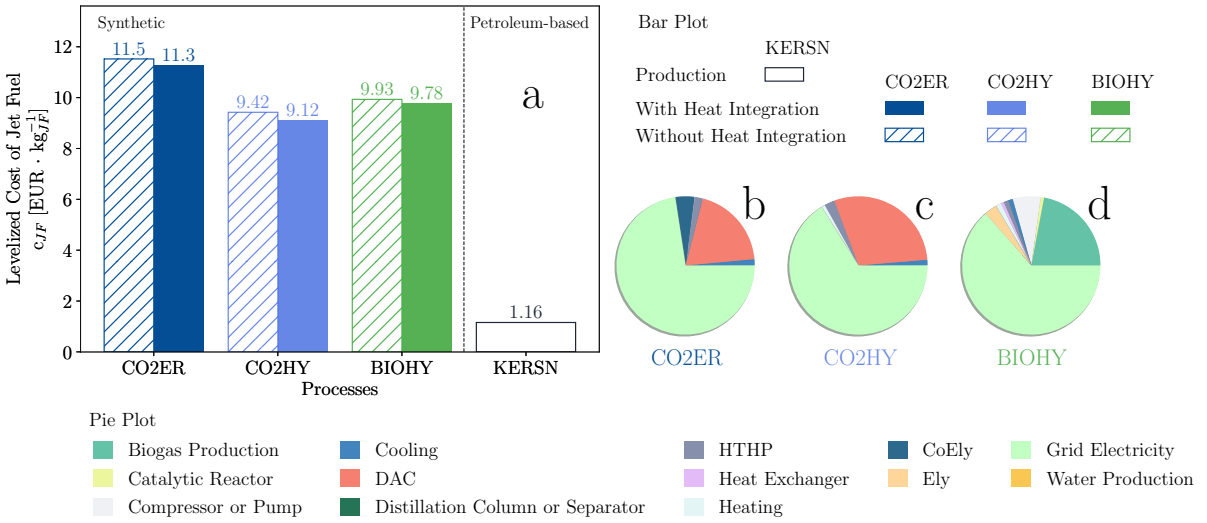

Figure 3.2. The variation in the levelized cost of jet fuel, c_{JF} (a), produced by the synthetic jet fuel production processes (*CO2ER*, *CO2HY*, *BIOHY*). The impact categories are shown for each process without and with heat integration, highlighting the significant reduction when recovering heat in these processes. The cost for producing the synthetic jet fuel of each process is compared to that of the conventional petroleum-based jet fuel. A breakdown of the cost for the *CO2ER* (b), *CO2HY* (c), and *BIOHY* (d) processes highlights the unit processes contributing to the costs of the heat integrated synthetic processes, highlighted using the pie charts. Feedstock-related units generate are the highest contributors to the cost for the 3 synthetic jet fuel production processes: the DAC unit to capture CO_2/biogas production and electricity (most of which to produce H_2) whose cost is set at 0.195 EUR · kWh^{-1} [147]. The cost values are determined using a 5% discount rate, plant lifetime of 20 years, and production scale of 10 Mton of jet fuel per year.

Figure 3.2 (a) shows the levelized cost of jet fuel, c_{JF}, for the 3 synthetic processes. At first glance, the effect of heat integration on the cost can be deduced to be relatively minimal. Nevertheless, this cost reduction is certainly beneficial since the synthetic processes produce jet fuel at a cost of 9-10 times higher than the petroleum-based jet fuel. Such a factor renders the synthetic jet fuel via the assessed processes noncompetitive with respect to the current market price of petroleum-based jet fuel at 1.16 EUR · kg^{-1}_{JF}.

Figures 3.2 (b), (c), and (d) decompose the synthetic jet fuel cost (for the heat integrated processes of Figure 3.2 (a)) by showing the cost distribution across the units. The costs of incurred by the units are either capital investments at year 0 or yearly operating costs, both of which are transformed to the present time via Equation 3.18. The contribution of the grid electricity in Figures 3.2 (b), (c), and (d) is clearly the highest, as it contributes to around 63-72% of the levelized cost of jet fuel. The high levelized costs of the synthetic jet fuels in Figure 3.2 (a) can then be explained by the high contribution of electricity, whose levelized cost is that of the Swiss households at 0.195 EUR · kWh^{-1}. Such a value for electricity is higher than the world average, but is also nearly half the cost of electricity charged by some countries [170].

Naturally, chemical plants producing sustainable fuels would not only be charged the rate sold to businesses, but these production plants also could benefit from financial incentives to encourage the production of climate-friendly fuels. Thus, while the presented costs are quite high compared to the conventional jet fuel, a cheaper electricity price can significantly reduce the overall cost since the electricity contribution, which is predominantly utilized for H_2 production (Figure 2.18).

The second highest cost contributor is that of the DAC unit for the *CO2ER* (19.5%) and *CO2HY* (29.4%) processes, and the biogas cost for the *BIOHY* (22%) process. The underlying similarity between these second highest cost contributors is that they correspond to the second feedstock for all 3 processes. The cost of direct air capture was conservatively sized to avoid the unrealistically optimistic sizing methods in the literature, which lead to a very low levelized cost of 150 EUR $\cdot$ $t^{-1}_{CO_2}$ [88]. Such a levelized cost of CO_2 is over a third of the more realistic levelized costs reported by Climeworks at roughly 500 EUR $\cdot$ $t^{-1}_{CO_2}$ [24]. The costing method used here developed by Young et al. [158] is rather more conservative, since the cost is estimated to be linearly increasing as a function of capacity. In practice, the effect of economies of decreases the levelized cost with growing capacity, which is a feature not present in this model due to lack of data. Particularly, the evaluated plant was that of Climeworks in Hinwil [158], whose output is rather low and thus overestimates the cost when extrapolating linearly into higher scales and larger capacities. Thus, the contribution of direct air capture to the cost can decrease significantly, with continuous production and capacity increases over time promising cost reductions [24].

The remaining costs in Figures 3.2 (b), (c), and (d) are mainly attributed to the HTHP, cooling, heating, compressor/pumps, and the electrochemical units. The CoEly unit contributes to 4.5% of the levelized cost, which is an added cost not incurred in the other processes. Nevertheless, this unit does on average enable lower required heating and cooling loads, and thus provides savings elsewhere (Figure 2.19). The remaining energy sources, such as HTHP, absorption chiller, and fired furnace contribute to a combined 3.4%, 4.53%, and 3.5% in the *CO2ER*, *CO2HY*, and *BIOHY* processes respectively. Furthermore, the electrolyzer unit accounts for 2.93% of the cost of synthetic jet fuel produced via the *BIOHY* process; in contrast, Figures 3.2 (b) and (c) show no cost contribution by the electrolyzer. The reason behind the electrolyzer's lack of contribution is that at such high scales of production (10 Mton of jet fuel), the nonlinearly scaling electrolyzer cost is outweighed by revenue incurred by selling the oxygen byproduct, even at a relatively low selling price of 40 USD/ton of O_2. This behavior is not present for the *BIOHY* process, because the electrolyzers are sized separately for one biogas production plant, and then scales linearly, Thus, the equipment in the first part (Section **??**) of the *BIOHY* process do not benefit from economies of scale. For this reason, Figures 3.2 (d) also shows visible cost contributions by the compressors/pumps, heat exchangers, and reactors, amassing 8% of its levelized cost.

The takeaway from Figure 3.2 is that despite the high costs, promise still exists for decarbonizing aviation with a relatively cost competitive fuel. The high levelized costs of 9-11 EUR $\cdot$ kg^{-1}_{JF} are generated using a very conservative costing approach, hence indicating potential for cost reductions once more data is available and if electricity costs decrease. These cost values thus present an upper bound to the synthetic jet fuel costs using the technology available. In addition, the cost breakdown identifies which facets are in fact contributing to such high costs. The breakdown would then help in process design decisions in an iterative process design-life cycle assessment approach to minimizing synthetic jet fuel costs and emissions.

3.3.2. Cost of Electricity

To establish a better comparison with the literature cost values for synthetic values and investigate the effect of electricity, a benchmarking of the levelized cost of jet fuel is performed. Data points corresponding to results from literature studies are plotted at the cost of electricity used, such that a more valid comparison is established. The benchmarking is thus visualized in Figure 3.3.

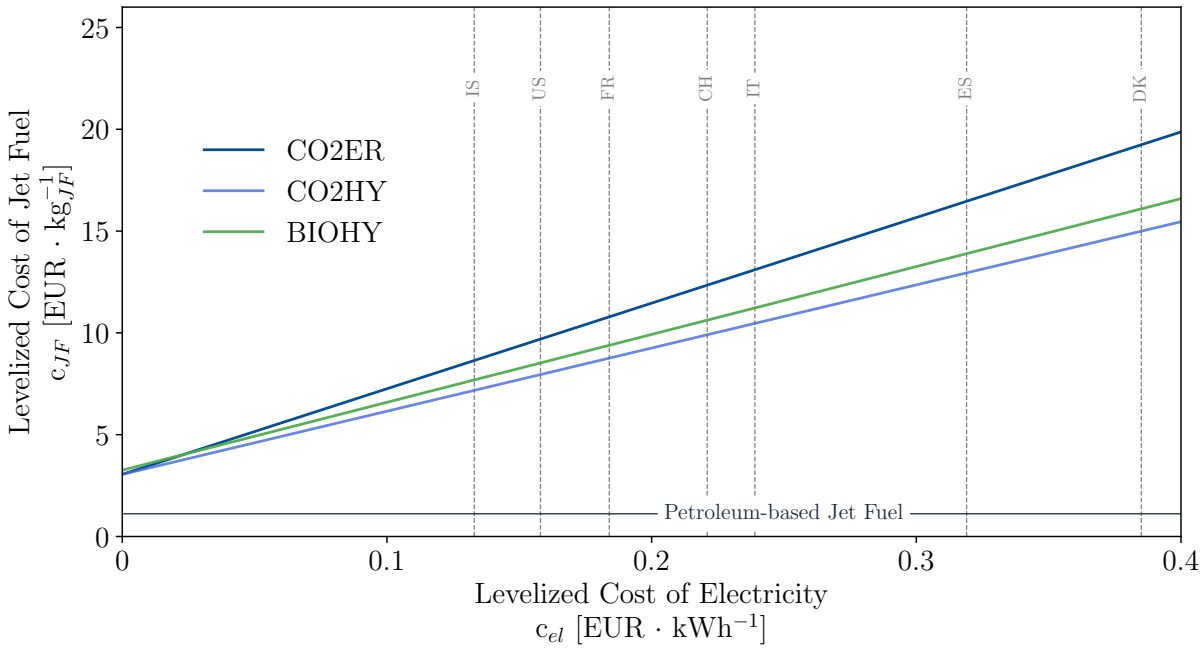

Figure 3.3. The evolution of the levelized cost of synthetic jet fuel, c_{JF}, as a function of the levelized cost of electricity, c_{el}, for the 3 production processes (*CO2ER*, *CO2HY*, *BIOHY*). The value is referenced to the petroleum-based jet fuel, denoted by the horizontal line, whose cost is 1.115 EUR · kg_{JF}^{-1} [35]. The dashed lines represent the cost of electricity of selected countries [170] such as: Switzerland (CH; without DE imports), France (FR), Germany (DE), Italy (IT), Spain (ES), Denmark (DK), and Iceland (IS). The levelized cost is determined at a yearly jet fuel output of 10 Mton, plant lifetime of 20 years, and 5% discount rate.

Figure 3.3 highlights the dependence of the levelized cost of jet fuel, c_{JF}, on the cost of electricity, c_{el}, for each of the 3 synthetic processes. The importance of this dependence was indicated in Figure 3.2, where the electricity cost contribution was shown to be around 65% of the levelized cost of jet fuel. The dependence of the levelized cost of jet fuel on the cost of electricity is naturally linear for all the processes, with the *CO2ER* and *CO2HY* processes both showing the lowest cost at 3.05 EUR · kg_{JF}^{-1} , followed *BIOHY* process with 3.25 EUR · kg_{JF}^{-1} . Even if electricity were free, the levelized cost of the 3 processes would be 3 EUR · kg_{JF}^{-1}, 3 times higher than the petroleum-based one. These electricity-free costs render synthetic jet fuels using the current state of these process completely noncompetitive. Moreover, due to the varying quantities of electricity required by each process, as portrayed in Figure 2.18, the difference in levelized cost of the processes diverges as the cost of electricity increases. The *CO2ER* specifically diverges and could reach as high as 19 EUR · kg_{JF}^{-1} if produced in Denmark. Upon considering the selected countries, the production cost of synthetic jet fuel via *CO2HY* process, which has the lowest cost, would range from 7 EUR · kg_{JF}^{-1} in Iceland to 15 EUR · kg_{JF}^{-1} in Denmark. These costs of electricity are assumed to be fix, and do not take into account the variation in cost due to the increase in demand, which could even further increase the cost of jet fuel production in Switzerland beyond 9.12 EUR · kg_{JF}^{-1}. Nevertheless, the selected countries are in Europe and the US, which typically are marked by relatively high electricity prices. Electricity prices below 0.1 EUR · kWh^{-1} exist in several countries [170], which could lead to synthetic jet fuel costs of below 6 EUR · kg_{JF}^{-1}. The

problem therein lies with the often high-carbon electricity associated with low costs of electricity in these countries.

In summary, the levelized cost of jet fuel via synthetic processes remains relatively high relative to the conventional process, even if electricity costs are completely abolished. The electricity prices will not unrealistically decrease in the future, which necessitates that more research and development instead be diverted to decrease the amount of electricity needed per kg of jet fuel (Figure 2.18), which would decrease slope of the lines in Figure 3.3 and make the cost a weaker function of the price electricity price. Nevertheless, a consequence of the trend shown in Figure 3.3 is the highlighted notable effect of geography in the production of jet fuel, which necessitates the consideration of the global supply chain when considering jet fuel production in light of the high electricity demands that would arise.

4

Global Supply Chain Optimization

Synthetic jet fuel production should not be examined through the limited scope of a single country. Instead, a global supply chain should be examined to identify the optimal locations for jet fuel production. Since the environmental footprint and economic metrics associated with jet fuel are largely location-dependent (refer to Figure 2.20 and 3.3), a more realistic assessment of the cost and carbon footprint of jet fuel can be achieved by evaluating the production in various countries. Consequently, such an assessment can incorporate the transportation of jet fuel to account for and minimize transport costs and GHG emissions.

The current situation regarding electricity production capacity proves that it is very difficult to produce sufficient amounts of synthetic jet fuel. This difficulty is shown upon combining the values of the current jet fuel demand globally (330 Mtons [53]) and the required electricity to convert CO_2 and H_2O to the synthetic jet fuel (31 kWh $\cdot$ kg_{JF}^{-1}), which would amount to a third of the global electricity production (27000 TWh in 2021 [171]). For this reason, the production of jet fuel will be examined using projected electricity production in 2050.

By leveraging datasets covering current and future electricity characteristics, transportation routes, as well as the global jet fuel demand, country-based metrics for GHG and cost are utilized in a global supply chain optimization algorithm to determine the optimal hubs for synthetic jet fuel production. The supply chain considers as many nations as possible, which is limited by the available dataset entries, in order to determine the optimal hubs for producing and supplying synthetic jet fuel to meet the global demand. By virtue of its low GHG emissions and low costs compared to the remaining processes, the *CO2HY* process is selected as the process by which synthetic jet fuel is produced.

4.1. Geography-dependent Inputs

The utilized datasets enable the economic and environmental assessment of jet fuel produced in the considered countries and establish connecting routes between these countries. Moreover, this data serves as an input into the optimization model, and it reflects the most recent data available.

Each dataset consists of a unique set of countries, which is not necessarily the same for other datasets. As a result, the jet fuel supply and demand of a given country is modeled if it possesses an entry in all the utilized datasets. Otherwise, the country is filtered out and not modeled. The final set of modeled countries in the global supply chain amounts to 140 countries.

4.1.1. Meteorological Parameters

Each country exhibits distinct meteorological patterns that can distinguish it in terms of renewable energy production capacity. Such a factor is quantified in the capacity factor, CF,

which quantifies the ratio of total energy produced by an energy system to a theoretical maximum energy produced.

The renewable energy systems whose capacity factors are utilized are wind turbines and photovoltaic (PV) cells. The capacity factor value for each country was collected by using the country's longitude and latitude coordinates in PV [172] and wind [173] potential maps. While a generalized coordinate pair for each country might not represent the regions with the highest potentials and could instead represent densely population locations with limited land for a chemical plant, this input will be utilized to approximate the country's meteorological parameters. Furthermore, the solar dataset was limited and did not cover high latitudes, thus omitting countries such as Iceland and Finland. Because both countries consist of economies with relatively high jet fuel demand and high potential for jet fuel production [48, 174], their capacity factor was approximated by using that of Sweden, since both Iceland and Finland are situated at very similar latitudes as Sweden.

4.1.2. Grid Electricity

The electricity required by the chemical plants is supplied by the local electricity grid of each country. As previously highlighted, the electricity production capacity in 2022 is not sufficient to realistically incorporate the production of synthetic jet fuels in volumes that can mark a transition away from petroleum-based jet fuel. As a result, the modeled grid electricity mixes refer to those that are projected to be built and integrated in the year 2050. These projections are derived from the study of Jacobson et al. [175], whose work estimated the distribution of various renewable energy technologies (solar, onshore/offshore wind, hydro, etc.) that would form entirely renewable electricity mixes of 145 countries in 2050. This distribution was specific to the countries and reflected their capability of leveraging their available natural resources to shift their grid electricity mixes to become independent of fossil fuels. The calculations provided by Jacobson et al. [175] also quantify the total electrical energy produced by the countries in 2050, while also accounting for the intermittency of these energy sources. The estimated increase in the generated electrical energy factors the residential and industrial requirements/needs of the 145 countries considered, which renders this study suitable to reflect reasonable projections of the electrical production capacity and the mix constituents. In particular, the data derived from this study [175] can demonstrate the relative increase in electrical capacity, which can be associated with a country's capability of producing synthetic jet fuel by utilizing part of this added capacity. This production capability is expressed using:

$$\Delta E_{avail,j} = E_j^{2050} - E_j^{2020} \tag{4.1}$$

In Equation 4.1, $\Delta E_{avail,j}$ is the increase of annual electrical energy production of a country j, while E_j^{2050} and E_j^{2020} are the electrical energy production in country j in years 2050 and 2020 respectively. E_j^{2050} is derived from the study of Jacobson et al. [175], while E_j^{2020} is derived from that of Ritchie & Roser [171]. By limiting the jet fuel production using electrical energy to the amount of energy quantified by $\Delta E_{avail,j}$, the synthetic jet fuel production is ensured not to interfere with the current local population demand for electricity. In fact, Jacobson et al. [175] accounted for the need for kerosene and other synthetic fuels as part of the renewable energy expansion. However, this data is not directly accessible. For this reason, a fraction of the increase in energy $\Delta E_{avail,j}$ is considered herein to represent the maximum available energy for synthetic jet fuel production.

Following the establishment of the electrical capacity increase, the environmental and economic metrics associated with the local grid electricity are derived. These metrics define the characteristics of the electricity mix utilized to produce synthetic jet fuel. As such, the carbon intensity of electricity is defined based on the share of renewable energy technologies projected by Jacobson et al. [175]. Thus, the climate change impact of electricity in 2050, $GHG_{el,j}^{2050}$, is defined by:

$$GHG_{el,j}^{2050} = \sum_{k \in RET} f_{j,k} \cdot GHG_{ref,k} \cdot s_{j,k} \tag{4.2}$$

In Equation 4.2, $f_{j,k}$ denotes the fraction of RET k used in country j, $GHG_{ref,k}$ refers to the climate change impact of a RET in set k of a reference country, and $s_{j,k}$ is a scaling factor for the GHG of the RET k in country j. The same equation form of Equation 4.2 is utilized to reflect the life cycle impact metrics denoting the remaining examined emissions (refer to Chapter 2). Such a formulation determines a weighted average emissions of the various renewable energy systems implemented. The scaling factor quantifies the added or reduced electricity emissions, which is correlated with the country's capacity factor of a given RET. This is particularly important for solar and wind production. For the remaining RET, the scale is set to 1, which approximates that the emissions due to energy production via geothermal, hydro power, wave device, and tidal turbine, do not change as a function of location. Thus, the equation is shown in:

$$s_{j,k} = \frac{CF_{ref,k}}{CF_{j,k}} \tag{4.3}$$

In Equation 4.3, $CF_{j,k}$ and $CF_{ref,k}$ are the capacity factors of the renewable energy technology k in country j and a reference country respectively. The capacity factors are derived using the methodology highlighted in Section 4.1.1.. Because the utilized life cycle inventory [51, 143] accounts for the country-specific yields and weather patterns in the production of a unit of energy (1 kWh), it is imperative to adjust the emissions by scaling the emissions using country-specific intermittency factors, which is quantified by the capacity factor. Particularly, the solar PV inventories [143] are based on an average annualized value of solar energy production in kWh·kWp^{-1}, which is a metric that is directly correlated with the solar capacity factor. Thus, the emissions associated with generating 1 kWh in country j is inversely scaled by the ratio of its capacity factor for RET k to that of a reference country, whose emissions are accounted for in $GHG_{ref,k}$. In other words, if a country has a higher potential for harvesting solar power relative to a reference country, then its solar capacity factor would be higher than that of the reference country. As a result, producing 1 kWh via solar panels would require less emissions in that country compared to the reference country due to the reduction in required equipment or area required because of intermittency. The reference values and countries are tabulated in Table A.17 in the appendix. Utilizing the carbon intensity of today's RET could be a limiting factor, since emissions would decrease as the technologies become more efficient. Utilizing today's carbon intensities is nevertheless a good starting point in the prediction of future emissions.

The electricity costs utilized herein are based on the household electricity prices that are available in the globalpetrolprices database [170]. The entries of this database were compared and validated with the OECD database for European entries [176]. While these values do not necessarily represent the prices that will be in effect in 2050, this approximation remains useful since electricity prices are rather reflected by local supply and demand [177], which is assumed to remain similar in 2050. Thus, the local population and business demand is assumed to remain similar between today and 2050 in a given country. As a result, similar supply-demand dynamics and should lead to maintaining similar electricity prices as those of today.

To summarize, the electricity mixes of countries in 2050 are derived from the projected distribution of Jacobson et al. [175]. The increase in capacity for electricity production is used as a pivotal quantity describing the available electricity for synthetic jet fuel production in 2050. The carbon intensity of these mixes is estimated by correlating the emissions with the country's capacity factors for certain renewable energy technologies (Table A.17), while the 2050 electricity cost per kWh is retained from the 2021 prices [170].

4.1.3. Shipping Routes

The shipping routes are determined via the CERDI-seadistance database [178], which provides the shortest and conventionally utilized shipping distances between 227 countries. The database showcases the shortest sea distance between each pair of countries, and when possible the shortest distance by land connecting the pair of capitals. In the case of the former, additional land distance is included that connects each of the countries' ports to their corresponding capital. Thus, the country capital cities are connected, which is a reasonable generalization of jet fuel transport since these cities typically possess the countries' largest airports, which would require more jet fuel supply. Similarly, it is assumed that the chemical plants are set up near the capital cities.

When establishing the shipping distance (in km) to country i from country j, $x_{i,j}$, the shortest distance between land or sea is chosen. However, the chosen value for $x_{i,j}$ might not necessarily be the distance generating the lowest GHG emissions. Nevertheless, the GHG emissions between train and sea are both typically low, so this is considered an adequate approximation.

The selection of supply routes amongst different countries is influenced by incorporating transport GHG emissions, GHG_{tpt}, and costs, c_{tpt}. If the shortest shipping route is by land, then GHG_{tpt} and c_{tpt} strictly refer to those of land transportation. In contrast, both land and sea transport are accounted for if the sea transportation is the shortest distance, accounting for the transport from port j to port i and the land distance from capital city j to port j and that from port i to capital city i. Moreover, transportation by sea is modeled as using a tanker ship, while land transportation is assumed to utilize rail transport. However, the land distance in the CERDI-seadistance database represents the shortest distance between the capitals [178], which is not necessarily the paths typically followed by rail transport. In addition, some countries are completely devoid of railway networks. Nevertheless, it is assumed that the shortest direct distance applies for railways in all countries since GHG emissions due to railway transport are amongst the lowest in terms of transportation modes [179]. Another key assumption is using a general value of GHG emissions for transporting the jet fuel via railway, which helps in simplifying the model. The emission and cost metrics for sea and land transport are thus shown in Table 4.1.

	Transport Mode	c_{tpt} [EUR · km^{-1} · ton^{-1}]	GHG_{tpt} [kg_{CO_2} · km^{-1} · ton^{-1}]
Sea	Tanker	0.0049	0.0075
Land	Rail	0.04	0.036

Table 4.1. The emission and cost metrics utilized for sea and land transport. The emission values consist of ecoinvent data (sea: "transport, freight, sea, tanker for liquid goods other than petroleum and liquefied natural gas", land: "transport, freight train, electricity") [51], in addition to transport cost values [180]. These values are utilized to optimize jet fuel transport and production. Note that the EUR values are in 2018 EUR.

4.1.4. Jet Fuel Demand

Determining the optimal synthetic jet fuel production locations globally necessitates accounting for the jet fuel demand and consumption of as many countries as possible. The amount of jet fuel required by each country affects the flow of synthetic jet fuel between countries, and the variation of this demand could result in relocating the jet fuel production locations. Such changes would be owed to the cost and GHG emissions generated by transport, as explained in Section 4.1.3.. For this reason, the domestic jet fuel demand can significantly impact the global supply chain, and it is determined by the US Energy Information Adminstration (EIA) database [53]. The total jet fuel demand in 2019 was roughly 330 Mtons.

Following the filtration of countries that do not have sufficient data entries to be modeled, the demand of the selected countries represents 99.1% of the global demand, which would in turn validate the results as being representative of the global situation. As a result, 140 countries consume 99.1% of the global jet fuel demand.

4.1.5. Life Cycle Metrics

The life cycle metrics are imported directly from the results from Sections 2.4. and 3.3.. The synthetic jet fuel production GHG emissions are defined by $GHG_{JF,j}$, which refers to the amount of CO_2 emitted when producing 1 kg of jet fuel in country j. The total production GHG emissions scale linearly as a function of $GHG_{JF,j}$ due to the nature of the life cycle assessment methodology [181]. Compared to the LCA of synthetic jet fuel production in Switzerland (Section 2.4.1.), the main geography-dependent activity is only that of electricity. The reason behind this is that electricity GHG emissions are the main contributors to GHG emissions (Figures 2.18 and 2.20), which implies that the other units do not have notable contributions and thus not changing them to regional activities maintains the model's simplicity through this reasonable approximation. Similarly, the electricity utilized in the background for manufacturing equipment is kept the same (high voltage, electricity production in Switzerland), which is a reasonable approximation due to low contribution of manufacturing of equipment. Other activities, such as the production of metals are often specific to certain locations, as is the case for platinum production in South Africa or Russia [81].

The cost function established in Section 3.3. is highly nonlinear and accounts for the economies of scale exhibited by chemical plants. Thus, the production cost can be expressed as a nonlinear function of produced synthetic jet fuel; however, to simplify the model, a linear approximation is utilized. The LCOJF (Equation 3.19) is used directly at a production capacity instead of using a nonlinear cost as a function of jet fuel output (Figure 5.1). The cost of producing jet fuel in country j, denoted by $c_{JF,j}$, is the levelized cost of jet fuel. This quantity is assumed to scale linearly. If more countries are producing synthetic jet fuel, then the total incurred cost would be higher in more countries since more plants are built and operated. This implies that the estimated cost of jet fuel via this linearization potentially underestimates its actual cost. Nevertheless, this simplification allows the optimization model to remain linear in nature. In addition, if various processes are considered in the optimization, then a nonlinear cost expression could change the relative assessment of the processes at different scales, since the processes have different units that scale differently with size. For example, process A could produce cheaper jet fuel than process B at low production scales, but produce more expensive jet fuel at higher scales if A scales linearly and B scales logarithmically. Such an error presented

by non-linear effects has no influence herein since only one process is considered as a pathway to produce synthetic jet fuel.

4.2. Problem Formulation

The purpose of this optimization problem is to minimize the emissions and costs associated with the life cycle of synthetic jet fuel. The life cycle is extended to include transportation of jet fuel, which elevates production locations of synthetic jet fuel to an important parameter. As shown in Figures 2.20 and 3.3, the effect of production location can be substantial in making synthetic jet fuel a feasible petroleum substitute. Thus, the goal of this section is to introduce and discuss the parameters and their relationships, in order to answer the following question: where should synthetic jet fuel be produced if the target is cost or GHG emission minimization?

Accounting for realistic transport and jet fuel supply necessitates the inclusion of transportation costs and GHG emissions. Thus, the general optimization framework is detailed herein, which will feed into the 3 optimization schemes (Sections 4.2.1., 4.2.2., and 4.2.3.) as constraints and objective functions. The optimization problems are solved using MATLAB's "linprog" function, which is a linear programming function. The solver was set to utilize the interior point method to determine the global optimum [182].

The primary optimization variable, $n_{i,j}$, is defined as the amount of jet fuel (in kg) that would be supplied to country i from country j. When non-zero, $n_{i,j}$ denotes that a shipping route between country i and country j is favored. This continuous variable is thus constrained by:

$$n_{i,j} \geq n^{UB} \tag{4.4}$$

In Equation 4.4, n^{UB} is an upper bound that is set to the total global demand as a practical upper limit. A lower bound is also defined by:

$$n^{LB} \leq n_{i,j} \tag{4.5}$$

In Equation 4.5, n^{LB} is a value for the lower bound, which in this case is set to zero, such that negative or reverse supplies are avoided. No constraints are enforced on a country supplying jet fuel to itself, which implies that $n_{j,j} \geq 0$.

Moreover, the supply of country i is satisfied by reaching a supply that is equal to its demand, ∂_i. This constraint is expressed in Equation 4.6:

$$\sum_{\forall\, j \in C} n_{i,j} = \partial_i \tag{4.6}$$

From a production perspective, the total amount of jet fuel produced from a supplying country j is expressed as:

$$\sum_{\forall\, i \in C} n_{i,j} = S_j \tag{4.7}$$

In Equation 4.7, S_j refers to the amount of jet fuel produced in a country j. This variable contributes directly to the total GHG emissions or cost.

To establish a realistic production capacity that reflects each country's available electricity, current and projected electricity production capacities are utilized. The increase in the electricity production of each country between 2020 and 2050 reflects in part the energy production that is increased to support the transition from fossil fuel-based systems to sustainable energy systems. Thus, this available electricity is expressed as:

$$E_{JF,j} = \alpha \cdot \Delta E_{avail,j} \tag{4.8}$$

In Equation 4.8, $E_{JF,j}$ is defined as the electricity that is considered available in country j to be dedicated to synthetic jet fuel production, while α is the fraction of the available electricity dedicated to jet fuel production. α is difficult to estimate with high certainty since the available electricity in each country that can be attributed to jet fuel production depends on countless factors that include the countries' economic and population growth and requirements. This fact renders α as country-specific; in this formulation, it is assumed to be the same in all countries due to insufficient data for its quantification. For this reason, the α is parametrized to cover a range of potential values. Naturally, these values would range between 0 and 1, but it is parametrized to consist of values beyond 1 to account for potential scenarios that surpass the electricity increase quantified by ΔE, such as for a projection beyond 2050. The significance of $E_{JF,j}$ is thus highlighted through the relative production capacity of the countries, which would limit the produced jet fuel in a given country based on its available capacity. This is highlighted in the following equation:

$$S_j \cdot W_{CO2HY} \leq E_{JF,j} \tag{4.9}$$

In Equation 4.9, W_{CO2HY} refers to the electric energy required to produce 1 kg of synthetic jet fuel via the *CO2HY* process, whose electricity input is the lowest amongst the 3 evaluated processes (31 kWh; Figure 2.18). This inequality limits S_j by establishes an upper limit as a function of available electricity, $E_{JF,j}$, which demonstrates a more realistic production capacity limitation.

Finally, the cost and GHG emissions per kg of jet fuel (including production and transportation) are expressed respectively in Equations 4.10 and 4.11:

$$C^{sc} = \underbrace{\sum_j \left[c_{JF,j} \cdot S_j\right]}_{\text{production}} + \underbrace{\sum_j \sum_i \left[c_{tpt} \cdot x_{i,j} \cdot n_{i,j}\right]}_{\text{transportation}} \tag{4.10}$$

$$GHG^{sc} = \underbrace{\sum_j \left[GHG_{JF,j} \cdot S_j\right]}_{\text{production}} + \underbrace{\sum_j \sum_i \left[GHG_{tpt} \cdot x_{i,j} \cdot n_{i,j}\right]}_{\text{transportation}} \tag{4.11}$$

In Equation 4.10, C^{sc} represents the total cost of synthetic jet fuel production and transportation, while GHG^{sc} refers to the total GHG emissions generated due to synthetic jet fuel production and transportation in Equation 4.11. C^{sc} and GHG^{sc} are divided by the fixed value of the total jet fuel demand, represented by $\sum_j S_j$, to determine the resulting cost and emission values per unit of synthetic jet fuel.

Table 4.2 summarizes the key parameters and variables utilized that are utilized in the optimization problems.

Given that all variables highlighted in Table 4.2 are expressed in a linear formulation (as

Symbol	Unit	Brief Description
$n_{i,j}$	$kg_{JF} \cdot yr^{-1}$	Amount of synthetic jet fuel produced in country j and delivered to country i
∂_i	$kg_{JF} \cdot yr^{-1}$	Yearly jet fuel demand of country i (based on 2019 data) [53]
S_j	$kg_{JF} \cdot yr^{-1}$	Total production of synthetic jet fuel in country j
W_{CO2HY}	$kWh \cdot kg_{JF}^{-1}$	Amount of electricity needed to produce 1 kg of synthetic jet fuel via *CO2HY*
$\Delta E_{avail,j}$	TWh	Maximum available electricity, defined by the increase in annual electricity production (2020 to 2050)
α	-	Fraction of electricity that can be dedicated to synthetic jet fuel production
$GHG_{JF,j}$	$kg_{CO_2} \cdot kg_{JF}^{-1}$	GHG emissions associated with producing 1 kg of synthetic jet fuel in country (via CO2HY process) j
$c_{JF,j}$	$EUR \cdot kg_{JF}^{-1}$	Levelized cost of synthetic jet fuel if produced in country j (via CO2HY process)

Table 4.2. The variables and parameters that define the supply chain optimization algorithm as constraints and objective functions. These main optimization variable is $n_{i,j}$, with most of remaining quantities serving as input parameters from the datasets or derived from Chapter 2 and 3. W_{CO2HY} and α have a direct effect on the quantity of synthetic jet fuel that can be produced: if α increases, then there is more available electricity that can be used for synthetic jet fuel; if W_{CO2HY} decreases, then more electricity is available since the process would be less electricity-intensive.

highlighted in Section 4.1.5.), the optimization problem is a linear program, regardless of whether cost or GHG emissions are minimized. A linear program is particularly useful to ensure global optimality of the generated results [100]. 3 optimization schemes are thus assessed in each of sections 4.2.1., 4.2.2., and 4.2.3., with varying constraints and objective functions. The developed schemes are simple and consist of only a few constraints but consist of abundant geographical data inputs (Section 4.1.).

4.2.1. Cost Minimization

The optimization problem herein strictly targets the minimization of the cost of synthetic jet fuel that will satisfy the global demand and determine the optimal supply chain. No emission constraints are included since the objective of this problem is to assess the range of synthetic jet fuel cost. The scheme for the aforementioned problem is defined in Scheme S1.

$$\text{minimize} \quad \sum_j \left[c_{JF,j} \cdot S_j\right] + \sum_j \sum_i \left[c_{tpt} \cdot x_{i,j} \cdot n_{i,j}\right] \tag{S1.1}$$

$$\text{subject to} \quad S_j - \sum_i n_{i,j} = 0 \qquad \forall j \in C \tag{S1.2}$$

$$\partial_i - \sum_j n_{i,j} = 0 \qquad \forall i \in C \tag{S1.3}$$

$$n^{LB} - n_{i,j} \leq 0 \qquad \forall i,j \in C \tag{S1.4}$$

$$n_{i,j} - n^{UB} \leq 0 \qquad \forall i,j \in C \tag{S1.5}$$

$$S_j \cdot W_{CO2HY} - E_{JF,j} \leq 0 \qquad \forall j \in C \tag{S1.6}$$

Scheme S1. The scheme describing the optimization problem formulation that minimizes synthetic jet fuel cost (Equation S1.1).

The life cycle cost of synthetic jet fuel that will be documented reflects the production and transportation costs. In addition, the optimal solution ensures that the local jet fuel demand of countries is satisfied (Equation S1.4) while the production and supply of jet fuel from each country j to country i is determined based on the total cost (Equation S1.1 and S1.3) and the available electricity (Equation S1.6). The fraction of electricity dedicated to jet fuel, α, is altered so that $E_{JF,j}$ varies (Equation S1.6) to show the minimal synthetic jet fuel cost in various possible supply chain scenarios.

4.2.2. Emission Minimization

The considered optimization problem aims to minimize the total GHG emissions of synthetic jet fuel, in order to determine the resulting GHG emissions irrespective of the cost per unit of jet fuel. This problem is shown in Scheme S2.

$$\text{minimize} \quad \sum_j \left[GHG_{JF,j} \cdot S_j\right] + \sum_j \sum_i \left[GHG_{tpt} \cdot x_{i,j} \cdot n_{i,j}\right] \tag{S2.1}$$

$$\text{subject to} \quad S_j - \sum_i n_{i,j} = 0 \qquad \forall j \in C \tag{S2.2}$$

$$\partial_i - \sum_j n_{i,j} = 0 \qquad \forall i \in C \tag{S2.3}$$

$$n^{LB} - n_{i,j} \leq 0 \qquad \forall i,j \in C \tag{S2.4}$$

$$n_{i,j} - n^{UB} \leq 0 \qquad \forall i,j \in C \tag{S2.5}$$

$$S_j \cdot W_{CO2HY} - E_{JF,j} \leq 0 \qquad \forall j \in C \tag{S2.6}$$

Scheme S2. The scheme describing the optimization problem formulation that minimizes synthetic jet fuel GHG emissions (Equation S2.1).

The life cycle GHG emissions of synthetic jet fuel are divided into production and transportation emissions. Similarly, the solutions account for countries' demand requirements (Equation S2.3) by respecting supply limitations invoked by the available electricity (S1.6). The supply routes and production locations are determined with the objective of minimizing the total emissions (Equation S2.1 and S1.3). The parameter α, and thus $E_{JF,j}$, are varied to study the optimal supply chain as a function of the available electricity, as in Section 4.2.1..

4.2.3. Cost-Emission Tradeoff

The problem attempts to demonstrate the tradeoff between to minimization of synthetic jet fuel cost and GHG emissions to present. This multi-objective optimization is shown in Scheme S3.

$$\text{minimize} \quad \sum_j \left[c_{JF,j} \cdot S_j\right] + \sum_j \sum_i \left[c_{tpt} \cdot x_{i,j} \cdot n_{i,j}\right] \tag{S3.1}$$

$$\text{subject to} \quad \sum_j \left[GHG_{JF,j} \cdot S_j\right] + \sum_j \sum_i \left[GHG_{tpt} \cdot x_{i,j} \cdot n_{i,j}\right] \leq GHG_{target} \cdot \sum_j S_j \tag{S3.2}$$

$$S_j - \sum_i n_{i,j} = 0 \qquad \forall j \in C \tag{S3.3}$$

$$\partial_i - \sum_j n_{i,j} = 0 \qquad \forall i \in C \tag{S3.4}$$

$$n^{LB} - n_{i,j} \leq 0 \qquad \forall i,j \in C \tag{S3.5}$$

$$n_{i,j} - n^{UB} \leq 0 \qquad \forall i,j \in C \tag{S3.6}$$

$$S_j \cdot W_{CO2HY} - E_{JF,j} \leq 0 \qquad \forall j \in C \tag{S3.7}$$

Scheme S3. The scheme describing the multi-objective optimization problem formulation, targeting cost minimization as its objective function (Equation S3.1).

The problem shown in Scheme S3 targets the development of a pareto optimal front that explores the variation in the optimal cost as a function of varying life cycle jet fuel emission targets. This pareto front is derived by the introduction of an emission constraint (Equation S3.2), by varying the value of the climate change impact, GHG_{target}. Thus, trade-offs between cost and GHG emissions are demonstrated for a number of values of α, which can be associated with the available electricity as a function of time.

4.3. Results & Discussion

The aim of a global supply chain optimization is to determine the optimal production locations and supply routes that minimize climate change impact of synthetic jet fuel (Scheme S2) and minimize global cost of synthetic fuel (Scheme S1). Since the minimization of one does not lead to that of the other, the the trade-off between the cost and emissions is similary investigated (Scheme S3). The results of such optimization problems depend on the established constraints, particularly parameters such as α. A value of $\alpha = 1$ corresponds to the realistic capacities than can be applied for different technologies based on the countries' capacities [175]. Nevertheless, values of $\alpha = 1$ denote hypothetical possibilities in years beyond the year of 2050, should capacities require further expansion. The minimized emissions and jet fuel costs, based on Schemes S1 and S2 respectively, are shown in Figure 4.1.

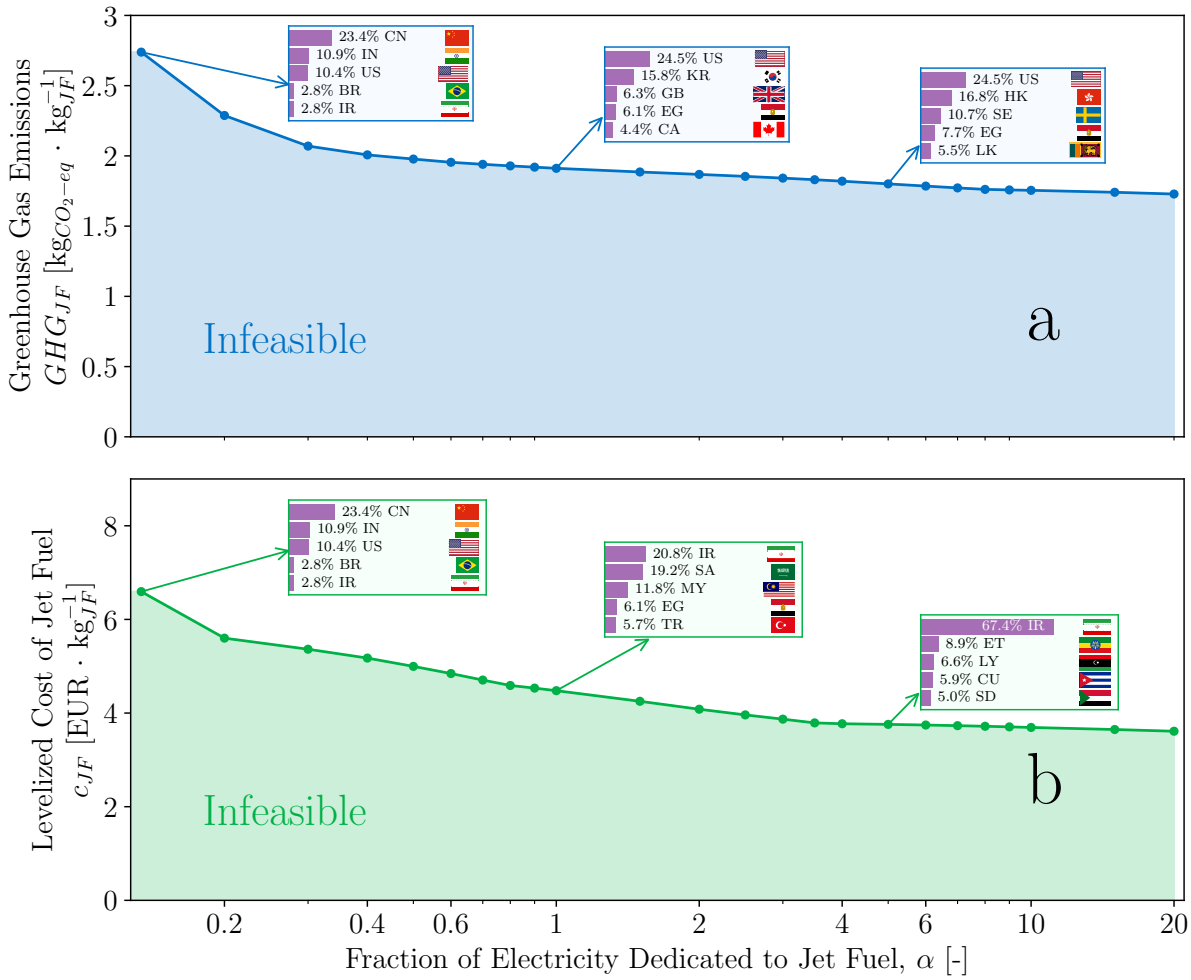

Figure 4.1. The evolution of the optimal (minimal) synthetic jet fuel climate change impact (a), GHG_{JF}, and the synthetic jet fuel cost (b), c_{JF}, for different values of the fraction of electricity dedicated to jet fuel, α. The presented curve represents a pareto optimal front for optimal climate change impact (a) and cost (b), for which lower values are infeasible at the same value of α. The boxes in each plot show 5 countries with the highest synthetic jet fuel production share for (from left to right) the values of α =0.1336, 1, and 5. The complete set of country names and codes can be found in Table A.18.

Figures 4.1 (a) and (b) respectively depict the variation of the minimized synthetic jet fuel climate change impact, GHG_{JF}, and the cost of synthetic jet fuel, c_{JF}, as a function of the fraction of electricity dedicated to jet fuel, α. The potential range of optimal GHG values in Figure 4.1 (a) ranges from around 2.74 to 1.73 $kg_{CO_2} \cdot kg_{JF}^{-1}$. The conditions of these minimized metrics

pertain to the projected electricity mixes in 2050, as highlighted in Section 4.1.. The available electricity that is dedicated to synthetic jet fuel production is quantified by α. Similarly, the range of minimized cost presented in Figure 4.1 (b) ranges between 6.59 and 3.61 EUR $\cdot$ kg_{JF}^{-1} . These values are minimized values attained at specific values of α; in other words, a value of GHG or cost below the pareto optimal front is infeasible without varying the fraction of electricity dedicated to electricity. The preliminary implications of Figure 4.1 show that when considering the global supply chain, the emissions of jet fuel and including transport burdens could generate synthetic jet fuel with GHG emissions of 1.73 $kg_{CO_2} \cdot kg_{JF}^{-1}$ on one hand. This GHG emission value corresponds to a 50.8% reduction compared to that of petroleum-based jet fuel. On the other hand, the cost could be around 3.16 EUR $\cdot$ kg_{JF}^{-1} , which is very close to the current cost of petroleum-based jet fuel at 1.115 EUR $\cdot$ kg_{JF}^{-1} . Such a cost is particularly interesting, since this minimized cost includes transportation and production of jet fuel. However, both minimized GHG and cost of jet fuel are not achieved simultaneously since the results of Figures 4.1 (a) and (b) correspond to distinct optimization problems, with each strictly focusing on GHG and cost respectively. Additionally, these competitive metrics are only achieved if the electricity dedicated to jet fuel is 5 to 20 times greater than the capacity increase projected to the year 2050. Thus, such values are considered rather impractical, even in 2050, and instead serve as a lower limit projection using excess electricity. A key takeaway from Figure 4.1, however, is the quantification via α of how much additional electricity would be required to attain desired values of climate change impact and costs. This quantity naturally is restricted to the selected *CO2HY* process and is based on the projected electricity mixes proposed by Jacobson et al. [175], whose distribution significantly impacts the carbon intensity of electricity and thus the jet fuel GHG.

Moreover, the minimized metrics shown in Figures 4.1 (a) and (b) correspond to an optimal geographical distribution of hubs for synthetic jet fuel production. For the value of $\alpha = 0.1336$, which is the minimum value sufficient to satisfy the global jet fuel demand, the distribution of synthetic jet fuel producing countries is divided amongst China (23.3 %), India (10.8%), USA (10.4%), Brazil (2.8%), and Iran (2.8%). This distribution is true for both minimized GHG and cost at $\alpha = 0.1336$ because at such a low value of dedicated electricity, the optimization solver's solution is greatly limited by the constraints. As a result, the top 5 chosen countries at $\alpha = 0.1336$ are in fact the countries with the highest expansion rate between 2020 and 2050 (i.e. greatest $\Delta E_{avail,j}$).

Thus, for low values of available electricity (low α), the burden of producing jet fuel is shared amongst many countries (123 countries), which leads to high emissions and costs per unit of jet fuel due to the solver's constraint on the available electricity. As more electricity becomes available to use for synthetic jet fuel production, the solver is capable of diverting more synthetic jet fuel production (at $\alpha = 1$) to countries with lower carbon intensity of electricity, such as South Korea (15.8%) whose electricity is mostly made up of offshore wind according to the Jacobson et al. [175] projections. This production distribution leads to a GHG of synthetic jet fuel of 1.9 $kg_{CO_2} \cdot kg_{JF}^{-1}$, assuming the entire electricity production expansion can be dedicated to synthetic jet fuel in 2050 ($\alpha = 1$). Similarly in Figure 4.1, the production distribution shifts to countries with cheaper electricity as more electricity is dedicated to jet fuel, with the production shifting mostly to Iran (20.8%, $c_{el} = 0.05$ EUR$\cdot$ kWh^{-1}), Saudi Arabia (19.2%, $c_{el} = 0.048$ EUR$\cdot$ kWh^{-1}), Malaysia (11.8%, $c_{el} = 0.05$ EUR$\cdot$ kWh^{-1}), Egypt (6.1%, $c_{el} = 0.044$ EUR$\cdot$ kWh^{-1}), and Turkey (5.7%, $c_{el} = 0.055$ EUR$\cdot$ kWh^{-1}). In this scenario, the cost is minimized at 4.47 EUR/kgJF for $\alpha = 1$, wherein the countries are geographically distributed across Africa, the Middle East, and South Eastern Asia, which is a first indication of the effect of accounting for transportation

of synthetic jet fuel. In fact, Egypt is the country with lowest cost of electricity cost among the top 5 ranking countries, but its rank is only 4th highest synthetic jet fuel contributor.

As aforementioned, values of α greater correspond to a hypothetical scenario in which more electricity than is projected for 2050 is available. This scenario could correspond to scenarios of years beyond 2050, assuming renewable energy systems continue to expand at such high rates. Thus, the scenario of $\alpha = 5$ shown in Figures 4.1 either demonstrates an overly optimistic scenario for the year 2050, or a scenario well beyond the year 2050. The minimum GHG for this scenario reaches an overall minimum of 1.8 $kg_{CO_2} \cdot kg_{JF}^{-1}$, which includes global transportation and is almost a 50% reduction compared to GHG of petroleum-based jet fuel. This shows that with greater access to cleaner electricity, such as that in Sweden and Hong Kong, the life cycle carbon footprint of synthetic jet fuel can decrease further. The clean electricity of the aforementioned countries is mostly based on offshore wind technologies in their grid mixes, which highlights the importance of these technologies in the energy transition and in a sustainable future. In a similar manner, the minimized cost when $\alpha = 5$ is nearly globally optimum at $c_{JF} = 3.75$ EUR $\cdot kg_{JF}^{-1}$. This cost of jet fuel is still not competitive. In that case, the optimizer selects Iran, Ethopia, Libya, Cuba, and Sudan as the locations for the production of the cheapest synthetic jet fuel. However, these electricity costs are not expected to remain very low as they are today, even if the cost is predominantly are determined by supply and demand. Such massive increases in capacity for electricity production would have to be accompanied by an increase in costs. Thus, these lower bounds for cost of jet fuel should be examined with caution, since they are optimistic lower bounds of the potential synthetic jet fuel costs in 2050.

While the cost and GHG metrics can become very attractive relative to the conventional jet fuel, such scenarios still corresponds to one in which the generated electricity exceeds Jacobson et al.'s projections ($\alpha > 1$). Nevertheless, the GHG emission of producing jet fuel using the 2050 grid mixes for values of $\alpha < 1$ still proves to be much more environmentally friendly than today's petroleum-based method, which emits 3.52 $kg_{CO_2} \cdot kg_{JF}^{-1}$ between combustion and production. The GHG range shown in Figure 4.1 shows GHG values of less than 2.74 $kg_{CO_2} \cdot kg_{JF}^{-1}$, even at a low fraction of electricity dedicated to jet fuel equal to 0.1336. These GHG values cover production, transportation, and combustion. To further understand these optimal values, a breakdown of the contribution of the combustion and production and transportation in the GHG and cost metrics is highlighted in Figure 4.2 for a selected range of α.

Figures 4.2 (a) and (b) show the contribution of production and transport in the minimized synthetic jet fuel climate change impact, GHG_{JF}, and the cost of synthetic jet fuel, c_{JF}, as a function of the fraction of electricity dedicated to jet fuel, α. Similar to Figures 4.1 (a) and (b), the total value of GHG and cost in Figures 4.2 (a) and (b) decrease with higher available electricity. The contributions of transportation for both GHG and cost is non-monotonic as a function of α. At low values of α, the production is initially scattered around the world so that the jet fuel demand is satisfied in light of the limited availability of electricity. Thus, the 123 countries producing synthetic jet fuel renders the geographical supply more accessible, so transportation is facilitated and comprises. As more electricity is dedicated to jet fuel, the total GHG and cost continue to decrease, with generally decreasing production emissions and costs. At $\alpha = 4$, the contribution of cost of transport in Figure 4.2 (b) becomes more prominent compared to that of the production, as the transportation cost reaches 16% of the production cost. This transportation contribution emphasizes how significant the transportation is in the determination of the optimal production location, which is shown by the increase of the GHG of production from

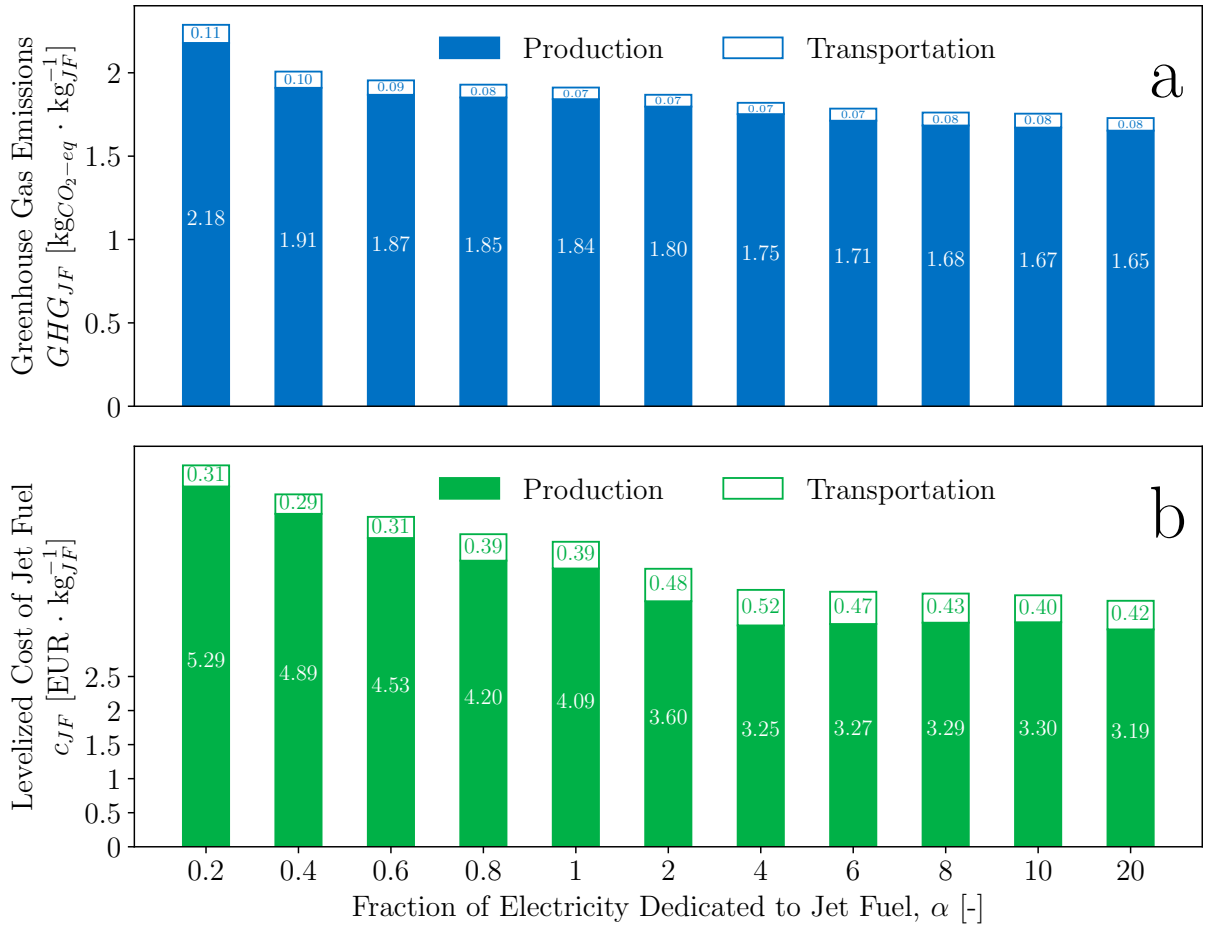

Figure 4.2. The contribution of production/combustion and transportation in the optimized synthetic jet fuel climate change impact (a), GHG_{JF}, and the cost of synthetic jet fuel (b), c_{JF}. The GHG and cost metrics are assessed at selected fractions of electricity dedicated to jet fuel, α. The progression of the split of GHG and cost between production/combustion and transportation as a function α shows that the transportation emissions and cost grow to be significant and non-negligible.

3.25 to 3.27 as α increases from 4 to 6. The reason for this increase lies in the solver's attempt to minimize the total GHG, and in doing so sacrifices the GHG of production slightly to achieve a greater reduction in transport GHG. Such a pattern also appears for subsequent α values, but does not appear in the case of GHG emissions in Figure 4.2 (a). This pattern is exhibited when α increases and thus more electricity is made available in all countries, which implies that the solver diverts the production to locations that are more geographically optimal.

Finally, a direct evaluation of the trade-off between cost and emissions is established. The pareto optimal front showcased in Figure 4.3 highlights the trade-off between synthetic jet fuel cost and emissions.

In Figure 4.3, the synthetic jet fuel greenhouse gas emissions, GHG_{JF}, is portrayed as a function of the minimized synthetic jet fuel cost, c_{JF}. The results of this multi-objective optimization highlight a curve of potential operating points at a specific α. As more electricity is made available, highlighted by the gradual shift in color from red to yellow, the pareto optimal curve shifts inwards towards the origin. This shift signifies the existence of lower GHG and cost values. In particular, the tradeoff shows that in the best case scenario, the extremities at $\alpha = 5$ shows synthetic jet fuel production with potential sustainability metrics of 1.8 $kg_{CO_2} \cdot kg_{JF}^{-1}$ and 7.35 EUR $\cdot$ kg_{JF}^{-1} on one end of the curve, while these metrics show 2.63 $kg_{CO_2} \cdot kg_{JF}^{-1}$ and 3.75

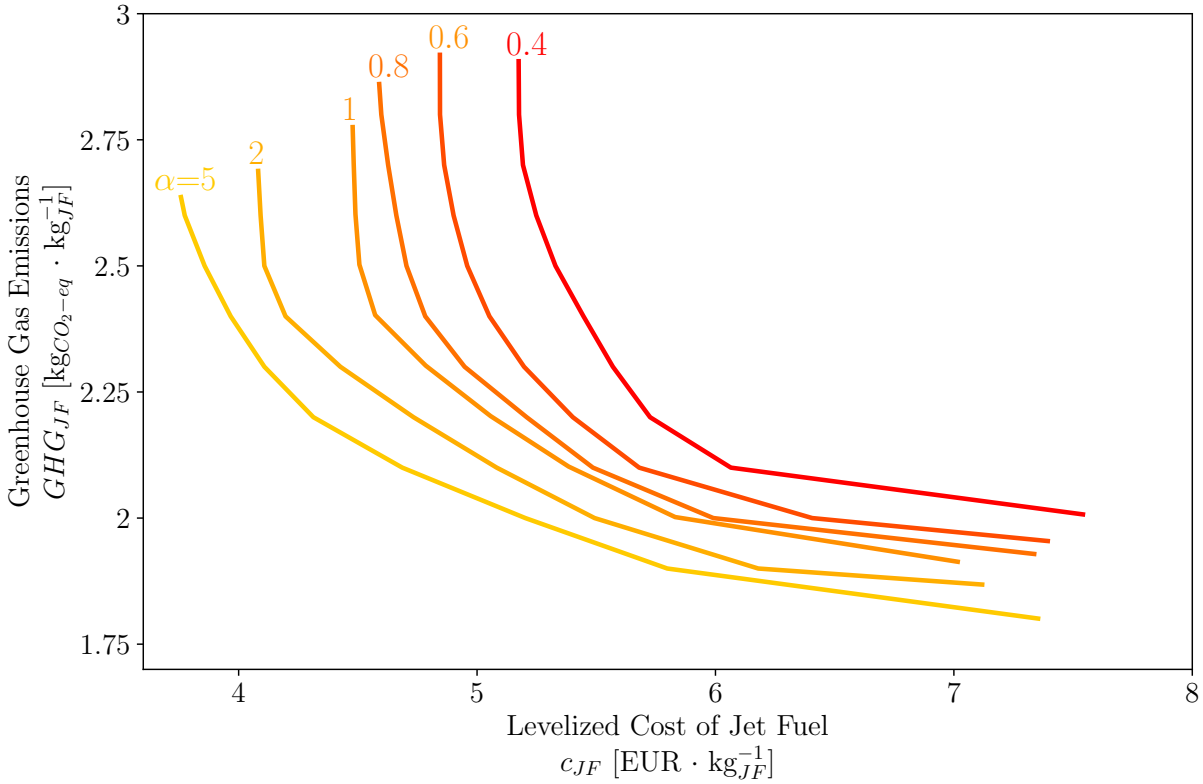

Figure 4.3. The pareto optimal front showing the variation of the synthetic jet fuel greenhouse gas emissions, GHG_{JF}, as a function of the synthetic jet fuel cost, c_{JF}. This multi-objective optimization demonstrates the varying cost-emission relations at fixed fractions of electricity dedicated to jet fuel (α =0.4, 0.6, 0.8, 1, 2, 5). Higher α factors shift the curves closer to the origin, and lead to lower emissions and costs.

EUR · kg_{JF}^{-1} on the other end of the curve. The optimal operating point thus lies on the curve in between, and choosing this operating point depends on the global situation with regards to climate change. For instance, if the energy transition is not on schedule and climate disasters are projected to occur, then greater carbon reductions must take place, and the operator would choose an operating point with much lower GHG at the expense of higher jet fuel costs. However, the value of $\alpha = 5$ implies a significantly higher amount of available electricity than the one projected for the year 2050. Thus, a more realistic fraction of available electricity for jet fuel production is 0.4, whose pareto optimal curve is bounded by sustainability metrics of 2 $kg_{CO_2} \cdot kg_{JF}^{-1}$ and 7.54 EUR · kg_{JF}^{-1} on one end, and 2.9 $kg_{CO_2} \cdot kg_{JF}^{-1}$ and 5.17 EUR · kg_{JF}^{-1} on the other end. Similarly, the optimal point would lie along the curve and between these extremities, such as the point at 2.3 $kg_{CO_2} \cdot kg_{JF}^{-1}$ and 5.57 EUR · kg_{JF}^{-1} . These more practical values are nevertheless high, which could hinder the shift to sustainable aviation. Consequently, it is imperative to revise electricity capacity expansion targets to make the expansion more in-line with the sustainability targets of 2050. Targeting different decarbonization approaches is also fundamental, such as working on further lowering the carbon intensity of renewable energy technologies in 2050 and lowering transportation emissions. For instance, this could be accomplished by targeting higher energy efficiencies. With higher energy efficiencies, the cost of the synthetic jet fuel production can also decrease significantly, especially following decades of mass production of units such as the DAC units, electrolyzers, and renewable energy systems. The values presented herein are thus lower than the current status quo in emissions and relatively competitive in terms of price, but further enhancements and reductions can be conducted using emissions and costs in the year 2050 following years of mass production and research and development.

The results highlighted by Figures 4.1 and 4.3 show potential in global decarbonization of the aviation industry and its supply chain in the year of and after 2050. The global supply chain optimization algorithm attempts to present practical results by including as many realistic constraints as possible. However, this model still exhibits some limitations. For instance, certain political limitations exist due to international relations, which can be added to the model as constraints. Such constraints, however, are beyond the scope of this economic and environmental supply chain assessment. Moreover, the topic of supply security is particularly important in a supply chain optimization. Thus, regionalizing the production and ensuring that each continent possesses at least one synthetic jet fuel supplier could provide a more accurate distribution of the synthetic jet fuel production hubs. By introducing such a constraint, the supply security is ensured by preventing countries from monopolizing the supply of jet fuel and endangering the supply security.

5

Conclusions & Outlook

In this thesis, a thorough life cycle analysis of 3 synthetic jet fuel production processes was conducted. The processes convert biogenic CO_2 feedstocks and water to jet fuel via methanol as an intermediate. Two of these processes use pure CO_2 from direct air capture units and reach methanol either through direct hydrogenation or electrochemical reduction to CO/syngas. The final process converts biogas, generated from biomass waste, to methanol via hydrogenation. The analysis centered on the sustainability of these processes in terms of economic and environmental sustainability. A pragmatic view of the global aviation situation was assessed, wherein a supply chain optimization determined the optimal production locations of synthetic jet fuel (amongst 140 countries). The supply chain accounted for: (1) the burdens associated with transporting synthetic jet fuel from producing countries to demanding countries, (2) the country-based grid electricity mixes, prices, and greenhouse gas emissions to determine the synthetic jet fuel cost and greenhouse gas emissions, (3) the shortest shipping routes connecting countries, and (4) capacity for expansion of the electricity production to quantify the available electricity in each country by 2050. By combining such country-based data, the global supply chain was optimized based on different scenarios of available electricity, wherein the trade-offs between the environmental and economic sustainability metrics were highlighted and discussed to determine the optimal hubs for the production of synthetic jet fuel.

The results show that amongst the 3 processes discussed, the process converting CO_2 to jet fuel via direct hydrogenation (*CO2HY*) demonstrated synthetic jet fuel with the lowest greenhouse gas emissions (2.05 $kg_{CO_2} \cdot kg_{JF}^{-1}$ using carbon intensity of electricity of 0.045 $kg_{CO_2} \cdot kWh^{-1}$) and lowest levelized cost (9.12 EUR $\cdot kg_{JF}^{-1}$ using a cost of electricity of 0.195 EUR$\cdot kWh^{-1}$). The levelized cost of the other evaluated processes was similar (maximum of 11 EUR $\cdot kg_{JF}^{-1}$), while the other impact categories (water depletion, land usage, cumulative energy demand) were very similar across the processes. With the exception of greenhouse gas emissions, the aforementioned impact categories and the resulting cost of synthetic jet fuel of the 3 processes are significantly higher than that of the petroleum-based jet fuel (1.115 EUR $\cdot kg_{JF}^{-1}$ [35]). Finally, the main contributors to all environmental and economic metrics are clearly the direct air capture and grid electricity units. The supply chain optimization showed that satisfying the jet fuel demand can be met using synthetic jet fuel that reduces greenhouse gas emissions relative to the petroleum-based equivalent, even if transportation burdens are included. The reduction of both cost and greenhouse gas emissions depends significantly on the available electricity that can be dedicated to jet fuel. Patterns of sacrificing minimum cost or emissions of synthetic jet fuel production in favor of a greater reduction in synthetic jet fuel cost or emissions were shown.

5.1. Takeaways

Many implications can be highlighted based on on the results of the life cycle analysis and the global supply chain optimization. The key takeaways from this work are highlighted as follows:

- The co-electrolysis unit renders the process in which CO_2 is electrochemically reduced to CO much more electricity-intensive, which questions the feasibility of its implementation in sustainable fuel production processes. This process generated the highest costs (11 EUR · kg_{JF}^{-1}), while its emissions were 2nd best (2.25 kg_{CO_2} · kg_{JF}^{-1}). Such results were utilizing an optimistic measure of its lifetime.
- Heat integration provides significant reductions in greenhouse gas emissions associated with these processes, which require high loads of heat. Reductions up to 0.8X kg_{CO_2} · kg_{JF}^{-1} were achieved by heat integration.
- The majority of cost and greenhouse contributions, for all 3 processes, are owed to processing the feedstocks (CO_2 from direct air capture & H_2 from water electrolysis). Thus, a combination of feedstock supply routes could be required to enhance the sustainability metrics of these processes.
- The satisfaction of sustainability targets is paramount not only in the eventual decarbonization of the aviation sector, but also in the transition from fossil fuel based jet fuel to its synthetic counterpart.
- Complete decarbonization (i.e. net zero emissions) of the aviation industry is not yet foreseeable. Carbon capture and storage thus proves its importance in offsetting the remaining but reduced life cycle emissions of synthetic jet fuels; in other words, the conversion of CO_2 to jet fuel via renewable energy technologies alone cannot lead to carbon-neutral aviation.
- Significant reductions in the carbon footprint of the aviation industry strongly depends on the amount of available electricity generated via renewable energy technologies. Thus, more electricity generation than that projected [175] could be required to enable a rapid and permanent transition away from fossil fuel dependencies by 2050.
- Transportation is an essential part of the well-to-tank life cycle of synthetic jet fuel, and cannot be ignored since it could, in some cases of cost/greenhouse gas emission minimization, contribute to costs or greenhouse emissions that surpass those of the production of synthetic jet fuel.
- The production locations with high capacities for implementing offshore wind farms are favored in the greenhouse gas emission minimization problem, thus highlighting this renewable energy technology as a key component in the generation of electricity with very low carbon intensity.
- Most of the datasets utilized in the supply chain optimization were based on data from today, rather than of 2050, which is the year of the supply chain optimization. The model requires more projections to provide more accurate supply chain solutions. While efficiencies are set to increase over the years, the cost of electricity based on such increase in demands and decarbonization most likely will increase, which is why the minimized emissions and presented herein likely represent an optimistic case.

5.2. Further Work

The developed methodology attempted to be as practical as possible in estimating for life cycle costs and emissions. However, the model is not without some limitations and uncertainties. Consequently, the model can be improved and expanded by:

- Enhancing and incorporating thorough life cycle evaluation of utilized catalysts. The contributions due to catalysts can grow significantly based on the rate of resupply. Thus, a generalized and consistent methodology for accurate catalyst life cycle assessment is required.
- Exploring alternate synthetic jet fuel production pathways that do not necessarily pass through methanol as an intermediate, as well as enhancing the methanol to jet fuel reactor sequence.
- Developing upscaled direct air capture costing is need to accurately model the cost of direct air capture at high scales.
- Regionalizing of jet fuel production to minimize effects of geopolitical factors on global jet fuel supply.
- Investigating how much renewable electricity countries can dedicate to synthetic jet fuel, to obtain a country-specific capacity for production.
- Exploring of the non-linear effects of the global supply chain algorithm, which could include demand driven cost of electricity and including nonlinear expressions.
- Exploring different (more than one) synthetic jet fuel production in the global supply chain optimization.
- Extrapolating the jet fuel demand data to that which would represent the global jet fuel demand in 2050.
- Establishing projections in electricity prices for completely renewable grids in 2050, as well as projections due to increase in electricity demand per country, which would more accurately represent the future synthetic jet fuel costs.
- Including geography-dependent life cycle inventory of the processes and geography-dependent discount rates.
- Utilizing process data for the year 2050 in the supply chain optimization, such as: projections of renewable energy technologies emissions[183] and efficiency of water electrolysis [78].
- Validating the cost of emerging technologies, such as the co-electrolysis unit and direct air capture, using more sources and implemented equipment, to minimize the uncertainty associated with these units, which have significant economic and environmental contributions to synthetic jet fuel production.
- Conducting an extensive sensitivity analysis to assess the impact of uncertain variables on cost and emissions. This analysis would also extend to the supply chain optimization, wherein the parameters quantifying transportation burdens are varied to assess potential changes in optimal synthetic jet fuel production locations.

- Decreasing the cost and greenhouse gas emission contributions of the feedstocks by incorporating a CO_2 supply from point sources (example: cement plant) and producing H_2 via less electricity-intensive methods (example: methane/biogas pyrolysis).
- Incorporating the carbon tax as a part of the economic comparison of the levelized cost of synthetic jet fuel relative to the petroleum-based jet fuel.
- Accounting for the synthetic jet fuel cost-greenhouse gas emissions tradeoff in climate scenarios evaluations to determine favorable operating points as a function of the urgency of climate action.
- Exploring the complete decarbonization of the aviation industry by quantifying the added economic cost and additional emissions incurred by carbon capture and storage of the emissions due to synthetic jet fuel.

Appendix

I LCIA

Table A.1. A detailed breakdown of the LCIA utilized from ecoinvent [51].

Impact Category	**Ecoinvent Name**	Unit	Number of Characterization Factors
Climate Change Impact	IPCC 2013, climate change, GWP 100a	$kg_{CO_2\text{-eq}}$	211
Cumulative Energy Demand	cumulative energy demand, biomass, renewable energy resources, biomass	MJ-eq	1
	cumulative energy demand, fossil, non-renewable energy resources, fossil		6
	cumulative energy demand, geothermal, renewable energy resources, geothermal, converted		1
	cumulative energy demand, nuclear, non-renewable energy resources, nuclear		1
	cumulative energy demand, primary forest, non-renewable energy resources, primary forest		1
	cumulative energy demand, solar, renewable energy resources, solar, converted		1
	cumulative energy demand, water, renewable energy resources, potential (in barrage water), converted		1
	cumulative energy demand, wind, renewable energy resources, kinetic (in wind), converted		1
Land Occupation	ecological footprint, total, land occupation	$m^2 \cdot yr$	58
Water Depletion	ReCiPe Midpoint (E) V1.13, water depletion, WDP	m^3	5

II LCA of Unit Processes

Table A.2. The values of the life cycle impact categories of the individual unit processes across the 3 processes. These LCIA are expressed in their respective unit, and the value is per unit of functional unit of the unit process. The electrolyzer and co electrolyzer are after allocation. The functional unit is strictly for the output/outlet, except in the case of distillation columns and separators, where the inlet mass of the mixture to be separated is the functional unit.

		Life Cycle Impact Assessment Categories			
Unit Process	**Functional Unit**	GHG [$kg_{CO_2\text{-}eq}$]	LUO [$m^2 \cdot yr$]	WDP [m^3]	CED [MJ-eq]
Electricity (Grid)	1 kWh	0.04498	0.0196	0.01064	6.698
Direct Air Capture	1 kg	0.018385	0.000956	0.000516	0 .3229
Heating via HTHP	1 MJ	0.00022524	1.612e-05	1.23e-06	0.001278
Electrolyzer	1 kg	0.0222738	0.0043452	0.0013156	0.964058
H2 Compressor	1 kg	0.000282	4.26844e-05	4.92854e-06	0.0057013
Co-electrolyzer	1 kg	0.1011	2.1040e-02	6.4590e-03	4.6761
CO Compressor	1 kg	1.9964e-05	3.01896e-06	3.4858e-07	0.0004032
Heat Exchanger for CO+H2	1 kg	3.264419e-07	4.59380e-08	3.28219e-09	5.1265e-06
Reactor Syngas	1 kg	5.135790e-05	1.677113e-05	7.22672e-07	0.000839131
Cooler for MeOH	1 kg	1.437174e-06	2.022441e-07	1.445e-08	2.257e-05
Separator 4 MeOH (CO2ER)	1 kg	1.480601e-05	2.039451e-06	1.955276e-07	0.00025345
Heat Exchanger for MeOH	1 kg	4.35194273e-07	6.124204e-08	4.3756425e-09	6.83449626e-06
Reactor MTO	1 kg	0.00072474972	6.653907e-05	4.718597e-06	0.00713820504
Cooler for MTO Outlet	1 kg	2.950953e-06	4.1526832e-07	2.967023e-08	4.634316e-05
Separator 4 Hydrocarbons	1 kg	4.949627e-08	6.817853-09	6.53645e-10	8.47289e-07
Distillation Column 4 Hot Olefin and Water	1 kg	2.234255e-05	3.0949435e-06	2.7667e-07	0.0003742194
Olefin Pump	1 kg	0.00013599	2.038261e-05	1.05949e-06	0.0020742524
Heat Exchanger for Olefins	1 kg	3.40207853e-07	4.787522e-08	3.420605e-09	5.342784e-06
Reactor for Oligomerization	1 kg	3.690158e-06	7.20591389e-07	2.851701e-08	5.41898e-05
Cooler for JF Range Liquid Fuel	1 kg	4.580054e-07	6.445210e-08	4.604996e-09	7.1927336e-06
Reactor Final	1 kg	0.0021768	0.000200314	1.374424e-05	0.0354064
Cooler for Paraffin Liquid Fuel	1 kg	2.37252e-07	3.338703e-08	2.3854e-09	3.725929e-06
DistGasDies	1 kg	8.4228389e-05	1.1604939e-05	1.1092276-06	0.00144045
Heating via Furnace	1 MJ	0.07556044	0.00033450966	3.86633e-05	1.462014
Cooling via Chiller	1 MJ	0.001193	0.000422902	0.00021234	0.1333679
Water Production	1 kg	0.0003353650	3.2823e-05	3.19005e-05	0.00521364
Water Pump	1 MJ	5.832236e-06	8.7414370e-07	4.543842e-08	8.8957e-05
CO2 Compressor	1 kg	9.0715e-06	1.3717659e-06	1.5839e-07	0.000183226
Heat Exchanger for CO2+H2	1 kg	2.82913e-07	3.9812512e-08	2.8445381e-09	4.443001e-06
Reactor CO2 Hydrogenation	1 kg	0.01593549	0.00148648	0.000100608	0.25523896
Cooler for MeOH for CO2 Hydrogen	1 kg	8.57303e-07	1.20642e-07	8.6197191e-09	1.34634e-05
Separator 4 MeOH (CO2HY)	1 kg	1.3570533e-05	1.869e-06	1.792118e-07	0.00023230373
Distillation Column 4 MeOH (CO2HY/BIOHY)	1 kg	2.04247e-05	2.8324899e-06	2.49532e-07	0.000340575964
H2 Compressor 4 Biogas	1 kg	2.2531e-04	3.4071e-05	3.9340e-06	4.5509e-03
Compressor 4 Biogas	1 kg	1.9081e-05	2.8854e-06	3.3316e-07	3.8540e-04
Heat Exchanger Biogas+H2	1 kg	7.0398e-06	9.9067e-07	7.0782e-08	1.1056e-04
Biogas Production	1 kg	0	0	0	0
Biogas Reactor (cascade)	1 kg	2.3325e-04	3.2734e-05	1.9561e-06	3.4952e-03
Cooler (cascade)	1 kg	7.0398e-06	9.9067e-07	7.0782e-08	1.1056e-04
Separator (cascade)	1 kg	8.4811e-04	4.8306e-04	7.0483e-05	3.6788e-020

III LCC of Unit Processes

The costing of the unit processes of Section 3.1. based on the initial investment and the temporal cash flows is summarized in Table A.3.

Table A.3. A summary of the costing of the units, including initial capital investments and yearly costs incurred during operation based on the sizing parameters (SP) and their functional unit (FU, not rates). This includes only foreground units; for instance, catalysts for reactors are further elaborated in next section. The yearly maintenance costs are expressed as a function of the CAPEX. The power rating is calculated by dividing the energy by the total operating hours, thus assuming that the power remains constant over the hours of the year. Note that these flows are not expressed in the same currencies, and could be in either EUR, USD, or CHF. The currency can be retrieved via the references in the thorough documentation in Section 2.2.. The revenue cash flow is omitted because it is unit-specific. The references for these equations can be found in Section 3.1..

				Annual Cash Flows	
Unit Process	**FU**	**SP**	**CAPEX**	**OPEX**	$\frac{\text{MAINT}}{\text{CAPEX}}$ [%]
Electricity (Grid)	1 kWh	W	0	$0.1957 \cdot W$	0
Industrial Furnace	1 MJ	$\dot{Q}$, Q	$250 \cdot \dot{Q}$	$7.2 \cdot Q + c_{NG} \cdot Q + c_{DPE} \cdot m_{DPE}$	4
HTHP	1 MJ	$\dot{Q}$, Q	$660 \cdot \dot{Q}$	$2 \cdot \dot{Q} + 0.00180 \cdot Q$	3.5
Absorption Chiller	1 MJ	$\dot{Q}$	$2500 \cdot \dot{Q}$	$c_{NH_3} \cdot m_{NH_3}$	3.5
Electrolyzer	1 kg_{H_2}	$\dot{W}$	$1090388 \cdot \dot{W}^{0.8206}$	0	3.5
Co-electrolyzer	1 kg_{CO}	W	$1130514 \cdot \dot{W}^{0.8206}$	0	3.5
Direct Air Capture	1 kg_{CO_2}	$\dot{m}$	$6.0931 \cdot \dot{m}$	0	4
Compressor	1 kg	$\dot{W}$	$580000 + 20000 \cdot \dot{W}^{0.6}$	0	3.5
Heat Exchanger	1 kg	A	$28000 + 54 \cdot A^{1.2}$	0	3.5
Reactor	1 kg	$\dot{m}$	$61500 + 32500 \cdot \left(\frac{\dot{m}}{\beta \cdot \rho_{cat} \cdot WHSV}\right)^{0.8}$	$c_{cat} \cdot \frac{\dot{m}}{WHSV}$	3.5
Distillation Column/Separator	1 kg	D, H	$17640 \cdot D^{1.066} \cdot H^{0.802}$	0	3.5
Water Production	1 kg	m	0	$2 \cdot 10^{-4} \cdot m$	0
Pump	1 kWh	$\dot{W}$	$-1100 + 2100 \cdot \dot{W}^{0.6}$	0	3.5
Biogas Production	1 kg	m	0	$0.3339 \cdot m$	0

IV Life Cycle Inventories

IV.A Ecoinvent

Table A.4. The utilized ecoinvent datasets for unit processes that had activities identical or similar to what their inventories would be in the ecoinvent [51]. Only unit processes that can be described by a single activity and whose functional unit can be matched to the functional unit of the activity are shown in this table. These were used for Chapters 2 and 3 The electricity mix changes to that dictated by Table A.17 for the supply chain optimization of Chapter 4.

Unit Process	Product	Ecoinvent Activity	Unit	Location
Electricity Mix	electricity production	"market for electricity, low voltage"	kWh	CH
High Temperature Heat Pump	heat pump, brine-water, 10kW	"heat pump production, brine-water, 10kW"	unit	CH
Pump	water pump operation, electric	"water pump operation, electric"	MJ	DE
Water Production	water, deionised	"water production, deionised"	kg	CH
Biogas Production	biogas	"treatment of sewage sludge by anaerobic digestion"	m^3	CH
Petroleum-based Jet Fuel Production	kerosene	"petroleum refinery operation"	kg	CH

IV.B Literature-based LCI

IV.B.i Industrial Furnace

Table A.5. Life cycle inventory of Industrial Furnace. A closed loop furnace is used, wherein the heated fluid (diphenyl ether) is returned to be heated and not disposed of after one cycle.

Ecoinvent Activity	Quantity	Unit	Location
"heat production, natural gas, at industrial furnace low-NOx >100kW"	1	MJ	Europe without Switzerland
"diphenylether-compound production"	$\frac{m_{hf,\ell}}{E_{hf,\ell}}$	kg	RER

In Table A.5, the mass of propylene glycol in the furnace system, $m_{hf,\ell}$, is a fixed number since it is in a closed loop system. To determine the emissions associated with this mass of propylene glycol, the mass is normalized by the amount of energy, $E_{hf,\ell}$, (in MJ) that this heating fluid is expected to deliver during its lifetime. The lifetime is assumed to be one year (Section 2.2.2.).

IV.B.ii Absorption Chiller

Table A.6. Life cycle inventory of absorption chiller. The units are the corresponding activities' units per the functional unit of the unit process.

Ecoinvent Activity	Quantity	Unit	Location
"ammonia production, steam reforming, liquid"	$\frac{1}{E_{cf,\ell}}$	kilogram	Europe without RU
"absorption chiller production, 100kW"	$\frac{1}{E_{chiller,\ell}}$	unit	CH
"market for electricity, high voltage"	0.02	kWh	CH

Ammonia as the cooling fluid is in the closed loop absorption chiller. If 1 kg can extract $E_{cf,\ell}$ amount of heat over its lifetime, then the inventory mass for ammonia is the reciprocal of this value, which is the mass attributed to extract 1 MJ. The same approach is followed for the absorption chiller unit. During its lifetime (assumed to be equal to the plant lifetime), the unit can extract a value of $E_{chiller,\ell}$ MJ of heat. Thus, per MJ of heat extracted, number of units per MJ is the reciprocal of the total energy extracted during its lifetime. The used quantity of electricity in the inventory is used in the cooling via absorption chiller inventory in ecoinvent, so it is replicated herein as well for consistency purposes [51].

IV.B.iii Direct Air Capture

Table A.7. The utilized direct air capture inventory, is based on the work of Terlouw et al. [70].

Unit Process	Product	Activity	Unit	Location
Direct Air Capture	carbon dioxide, captured from atmosphere	"carbon dioxide, captured from atmosphere"	kg	CH

IV.B.iv Electrolyzer

Table A.8. Electrolyzer of capacity 1 MW [79] (explain what RER, GLO, etc. are)

Ecoinvent Activity	Quantity	Unit	Location
"market for aluminium, wrought alloy"	27	kilogram	GLO
"sheet rolling, aluminium"	27	kilogram	RER
"titanium production"	528	kilogram	GLO
"tetrafluoroethylene production"	16	kilogram	RER
"carbon black production"	9	kilogram	GLO
"market for platinum"	0.10318	kilogram	GLO
"copper production, cathode, solvent extraction and electrowinning process"	4.5	kilogram	GLO
"sheet rolling, copper"	4.5	kilogram	RoW
"sheet rolling, chromium steel"	100	kilogram	RER
"steel production, chromium steel 18/8, hot rolled"	100	kilogram	RER
"synthetic rubber production"	4.8	kilogram	RER

One electrolyzer unit rated at 1 MW requires the inventory of materials tabulated in Table A.8. However, over the lifetime (ℓ_{ely}) of 80000 hours [82] of the electrolyzer, an energy amount equal to $\ell_{ely} \cdot P_{ely}$ is utilized. Thus, the amount of H_2 produced during the lifetime, $m_{H_2,\ell}$, can be determined for $P_{ely} = 1$ MW. In this case, the inventory shown in Table A.8 corresponds to the

production of a mass of H_2 equal to $m_{H_2,\ell}$. These quantities of Table A.8 are thus scaled by the reciprocal of $m_{H_2,\ell}$, such that the inventory for the materials per kg of H_2 produced, which is the functional unit of the unit process, is determined.

IV.B.v Co-electrolyzer

Table A.9. The life cycle inventory of a co-electrolyzer of capacity 1 MW [79]. This inventory is based on that of the electrolyzer with changes in the membrane material and the anode catalyst [156].

Ecoinvent Activity	Quantity	Unit	Location
"market for aluminium, wrought alloy"	27	kilogram	GLO
"sheet rolling, aluminium"	27	kilogram	RER
"titanium production"	528	kilogram	GLO
"tetrafluoroethylene production"	8	kilogram	RER
"polysulfone production, for membrane filtration production"	8	kilogram	GLO
"carbon black production"	9	kilogram	GLO
"market for platinum"	0.075	kilogram	GLO
"copper production, cathode, solvent extraction and electrowinning process"	4.5	kilogram	GLO
"sheet rolling, copper"	4.5	kilogram	RoW
"sheet rolling, chromium steel"	100	kilogram	RER
"steel production, chromium steel 18/8, hot rolled"	100	kilogram	RER
"synthetic rubber production"	4.8	kilogram	RER
"market for silver"	0.3	kilogram	GLO

A co-electrolyzer unit rated at 1 MW needs the inventory of materials shown in Table A.9. However, over the lifetime (ℓ_{coely}) of 3000 hours [82] of the electrolyzer, an energy amount equal to $\ell_{coely} \cdot P_{coely}$ is used. Thus, the amount of CO produced during the lifetime, $m_{CO,\ell}$, is determined for $P_{coely} = 1$ MW. Hence, the inventory shown in Table A.9 corresponds to the production of a mass of CO equal to $m_{CO,\ell}$. These quantities of Table A.9 are thus scaled by the reciprocal of $m_{CO,\ell}$, to obtain the inventory for the materials per kg of CO produced, which is the functional unit of the unit process.

IV.B.vi Compressor

Table A.10. The life cycle inventory of a centrifugal compressor of rated power 18404 kW [92]. Based on the compressed fluid properties, the inventory needed for the compression of 1 kg of a given fluid is the materials and their quantities scaled by $m_{cmp,\ell}$ (Equation 2.10).

Ecoinvent Activity	Quantity	Unit	Location
"steel production, chromium steel 18/8, hot rolled"	51460	kilogram	RER
"steel production, alloy"	11004	kilogram	RER
"steel production, unalloyed"	25.65	kilogram	RER
"synthetic rubber production"	0.73	kilogram	RER
"market for electricity, high voltage"	261936.2	kWh	CH

The compressor inventory of materials tabulated in Table A.10 refers to the materials and energy required in the manufacturing of a 18404 kW rated compressor. The power rating is similarly identified as the key parameter. Thus, the amount of energy utilized by the compressor during the lifetime is $\ell_{cmp} \cdot P_{cmp}$. Depending on the fluid being compressed, the energy needed for the

compression is known via w_{cmp}. Thus, the amount of mass a compressor can compress over its lifetime can be determined using $m_{cmp,\ell}$ (Equation 2.10). In this case, the inventory shown in Table A.8 corresponds to the compression of an amount of mass of a fluid equal to $m_{cmp,\ell}$. These quantities of Table A.10 are scaled by the reciprocal of $m_{cmp,\ell}$ to attain the the quantity of the materials per kg of compressed flow.

IV.B.vii Heat Exchanger

Table A.11. Life cycle inventory of a shell and tube heat exchanger [79]

Ecoinvent Activity	Quantity	Unit	Location
"steel production, chromium steel 18/8, hot rolled"	$m_{hx,\ell}$	kilogram	RER
"market for electricity, high voltage"	$0.31 \cdot m_{hx,\ell}$	kWh	CH

The heat exchanger inventory consists of the stainless steel material and manufacturing energy, as shown in Table A.11 [79]. Unlike the electrolyzers, furnace, and the compressor, this inventory consists of only the relative amount of materials needed. The inventory is thus not based on any power rating or heat load. Nevertheless, based on the heat load required, the heat exchanger is sized (Section 2.2.9.), and the mass of steel (for shell and tube) is determined. This equipment, however, is assumed to last the entire lifetime of the plant. Thus, the mass of the steel needed, which is m_{hx} (Equation 2.15) is scaled by the total mass of heated fluid during the lifetime of the unit. Thus, the inventory is based on the mass of steel needed to heat 1 kg of fluid over the lifetime, $m_{hx,\ell}$ (Equation 2.19), thus forming the inventory in Table A.11.

IV.B.viii Reactor

Table A.12. Life cycle inventory of a reactor [79].

Ecoinvent Activity	Quantity	Unit	Location
"steel production, chromium steel 18/8, hot rolled"	$m_{RX,\ell}$	kilogram	RER
"market for electricity, high voltage"	$0.31 \cdot m_{RX,\ell}$	kWh	CH

Similar to the heat exchanger, the utilized inventory consists of only the material and manufacturing energy, as shown in Table A.12 [79]. Unlike the electrolyzers, furnace, and the compressor, this inventory consists of only the relative amount of materials needed. The inventory is thus not based on any power rating or heat load. Nevertheless, based on the reaction conditions, the reaction volume can be determined (Section 2.26), and thus mass of steel is obtained. This equipment, however, is assumed to last the entire lifetime of the plant. Thus, the mass of the steel required over the lifetime (m_{RX} in Equation 2.25) is divided by the total reacted mass during the lifetime of the unit. Hence, the inventory is based on the mass of steel needed to react 1 kg of fluid over the lifetime (Equation 2.26), thus forming the inventory in Table A.12.

IV.B.ix Distillation Column & Separator

The inventory of the distillation column and separators are attained in the same way as the reactor and heat exchanger. The distillation mass is determined by Equation 2.28. This corresponds

Table A.13. LCI for a distillation column for a column vessel weight of 285 kg [136].

Ecoinvent Activity	Quantity	Unit	Location
"steel production, chromium steel 18/8, hot rolled"	285	kilogram	RER
"market for electricity, high voltage"	715	kWh	CH
"water production, deionised"	0.15	kilogram	CH
"flat glass"	2	kilogram	RER
"alumunium oxide, metallurgy"	3.7	kilogram	RER
"synthetic rubber production"	3.5	kilogram	RER
"steel production, unalloyed"	65	kilogram	RER
"iron-nickel-chromium"	3.5	kilogram	RER

to the steel mass. Using the inventory proposed by Brondani et al. [136], 285 kg of steel are associated with the remaining materials shown in Table A.13. First, a relative inventory is obtained by normalizing it by a factor of 285 (steel mass) to establish the steel mass as the reference. Then, the amount of distillation column steel can be converted to the steel mass needed per kg of separated input, which is shown in Equation 2.29. Thus, the entire inventory is scaled by $m_{DC,\ell}$ (Equation 2.29), which accounts for the exact quantities that would be needed to build the distillation column and attributes its emissions over the distillation lifetime by dividing it by the total inlet mass separated during the lifetime. Thus, the inventory is transformed to quantities needed per kg of separated inlet.

IV.B.x Catalysts

Table A.14. Modeled environmental contributions of catalysts via allocation scales
For zeolites, the reference used is that of Grimaldi et al. [184], and their modeling shows that per kg of zeolite produced, 2.132 kg of Si and Al material are needed. Maintaining a fair comparison in this study with other modeled catalysts is of great importance. Thus, the wasted material herein is not considered during synthesis. Thus, per kg of their zeolite needed, we need 0.49344 kg of Al trihydrated and 1.5066 kg of Sodium silicate, implying needing almost double the mass to produce a kilogram of this zeolite. The assessed zeolite in their paper uses 1:1 ratio of Si/Al [184], so for the ones where Si/Al greater than 1, the amount of Si needed is scaled and then normalize.

Catalyst Element	Ecoinvent Activity	Unit	Location
Pt	"market for platinum"	kg	GLO
Pd	"market for palladium"	kg	GLO
Ir	"market for Platinum"	kg	RU
CeO_2	"rare earth oxides production, from rare earth oxide concentrate, 70% REO"	kg	CN-SC
Si	"silica sand production"	kg	DE
Al	"market for aluminium hydroxide"	kg	GLO
Ag	"market for silver"	kg	GLO
Al_2O_3	"aluminium oxide, metallurgical, import from Northern America"	kg	IAI area
ZnO	"zinc oxide production"	kg	RER
CuO	"copper oxide production"	kg	RER

V Catalyst Properties

Table A.15. Catalyst database showing the data for density and costs. This data was specified from Alfa [185], except for Platinum and Iridium costs [165]. The weights do not often add up to 1 since only the ingredients are given. The zeolite densities could not be found, so a worst case density of 10000 kg · m^{-3} was assumed. The cost is calculated via the weighted average of the individual compound costs using the mass percentage. For the AlPd catalyst, the exact one was found online, so it is used as one entry, but the emissions of Al and Pd are accounted for separately based on the split.

Process	Unit	Compound	Mass Percentage [%]	Density [kg · m^{-3}]	Price [EUR · kg^{-1}]	Cost [EUR · kg^{-1}]
CO2ER	Syngas Reactor	CuO ZnO Al_2O_3	40 51 4.5	6300 5606 3965	81.4 43.2 156	61.612
CO2HY	CO_2 Hydrogenation Reactor	Pd ZnO CeO_2	5 5 90	12200 5606 7132	187900 43.2 346	9713
ALL	MTO Reactor	Si [in Zeolite] Al [in Zeolite] CeO_2	146.8 2.405 30	10000 10000 7132	773.3 43.2 346	1257.9
ALL	Oligomerization Reactor	Si [in Zeolite] Al [in Zeolite]	211.8 1.3875	10000 10000	773.3 43.2	1664.8
ALL	Jet Fuel Range Hyrogenation	Pd on Al	100	12200	8680	8680
BIOHY	Biogas Reactor	CuO ZnO Al_2O_3	50 30 20	6300 5606 3965	81.4 43.2 156	84.86

For catalysts comprising multiple components, the mass composition is used to determine a weighted average cost [101]. While this is not the most representative method to cost catalysts, due to the unknown amounts of solvents and intermediate compounds utilized, this method

provides a good indication of the relative catalyst costs, which enables a useful comparison of the various synthetic jet fuel processes. For instance, it allows the comparison between the emissions generated from heavy noble metals etc.

VI Heat Integration

A simple heat integration approach was utilized. A pinch analysis code was used [186] to recover heat and minimize heating and cooling inputs. However, this code does not include latent heat in reboilers, condensers, or reactors. Thus, the input was limited to sensible heat changes.

The heated and cooling units that were used for heat recovery are shown in Table **??**. Table shows the streams that were utilized in the pinch analysis code. Not all heating and cooling

Table A.16. The heat exchanger (cooler/heater) units that were used in the pinch analysis code, using a pinch of 10°C. The stream names of the units are the same as those in Table 2.5. The cold stream is defined as a stream that requires cooling, while hot stream is defined as that which requires heating.

Process	Cold Stream	Hot Stream
CO2ER	MTO Reactor Outlet Syngas Reactor Outlet	Olefins pre reaction Syngas pre reaction MeOH pre reaction
CO2HY	MTO Reactor Outlet CO_2-H_2Reactor Outlet	Olefins pre reaction CO_2-H_2 pre reaction MeOH pre reaction
BIOHY	MTO Reactor Outlet	Olefins pre reaction

streams could be utilized due to the limitation imposed by lack of latent heat. The pinch was limited to 10 degrees. The *BIOHY* could not recover heat via more streams since the process units are spatially separated between a decentral methanol production plant near a biogas production facility and a centralized plant.

To bypass the inabiltiy to recover the latent heat, a second step for heat integration was done manually, by linking up the heat generated by the reactors with distillation column reboilers. The matched units for heat recovery were the reboilers of the jet fuel/heavies distillation column and the olefin/water distillation column, while the reactors were the MTO reactor and the methanol production reaction. These units in common with all processes, except for the methanol production reaction in the BIOHY process due to its spatial separation. The remaining heat or cooling load that was not captured was modeled as to be satisfied by the energy sources.

Once the fraction of heat and cooling that was recovered was calculated, this was accounted for by subtracting the avoided heating and cooling load from the final heating and cooling loads required per unit jet fuel, thus decreasing the contributions of heating and cooling via heat recovery.

VII Co-electrolysis Mass and Energy Balances

The half reaction characterizing the reduction of CO_2 is:

$$CO_2 \longrightarrow CO + \frac{1}{2} O_2$$

The change in Gibbs free energy [187] of this reaction is $\Delta G = 283.2$ kJ · mol^{-1}. Upon converting this value to kWh · kg$^{-1}_{CO}$, and accounting for an efficiency of 40% and a Faradic efficiency of 85%, the resulting energy needed for the conversion of CO_2 to CO is 7.5 kWh · kg$^{-1}_{CO}$.

The mass balances for the cathode of the CoEly unit are presented as follows:

$$\dot{m}_{CO_2,in} = X \cdot M_{CO_2} \cdot \frac{J}{2 \cdot y_{Faraday}}$$

$$\dot{m}_{CO_2,out} = (X - \eta_{F,CO}) \cdot M_{CO_2} \cdot \frac{J}{2 \cdot y_{Faraday}}$$

$$\dot{m}_{CO,out} = \eta_{F,CO} \cdot M_{CO} \cdot \frac{J}{2 \cdot y_{Faraday}}$$

$$\dot{m}_{H_2O,out} = \eta_{F,CO} \cdot M_{H_2O} \cdot \frac{J}{2 \cdot y_{Faraday}}$$

$$\dot{m}_{H_2,in} = (1 - \eta_{F,CO}) \cdot M_{H_2} \cdot \frac{J}{2 \cdot y_{Faraday}}$$

The mass balances for the anode of the CoEly unit are presented as follows:

$$\dot{m}_{H_2O,in} = X_w \cdot M_{H_2O} \cdot \frac{J}{2 \cdot y_{Faraday}}$$

$$\dot{m}_{H_2O,out} = (X_w - 1) \cdot M_{H_2O} \cdot \frac{J}{2 \cdot y_{Faraday}}$$

$$\dot{m}_{O_2,out} = \frac{1}{2} \cdot M_{O_2} \cdot \frac{J}{2 \cdot y_{Faraday}}$$

The values of the excess factors were chosen alongside the experimental collaborators in the synfuel initiative to be $X_w = 300$ and $X = 1.05$.

VIII Detailed Techno-economic Modeling

This section details extensive unit costing equations that were utilized initially. Upon iteration, these results of cost and GHG showed that these units had little contributions on both cost and GHG metrics. Thus, a more simplified method was used due to the negligible impact of these units on both metrics. Nevertheless, they are shown here:

VIII.A Heat Exchanger

The heat exchanger is a shell and tube heat exchanger, whose sizing was fixed based on standardized sizing parameters [95]:

- $a' = 0.2618$ ft2/ft; surface area per unit length
- $D_{shell} = 25$ inch
- $\delta_{tube} = 0.065$ inches
- $D_{tube} = 1$ inch
- $N_{tubes} = 252$

The overall heat transfer coefficient is a function of the heat exchanger fluid flow and the geometry (main geometric parameters are listed above). Herein, the pressure drop is assumed negligible and the interface between the tube thickness is assumed to be highly conductive. Thus, overall heat transfer coefficient, U, is expressed as:

$$U = \frac{h_o \cdot h_i}{h_o + h_i} \tag{5.1}$$

In Equation 5.1, h_i and h_o are respectively the tube (inner) and shell (outlet) heat transfer coefficients. If the process uses steam to heat the fluid, the steam convection coefficient can be assumed to be constant at $h_i = 5000$ W/m2 K [95]. It is considered as the fluid inside the tube because it is the hotter fluid [99]. h_o can be calculated by using the flow properties.

This extensive approach to modeling the overall heat transfer coefficient was shown to have no significant effect on the life cycle assessment and costing. Thus, it was aborted in favor of a simpler method using general values reported by Ulrich [96].

VIII.B Distillation Column

The number of trays in a distillation column can be expressed using [137]:

$$N_{trays} = 2.5 \frac{\log\left[\frac{FR_{A,dist}(1-FR_{B,dist})}{(1-FR_{A,dist})FR_{B,dist}}\right]}{\log \alpha_{AB}} \tag{5.2}$$

In Equation 5.2, the 2.5 factor is a heuristic to account tray inefficiencies.

Determining r_{reflux} requires an iterative solver to solve for ϕ in the following expression:

$$F_{feed}(1-q) - \frac{\alpha_{i/ref} \cdot F_{feed} \cdot z_{feed,i}}{\alpha_{i/ref} - \phi} = 0 \tag{5.3}$$

In Equation 5.3, q refers to the saturation state of the inlet. Once ϕ is determined (should be between alpha's of key components), the minimum vapor flowrate, F_V^{min}, can be determined via:

$$F_V^{min} = \frac{\alpha_{i/ref} \cdot F_{feed} \cdot z_{feed,i} \cdot FR_{i,dist}}{\alpha_{i/ref} - \phi} \tag{5.4}$$

Using the result of F_V^{min} from Equation 5.4, the minimum reflux ratio is determined using:

$$r_{reflux,min} = \frac{F_V^{min} - F_D}{F_D} \tag{5.5}$$

$$r_{reflux} = \beta_{reflux} \cdot r_{reflux,min} \tag{5.6}$$

The actual reflux ratio, r_{reflux}, is determined using Equations 5.5 and 5.6, where β_{reflux} is a scale factor, chosen as 1.3 [137].

IX Global Supply Chain

IX.A Effect of Production Scale

The jet fuel production in various countries is modeled using a fixed production output per year to avoid the incurred nonlinearities that could complicate the optimization model. Thus, the effect of the production scale is examined in Figure 5.1.

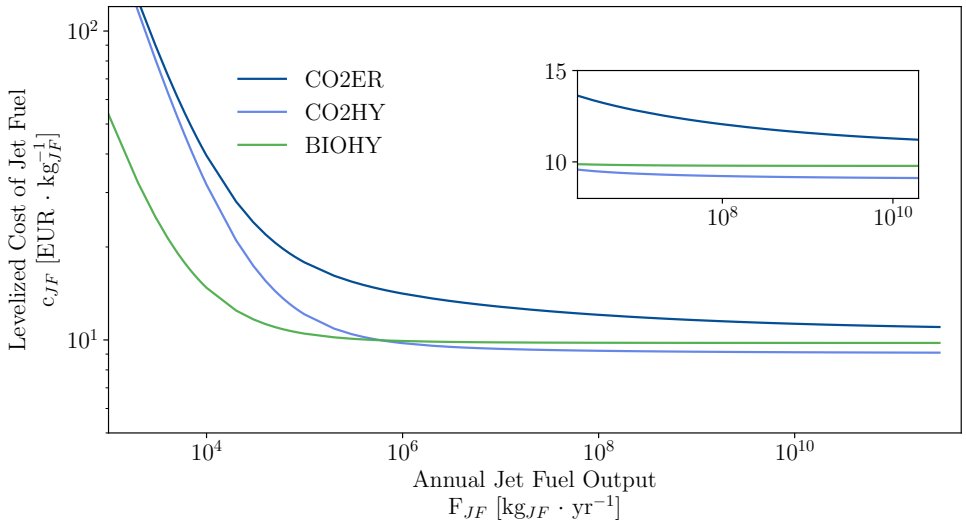

Figure 5.1. The effect of the production scale, expressed in annual jet fuel output, F_{JF}, on the resulting levelized cost of jet fuel. A close up on annual productions of $2 \cdot 10^6$-$2 \cdot 10^{10}$ kg_{JF} per year is shown. After a production rate of $2 \cdot 10^6$ kg per year, the jet fuel cost is stable and exhibits no sharp decreases.

Figure 5.1 shows that after $2 \cdot 10^6$ the value stabilizes with only negligible changes, which renders the assumption of using a fixed LCOJF a valid one. This production scale of $2 \cdot 10^6$ kg per year

corresponds to 0.0006% of the global jet fuel demand. It is thus unlikely that a chemical plant will be established in 2050 producing such low amounts per year in a sustainable society with high demands of synthetic jet fuel. Thus, the linear assumption brought by a fixed levelized cost of synthetic jet fuel is validated.

IX.B LCA of 2050 Electricity Mixes

Table A.17. The reference countries and their capacity factor values that are used to scale the emissions associated with producing 1 kWh of electricity in a country *j* whose electrical capacity and mix is defined by Jacobson et al. [175]. These electrical mixes include renewable energy technologies utilizing solar (residential, governmental, PV farm, solar tower), wind (onshore, offshore), hydro (run-of-river, pumped storage - non-alpine), geothermal, wave energy device, and tidal turbine. The cases for not applicable (N/A) reference capacity factors imply that no scaling was done (s=1) for the global warming potential of the considered RET.

RET	Product	Ecoinvent Activity	Reference Location	Reference CF
Onshore Wind	electricity, high voltage	electricity production, wind, ≥3MW turbine, onshore	DE	0.28404
Offshore Wind	electricity, high voltage	electricity production, wind, 1-3MW turbine, offshore	DE	0.28404
Rooftop Solar	electricity, low voltage	electricity production, photovoltaic, 3kWp slanted-roof installation, multi-Si, panel, mounted	ES	0.18386
Governmental Buildings Solar	electricity, low voltage	electricity production, photovoltaic, 3kWp slanted-roof installation, multi-Si, panel, mounted	ES	0.18386
PV Farm	electricity, low voltage	electricity production, photovoltaic, 570kWp open ground installation, multi-Si	ES	0.18386
CSP	electricity, high voltage	electricity production, solar tower power plant, 20 MW	ES	0.18386
Geothermal	electricity, high voltage	electricity production, deep geothermal	RoW	N/A
Pumped Hydro	electricity, high voltage	electricity production, hydro, reservoir, non-alpine region	RoW	N/A
Wave Device	electricity, high voltage	electricity production, hydro, run-of-river	RoW	N/A
Tidal Turbine	electricity, high voltage	electricity production, hydro, run-of-river	RoW	N/A

IX.C ISO 3166 Country Codes

Table A.18. The country codes utilized throughout this study (Figures 2.18, 2.19, and in Chapter 4) [188]. These are also applicable for the country codes of the ecoinvent databases.

Country	iso2	iso3
Switzerland	CH	CHE
Spain	ES	ESP
Iceland	IS	ISL
Denmark	ES	DNK
France	FR	FRA
Italy	IT	ITA
The United States	US	USA
China	CN	CHN
India	IN	IND
Brazil	BR	BRA
Iran	IR	IRN
South Korea	KR	KOR
Great Britain	GB	GBR
Egypt	EG	EGY
Canada	CA	CAN
Hong Kong	HK	HKG
Sweden	SE	SWE
Sri Lanka	LK	LKA
Saudi Arabia	SA	SAU
Malaysia	MY	MYS
Turkey	TR	TUR
Ethopia	ET	ETH
Libya	LY	LBY
Cuba	CU	CUB
Sudan	SD	SDN

Bibliography

[1] N. B. Grimm, F. S. Chapin III, B. Bierwagen, P. Gonzalez, P. M. Groffman, Y. Luo, F. Melton, K. Nadelhoffer, A. Pairis, P. A. Raymond, J. Schimel, and C. E. Williamson, "The impacts of climate change on ecosystem structure and function," *Frontiers in Ecology and the Environment*, vol. 11, 2013. DOI: 10.1890/120282.

[2] S. Jevrejeva, L. P. Jackson, R. E. M. Riva, A. Grinsted, and J. C. Moore, "Coastal sea level rise with warming above 2°C," *Proceedings of the National Academy of Sciences*, vol. 113, 2016. DOI: 10.1073/pnas.1605312113.

[3] Y. Malhi, J. Franklin, N. Seddon, M. Solan, M. G. Turner, C. B. Field, and N. Knowlton, "Climate change and ecosystems: threats, opportunities and solutions," *Philosophical Transactions of the Royal Society B: Biological Sciences*, vol. 375, 2020. DOI: 10.1098/rstb.2019.0104.

[4] COP, "Paris Climate Change Conference," 2015, p. 32.

[5] IEA (2020), "Tracking transport 2020," IEA, Paris, 2020.

[6] B. Graver, D. Rutherford, and S. Zheng, "CO_2 emissions from commercial aviation: 2013, 2018, and 2019," International Council on Clean Transportation (ICCT), Tech. Rep., 2020.

[7] R. Kotze, "Sustainability Analysis of the Airline Industry – Low Cost Carriers and Full Service Carriers," M.S. thesis, 2017.

[8] K. Button and E. Pels, *International Air Transport*. 2010. DOI: 10.1787/9789264072916-en.

[9] International Air Transport Association (IATA). (2018). "IATA Forecast Predicts 8.2 billion Air Travelers in 2037."

[10] IEA (2021), "Tracking transport 2021," IEA, Paris, 2021.

[11] S. I. Mussatto, I. L. Motta, R. M. Filho, L. van der Wielen, R. Capaz, J. Seabra, P. Osseweijer, J. Posada, M. de Freitas Gonçalves, P. R. Scorza, and G. Dragone, "Sustainable Aviation Fuels: Production, Use and Impact on Decarbonization," in *Reference Module in Earth Systems and Environmental Sciences*, Elsevier, 2021. DOI: 10.1016/B978-0-12-819727-1.00057-1.

[12] N. Pavlenko and S. Searle, "Assessing the sustainability implications of alternative aviation fuels," International Council on Clean Transportation (ICCT), Working Paper, 2021.

[13] C. E. Riboldi, L. Trainelli, and F. Biondani, "Structural Batteries in Aviation: A Preliminary Sizing Methodology," *Journal of Aerospace Engineering*, vol. 33, 2020. DOI: 10.1061/(ASCE)AS.1943-5525.0001144.

[14] J. Hileman and R. Stratton, "Alternative jet fuel feasibility," *Transport Policy*, vol. 34, 2014. DOI: 10.1016/j.tranpol.2014.02.018.

[15] V. K. Undavalli and B. Khandelwal, "Chapter 2 - General compositions and alternative aviation fuel approval process," in *Aviation Fuels*, B. Khandelwal, Ed., Academic Press, 2021. DOI: 10.1016/B978-0-12-818314-4.00002-9.

[16] A. Mancio, S. da Mota, C. Ferreira, T. Carvalho, O. Neto, J. Zamian, M. Araújo, L. Borges, and N. Machado, "Separation and characterization of biofuels in the jet fuel and diesel fuel ranges by fractional distillation of organic liquid products," *Fuel*, vol. 215, 2018. DOI: 10.1016/j.fuel.2017.11.029.

[17] G. Guest, F. Cherubini, and A. H. Strømman, "Global Warming Potential of Carbon Dioxide Emissions from Biomass Stored in the Anthroposphere and Used for Bioenergy at End of Life," *Journal of Industrial Ecology*, vol. 17, 2013. DOI: https://doi.org/10.1111/j.1530-9290.2012.00507.x.

[18] L. Li, E. Coppola, J. Rine, J. L. Miller, and D. Walker, "Catalytic Hydrothermal Conversion of Triglycerides to Non-ester Biofuels," *Energy & Fuels*, vol. 24, 2010. DOI: 10.1021/ef901163a.

[19] F. Cheng and C. E. Brewer, "Producing jet fuel from biomass lignin: Potential pathways to alkyl-benzenes and cycloalkanes," *Renewable and Sustainable Energy Reviews*, vol. 72, 2017. DOI: 10.1016/j.rser.2017.01.030.

[20] H. Wei, W. Liu, X. Chen, Q. Yang, J. Li, and H. Chen, "Renewable bio-jet fuel production for aviation: A review," *Fuel*, vol. 254, 2019. DOI: 10.1016/j.fuel.2019.06.007.

[21] W.-C. Wang and L. Tao, "Bio-jet fuel conversion technologies," *Renewable and Sustainable Energy Reviews*, vol. 53, 2016. DOI: 10.1016/j.rser.2015.09.016.

[22] J. Pechstein, U. Neuling, J. Gebauer, and M. Kaltschmitt, "Alcohol-to-Jet (AtJ)," in *Biokerosene: Status and Prospects*, M. Kaltschmitt and U. Neuling, Eds. Berlin, Heidelberg: Springer Berlin Heidelberg, 2018. DOI: 10.1007/978-3-662-53065-8_21.

[23] S. de Jong, R. Hoefnagels, A. Faaij, R. Slade, R. Mawhood, and M. Junginger, "The feasibility of short-term production strategies for renewable jet fuels – a comprehensive techno-economic comparison," *Biofuels, Bioproducts and Biorefining*, vol. 9, DOI: 10.1002/bbb.1613.

[24] V. Becattini, P. Gabrielli, and M. Mazzotti, "Role of Carbon Capture, Storage, and Utilization to Enable a Net-Zero-CO_2-Emissions Aviation Sector," *Industrial & Engineering Chemistry Research*, vol. 60, 2021. DOI: 10.1021/acs.iecr.0c05392.

[25] J. I. Hileman, D. S. Ortiz, J. T. Bartis, H. M. Wong, P. E. Donohoo, M. A. Weiss, and I. A. Waitz, *Near-Term Feasibility of Alternative Jet Fuels*. Santa Monica, CA: RAND Corporation, 2009.

[26] K. S. Ng, D. Farooq, and A. Yang, "Global biorenewable development strategies for sustainable aviation fuel production," *Renewable and Sustainable Energy Reviews*, vol. 150, 2021. DOI: 10.1016/j.rser.2021.111502.

[27] J. Han, L. Tao, and M. Wang, "Well-to-wake analysis of ethanol-to-jet and sugar-to-jet pathways," *Biotechnology for Biofuels*, vol. 10, 2017. DOI: 10.1186/s13068-017-0698-z.

[28] A. Contreras, S. Yiğit, K. Özay, and T. Veziroğlu, "Hydrogen as aviation fuel: A comparison with hydrocarbon fuels," *International Journal of Hydrogen Energy*, vol. 22, 1997. DOI: 10.1016/S0360-3199(97)00008-6.

[29] R. A. Roberts, S. R. Nuzum, and M. Wolff, "Liquefied Natural Gas as the Next Aviation Fuel," in *13th International Energy Conversion Engineering Conference*. DOI: 10.2514/6.2015-4247.

[30] Y. Bicer and I. Dincer, "Life cycle evaluation of hydrogen and other potential fuels for aircrafts," *International Journal of Hydrogen Energy*, vol. 42, 2017. DOI: 10.1016/j.ijhydene.2016.12.119.

[31] "Our Common Future," United Nations - World Commission on Environment and Development (WCED), Tech. Rep., 1987.

[32] W. Steffen, K. Richardson, J. Rockström, S. E. Cornell, I. Fetzer, E. M. Bennett, R. Biggs, S. R. Carpenter, W. de Vries, C. A. de Wit, C. Folke, D. Gerten, J. Heinke, G. M. Mace, L. M. Persson, V. Ramanathan, B. Reyers, and S. Sörlin, "Planetary boundaries: Guiding human development on a changing planet," *Science*, vol. 347, 2015. DOI: 10.1126/science.1259855.

[33] "CORSIA Sustainability Criteria for CORSIA Eligible Fuels," International Civil Aviation Organization (ICAO), Working Paper, 2019.

[34] M. Prussi, U. Lee, M. Wang, R. Malina, H. Valin, F. Taheripour, C. Velarde, M. D. Staples, L. Lonza, and J. I. Hileman, "CORSIA: The first internationally adopted approach to calculate life-cycle GHG emissions for aviation fuels," *Renewable and Sustainable Energy Reviews*, vol. 150, 2021. DOI: 10.1016/j.rser.2021.111398.

[35] International Air Transport Association (IATA). (2022). "Jet Fuel Price Monitor," [Online]. Available: https://www.iata.org/en/publications/economics/fuel-monitor/.

[36] M. D. Staples, H. Olcay, R. Malina, P. Trivedi, M. N. Pearlson, K. Strzepek, S. V. Paltsev, C. Wollersheim, and S. R. H. Barrett, "Water Consumption Footprint and Land Requirements of Large-Scale Alternative Diesel and Jet Fuel Production," *Environmental Science & Technology*, vol. 47, 2013. DOI: 10.1021/es4030782.

[37] S. de Jong, K. Antonissen, R. Hoefnagels, L. Lonza, M. Q. Wang, A. Faaij, and M. Junginger, "Life-cycle analysis of greenhouse gas emissions from renewable jet fuel production," *Biotechnology for Biofuels*, vol. 10, 2017.

[38] M. D. Staples, R. Malina, H. Olcay, M. N. Pearlson, J. I. Hileman, A. Boies, and S. R. H. Barrett, "Lifecycle greenhouse gas footprint and minimum selling price of renewable diesel and jet fuel from fermentation and advanced fermentation production technologies," *Energy Environ. Sci.*, vol. 7, 2014. DOI: 10.1039/C3EE43655A.

[39] U. Neuling and M. Kaltschmitt, "Techno-economic and environmental analysis of aviation biofuels," *Fuel Processing Technology*, vol. 171, 2018. DOI: 10.1016/j.fuproc.2017.09.022.

[40] I. Abrantes, A. F. Ferreira, A. Silva, and M. Costa, "Sustainable aviation fuels and imminent technologies - CO_2 emissions evolution towards 2050," *Journal of Cleaner Production*, vol. 313, 2021. DOI: 10.1016/j.jclepro.2021.127937.

[41] Y. Zhou, S. Searle, and N. Pavlenko, "Current and future cost of e-kerosene in the United States and Europe," International Council on Clean Transportation (ICCT), Working Paper, 2022.

[42] P. Schmidt, W. Weindorf, A. Roth, V. Batteiger, and F. Riegel, "Power-to-liquids: Potentials and perspectives for the future supply of renewable aviation fuel," Tech. Rep., 2016.

[43] P. Schmidt, V. Batteiger, A. Roth, W. Weindorf, and T. Raksha, "Power-to-Liquids as Renewable Fuel Option for Aviation: A Review," *Chemie Ingenieur Technik*, vol. 90, pp. 127–140, 2018. DOI: 10.1002/cite.201700129.

[44] K. Lokesh, V. Sethi, T. Nikolaidis, E. Goodger, and D. Nalianda, "Life cycle greenhouse gas analysis of biojet fuels with a technical investigation into their impact on jet engine performance," *Biomass and Bioenergy*, vol. 77, 2015. DOI: 10.1016/j.biombioe.2015.03.005.

[45] G. M. Souza, R. L. Victoria, C. A. Joly, and L. M. Verdad, *Bioenergy & Sustainability: bridging the gaps*. SCOPE, 2015.

[46] J. Herranz, A. Pătru, E. Fabbri, and T. J. Schmidt, "Co-electrolysis of CO_2 and H_2O: From electrode reactions to cell-level development," *Current Opinion in Electrochemistry*, vol. 23, 2020. DOI: 10.1016/j.coelec.2020.05.004.

[47] A. Meurer and J. Kern, "Fischer–tropsch synthesis as the key for decentralized sustainable kerosene production," *Energies*, vol. 14, no. 7, 2021. DOI: 10.3390/en14071836.

[48] K. Treyer, R. Sacchi, and C. Bauer, "Life Cycle Assessment of synthetic hydrocarbons for use as jet fuel: "Power-to-Liquid" and "Sun-to-Liquid" processes," Paul Scherrer Institute (PSI), Villigen, Switzerland, Commissioned by the Swiss Federal Office of Civil Aviation (FOCA), 2021.

[49] H. Grimmer, N. Thiagarajan, and E. Nitschke, "Conversion of Methanol to Liquid Fuels by the Fluid Bed Mobil Process (A commercial concept)," in *Methane Conversion*, ser. Studies in Surface Science and Catalysis, D. Bibby, C. Chang, R. Howe, and S. Yurchak, Eds., vol. 36, 1988. DOI: 10.1016/S0167-2991(09)60522-X.

[50] J.-M. Rödger, L. Kjær, and A. Pagoropoulos, "Life cycle costing: An introduction," in *Life Cycle Assessment: Theory and Practice*, M. Z. Hauschild, R. K. Rosenbaum, and S. Irving Olsen, Eds. Springer, 2018. DOI: 10.1007/978-3-319-56475-3_15.

[51] G. Wernet, C. Bauer, B. Steubing, J. Reinhard, E. Moreno-Ruiz, and B. Weidema, "The ecoinvent database version 3 (part I): overview and methodology," *The International Journal of Life Cycle Assessment*, vol. 21, 2016. DOI: 10.1007/s11367-016-1087-8.

[52] H. Verkerk, J. Fitzgerald, P. Datta, M. Dees, G. Hengeveld, M. Lindner, and S. Zudin, "Spatial distribution of the potential forest biomass availability in Europe," vol. 6, 2019. DOI: 10.1186/s40663-019-0163-5.

[53] U.S. Energy Information Administration. (2022). "EIA Data Sets, International Energy Data, Jet Fuel Production," [Online]. Available: https://www.eia.gov/opendata/v1/qb.php?category=2135043.

[54] M. Wang, R. Dewil, K. Maniatis, J. Wheeldon, T. Tan, J. Baeyens, and Y. Fang, "Biomass-derived aviation fuels: Challenges and perspective," *Progress in Energy and Combustion Science*, vol. 74, 2019. DOI: 10.1016/j.pecs.2019.04.004.

[55] "ISO 14044:2006: Environmental management — Life cycle assessment — Requirements and guidelines," International Organization for Standardization, Standard, 2006.

[56] E. Moioli, A. Wötzel, and T. Schildhauer, "Feasibility assessment of small-scale methanol production via power-to-X," *Journal of Cleaner Production*, vol. 359, 2022. DOI: 10.1016/j.jclepro.2022.132071.

[57] H. Fehrenbach, A. Liebich, N. Abdalla, K. Biemann, T. Fröhlich, and B. Simon, "Life Cycle Inventories of Petroleum Refinery Operation," ecoinvent Association, Zürich, Switzerland, Tech. Rep., 2018.

[58] S. Shiva Kumar and V. Himabindu, "Hydrogen production by PEM water electrolysis – A review," *Materials Science for Energy Technologies*, vol. 2, 2019. DOI: 10.1016/j.mset.2019.03.002.

[59] C. Dorris, E. Lu, S. Park, and F. Toro, "High-Purity Oxygen Production Using Mixed Ionic-Electronic Conducting Sorbents," Senior Design Reports (CBE), 2016.

[60] G. Maggio, G. Squadrito, and A. Nicita, "Hydrogen and medical oxygen by renewable energy based electrolysis: A green and economically viable route," *Applied Energy*, vol. 306, 2022. DOI: 10.1016/j.apenergy.2021.117993.

[61] R. Šulc and P. Ditl, "A technical and economic evaluation of two different oxygen sources for a small oxy-combustion unit," *Journal of Cleaner Production*, vol. 309, 2021. DOI: 10.1016/j.jclepro.2021.127427.

[62] C. van der Giesen, R. Kleijn, and G. J. Kramer, "Energy and Climate Impacts of Producing Synthetic Hydrocarbon Fuels from CO_2," *Environmental Science & Technology*, vol. 48, 2014. DOI: 10.1021/es500191g.

[63] O. Weiss, G. Pareschi, G. Georges, and K. Boulouchos, "The Swiss energy transition: Policies to address the Energy Trilemma," *Energy Policy*, vol. 148, 2021. DOI: 10.1016/j.enpol.2020.111926.

[64] A. H. Elsheikh, S. W. Sharshir, M. K. Ahmed Ali, J. Shaibo, E. M. Edreis, T. Abdelhamid, C. Du, and Z. Haiou, "Thin film technology for solar steam generation: A new dawn," *Solar Energy*, vol. 177, 2019. DOI: 10.1016/j.solener.2018.11.058.

[65] G. Towler and R. Sinnott, "Chapter 7 - Capital Cost Estimating," in *Chemical Engineering Design (Second Edition)*, G. Towler and R. Sinnott, Eds., Second Edition, 2013. DOI: 10.1016/B978-0-08-096659-5.00007-9.

[66] M. Alguacil, C. Prieto, A. Rodriguez, and J. Lohr, "Direct Steam Generation in Parabolic Trough Collectors," *Energy Procedia*, vol. 49, 2014. DOI: 10.1016/j.egypro.2014.03.003.

[67] A. Fernández-García, E. Zarza, L. Valenzuela, and M. Pérez, "Parabolic-trough solar collectors and their applications," *Renewable and Sustainable Energy Reviews*, vol. 14, 2010. DOI: 10.1016/j.rser.2010.03.012.

[68] NIST Chemistry WebBook. (2022). "Diphenyl ether," [Online]. Available: https://webbook.nist.gov/cgi/inchi?ID=C101848&Mask=4.

[69] Tom O'Donnell and Jay Farmerie. (2018). "How to Optimize Your Closed-Loop Systems," [Online]. Available: https://www.process-heating.com/articles/92845-how-to-optimize-your-closed-loop-systems.

[70] T. Terlouw, K. Treyer, C. Bauer, and M. Mazzotti, "Life Cycle Assessment of Direct Air Carbon Capture and Storage with Low-Carbon Energy Sources," *Environmental Science & Technology*, vol. 55, 2021. DOI: 10.1021/acs.est.1c03263.

[71] S. Deutz and A. Bardow, "Life-cycle assessment of an industrial direct air capture process based on temperature–vacuum swing adsorption," *Nature Energy*, vol. 6, 2021. DOI: 10.1038/s41560-020-00771-9.

[72] H. Bauder, "Hochtemperatur-Wärmepumpen: Möglichkeiten der Anwendung und ihre Grenzen," *Wärme*, vol. 86, 1980.

[73] C. Arpagaus, F. Bless, M. Uhlmann, J. Schiffmann, and S. S. Bertsch, "High temperature heat pumps: Market overview, state of the art, research status, refrigerants, and application potentials," *Energy*, vol. 152, 2018. DOI: 10.1016/j.energy.2018.03.166.

[74] A. Primas, "Life Cycle Inventories of new CHP systems," Swiss Center for Life Cycle Inventories, B&H AG, Dübendorf and Zürich, Tech. Rep. ecoinvent report No. 20, 2007.

[75] F. Boudéhenn, H. Demasles, J. Wyttenbach, X. Jobard, D. Chèze, and P. Papillon, "Development of a 5 kW Cooling Capacity Ammonia-water Absorption Chiller for Solar Cooling Applications," *Energy Procedia*, vol. 30, 2012, 1st International Conference on Solar Heating and Coolingfor Buildings and Industry (SHC 2012). DOI: 10.1016/j.egypro.2012.11.006.

[76] P. Srikhirin, S. Aphornratana, and S. Chungpaibulpatana, "A review of absorption refrigeration technologies," *Renewable and Sustainable Energy Reviews*, vol. 5, 2001. DOI: 10.1016/S1364-0321(01)00003-X.

[77] E. D. Sherwin, "Electrofuel Synthesis from Variable Renewable Electricity: An Optimization-Based Techno-Economic Analysis," *Environmental Science & Technology*, vol. 55, 2021. DOI: 10.1021/acs.est.0c07955.

[78] C. Minke, M. Suermann, B. Bensmann, and R. Hanke-Rauschenbach, "Is iridium demand a potential bottleneck in the realization of large-scale PEM water electrolysis?" *International Journal of Hydrogen Energy*, vol. 46, 2021. DOI: 10.1016/j.ijhydene.2021.04.174.

[79] N. Gerloff, "Comparative Life-Cycle Assessment Analysis of Power-to-Methane Plants Including Different Water Electrolysis Technologies and CO_2 Sources While Applying Various Energy Scenarios," *ACS Sustainable Chemistry & Engineering*, vol. 9, 2021. DOI: 10.1021/acssuschemeng.1c02002.

[80] P. Nuss and M. J. Eckelman, "Life cycle assessment of metals: A scientific synthesis," *PLOS ONE*, vol. 9, 2014. DOI: 10.1371/journal.pone.0101298.

[81] A. J. Naldrett, "Fundamentals of Magmatic Sulfide Deposits," in *Magmatic Ni-Cu and PGE Deposits: Geology, Geochemistry, and Genesis*, 2011. DOI: 10.5382/Rev.17.

[82] J. Yates, R. Daiyan, R. Patterson, R. Egan, R. Amal, A. Ho-Baille, and N. L. Chang, "Techno-economic Analysis of Hydrogen Electrolysis from Off-Grid Stand-Alone Photovoltaics Incorporating Uncertainty Analysis," *Cell Reports Physical Science*, vol. 1, 2020. DOI: 10.1016/j.xcrp.2020.100209.

[83] J. H. Hao, C. Chen, L. Li, L. Yu, and W. Jiang, "Preparation of bipolar membranes (I)," *Journal of Applied Polymer Science*, vol. 80, 2001. DOI: 10.1002/app.1260.

[84] P. Sharma, M. Manohar, S. Kumar, and V. K. Shahi, "Highly charged and stable cross-linked polysulfone alkaline membrane for fuel cell applications: 4,4,-((3,3'-bis(chloromethyl)-(1,1'-biphenyl)-4,4-diyl)bis(oxy))dianiline (BCBD) a novel cross-linker," *International Journal of Hydrogen Energy*, vol. 45, 2020. DOI: 10.1016/j.ijhydene.2019.10.221.

[85] U. O. Nwabara, E. R. Cofell, S. Verma, E. Negro, and P. J. A. Kenis, "Durable Cathodes and Electrolyzers for the Efficient Aqueous Electrochemical Reduction of CO2," *ChemSusChem*, vol. 13, 2020. DOI: 10.1002/cssc.201902933.

[86] F. P. G. de Arquer, C.-T. Dinh, A. Ozden, J. Wicks, C. McCallum, A. R. Kirmani, D.-H. Nam, C. Gabardo, A. Seifitokaldani, X. Wang, Y. C. Li, F. Li, J. Edwards, L. J. Richter, S. J. Thorpe, D. Sinton, and E. H. Sargent, "CO_2 electrolysis to multicarbon products at activities greater than 1 A cm^{-2}," *Science*, vol. 367, 2020. DOI: 10.1126/science.aay4217.

[87] H. Yang, J. J. Kaczur, S. D. Sajjad, and R. I. Masel, "Performance and long-term stability of CO2 conversion to formic acid using a three-compartment electrolyzer design," *Journal of CO2 Utilization*, vol. 42, 2020. DOI: 10.1016/j.jcou.2020.101349.

[88] M. Fasihi, O. Efimova, and C. Breyer, "Techno-economic assessment of CO_2 direct air capture plants," *Journal of Cleaner Production*, vol. 224, 2019. DOI: 10.1016/j.jclepro.2019.03.086.

[89] D. Sutter, M. van der Spek, and M. Mazzotti, "110th Anniversary: Evaluation of CO_2-Based and CO_2-Free Synthetic Fuel Systems Using a Net-Zero-CO_2-Emission Framework," *Industrial & Engineering Chemistry Research*, vol. 58, 2019. DOI: 10.1021/acs.iecr.9b00880.

[90] D. Slesinski and S. Litzelman, "How Low-Carbon Heat Requirements for Direct Air Capture of CO_2 Can Enable the Expansion of Firm Low-Carbon Electricity Generation Resources," *Frontiers in Climate*, vol. 3, 2021. DOI: 10.3389/fclim.2021.728719.

[91] C. Hank, L. Lazar, F. Mantei, M. Ouda, R. J. White, T. Smolinka, A. Schaadt, C. Hebling, and H.-M. Henning, "Comparative well-to-wheel life cycle assessment of OME3–5 synfuel production via the power-to-liquid pathway," *Sustainable Energy Fuels*, vol. 3, 2019. DOI: 10.1039/C9SE00658C.

[92] S. Peng, T. Li, M. Dong, J. Shi, and H. Zhang, "Life cycle assessment of a large-scale centrifugal compressor: A case study in China," *Journal of Cleaner Production*, vol. 139, 2016. DOI: 10.1016/j.jclepro.2016.08.105.

[93] M. Minutillo, A. Perna, A. Forcina, S. Di Micco, and E. Jannelli, "Analyzing the levelized cost of hydrogen in refueling stations with on-site hydrogen production via water electrolysis in the Italian scenario," *International Journal of Hydrogen Energy*, vol. 46, 2021. DOI: 10.1016/j.ijhydene.2020.11.110.

[94] The Engineering Toolbox. (2022). "Gases - Ratios of Specific Heat," [Online]. Available: https://www.engineeringtoolbox.com/specific-heat-ratio-d_608.html.

[95] A. M. Flynn, T. Akashige, and L. Theodore, "Shell-and-Tube Heat Exchangers," in *Kern's Process Heat Transfer*. John Wiley & Sons, Ltd, 2019, ch. 7. DOI: 10.1002/9781119364825.ch7.

[96] G. Ulrich, *A guide to chemical engineering process design and economics*. 1984.

[97] W. L. Luyben, "Distillation Economic Optimization," in *Distillation Design and Control Using Aspen™ Simulation*. John Wiley & Sons, Ltd, 2013, ch. 4. DOI: 10.1002/9781118510193.ch04.

[98] V. Karakoussis, N. Brandon, M. Leach, and R. van der Vorst, "The environmental impact of manufacturing planar and tubular solid oxide fuel cells," *Journal of Power Sources*, vol. 101, no. 1, 2001. DOI: 10.1016/S0378-7753(01)00482-7.

[99] W. D. Seider, D. R. Lewin, J. D. Seader, S. Widagdo, R. Gani, and K. M. Ng, *Product and Process Design Principles: Synthesis, Analysis and Evaluation*, 4th ed. John Wiley & Sons, Ltd, 2016, ISBN: 978-1-119-28263-1.

[100] D. M. Saad and S. Y. Alnouri, "The need for speed - optimal CO_2 hydrogenation processes selection via mixed integer linear programming," *Computers & Chemical Engineering*, vol. 164, 2022. DOI: 10.1016/j.compchemeng.2022.107852.

[101] D. M. Saad, R. A. Bilbeisi, and S. Y. Alnouri, "Optimizing network pathways of CO_2 conversion processes," *Journal of CO2 Utilization*, vol. 45, 2021. DOI: 10.1016/j.jcou.2020.101433.

[102] "Chapter 14 - design of pressure vessels," in *Chemical Engineering Design (Second Edition)*, G. Towler and R. Sinnott, Eds., Second Edition, 2013. DOI: 10.1016/B978-0-08-096659-5.00014-6.

[103] P. Tian, Y. Wei, M. Ye, and Z. Liu, "Methanol to Olefins (MTO): From Fundamentals to Commercialization," *ACS Catalysis*, vol. 5, 2015. DOI: 10.1021/acscatal.5b00007.

[104] B. Salieri, D. A. Turner, B. Nowack, and R. Hischier, "Life cycle assessment of manufactured nanomaterials: Where are we?" *NanoImpact*, vol. 10, 2018. DOI: 10.1016/j.impact.2017.12.003.

[105] O. G. Griffiths, R. E. Owen, J. P. O'Byrne, D. Mattia, M. D. Jones, and M. C. McManus, "Using life cycle assessment to measure the environmental performance of catalysts and directing research in the conversion of CO_2 into commodity chemicals: a look at the potential for fuels from 'thin-air'," *RSC Adv.*, vol. 3, 2013. DOI: 10.1039/C3RA41900B.

[106] P. Caramazana-González, P. W. Dunne, M. Gimeno-Fabra, M. Zilka, M. Ticha, B. Stieberova, F. Freiberg, J. McKechnie, and E. H. Lester, "Assessing the life cycle environmental impacts of titania nanoparticle production by continuous flow solvo/hydrothermal syntheses," *Green Chem.*, vol. 19, 2017. DOI: 10.1039/C6GC03357A.

[107] F. J. Broecker, K.-H. Gruendler, L. Marosi, M. Schwarzmann, B. Triebskorn, and G. Zirker, "Preparation of methanol synthesis catalyst comprising zinc, copper and aluminum," US Patent 4436833A, 1984.

[108] A. S. Malik, S. F. Zaman, A. A. Al-Zahrani, M. A. Daous, H. Driss, and L. A. Petrov, "Development of highly selective $PdZn/CeO_2$ and Ca-doped $PdZn/CeO_2$ catalysts for methanol synthesis from CO_2 hydrogenation," *Applied Catalysis A: General*, vol. 560, 2018. DOI: 10.1016/j.apcata.2018.04.036.

[109] K. M. V. Bussche and G. F. Froment, "A steady-state kinetic model for methanol synthesis and the water gas shift reaction on a commercial cu / zno / Al_2O_3 catalyst," vol. 161, 1996.

[110] U. Etim, Y. Song, and Z. Zhong, "Improving the Cu/ZnO-Based Catalysts for Carbon Dioxide Hydrogenation to Methanol, and the Use of Methanol As a Renewable Energy Storage Media," *Frontiers in Earth Science*, vol. 8, 2020. DOI: 10.3389/fenrg.2020.545431.

[111] Y. Slotboom, M. Bos, J. Pieper, V. Vrieswijk, B. Likozar, S. Kersten, and D. Brilman, "Critical assessment of steady-state kinetic models for the synthesis of methanol over an industrial $Cu/ZnO/Al_2O_3$ catalyst," *Chemical Engineering Journal*, vol. 389, 2020. DOI: 10.1016/j.cej.2020.124181.

[112] S. J. Park, H.-G. Jang, K.-Y. Lee, and S. J. Cho, "Improved methanol-to-olefin reaction selectivity and catalyst life by CeO_2 coating of ferrierite zeolite," *Microporous and Mesoporous Materials*, vol. 256, 2018. DOI: 10.1016/j.micromeso.2017.08.003.

[113] F. Dubray, V. Paunović, M. Ranocchiari, and J. A. van Bokhoven, "Production of jet-fuel-range olefins via catalytic conversion of pentene and hexene over mesoporous Al-SBA-15 catalyst," *Journal of Industrial and Engineering Chemistry*, 2022. DOI: 10.1016/j.jiec.2022.07.030.

[114] P. R. Gruber, M. W. Peters, J. M. Griffith, Y. A. Obaidi, L. E. Manzer, J. D. Taylor, and D. E. Henton, US Patent 8193402B2, 2012.

[115] V. Dieterich, A. Buttler, A. Hanel, H. Spliethoff, and S. Fendt, "Power-to-liquid via synthesis of methanol, DME or Fischer–Tropsch-fuels: a review," *Energy Environ. Sci.*, vol. 13, 2020. DOI: 10.1039/D0EE01187H.

[116] A. C. Dimian and C. S. Bildea, "Energy efficient methanol-to-olefins process," *Chemical Engineering Research and Design*, vol. 131, 2018. DOI: 10.1016/j.cherd.2017.11.009.

[117] T. Wassermann, C. Schnuelle, P. Kenkel, and E. Zondervan, "Power-to-Methanol at Refineries as a Precursor to Green Jet Fuel Production: a Simulation and Assessment Study," in *30th European Symposium on Computer Aided Process Engineering*, ser. Computer Aided Chemical Engineering, S. Pierucci, F. Manenti, G. L. Bozzano, and D. Manca, Eds., vol. 48, 2020. DOI: 10.1016/B978-0-12-823377-1.50243-3.

[118] B. Lu, H. Luo, H. Li, W. Wang, M. Ye, Z. Liu, and J. Li, "Speeding up CFD simulation of fluidized bed reactor for MTO by coupling CRE model," *Chemical Engineering Science*, vol. 143, 2016. DOI: 10.1016/j.ces.2016.01.010.

[119] S. Xu, Y. Zhi, J. Han, W. Zhang, X. Wu, T. Sun, Y. Wei, and Z. Liu, "Chapter Two - Advances in Catalysis for Methanol-to-Olefins Conversion," in, ser. Advances in Catalysis, C. Song, Ed., vol. 61, 2017. DOI: 10.1016/bs.acat.2017.10.002.

[120] I. Castellanos-Beltran, G. Assima, and J.-M. Lavoie, "Effect of temperature in the conversion of methanol to olefins (mto) using an extruded sapo-34 catalyst," *Frontiers of Chemical Science and Engineering*, vol. 12, 2018. DOI: 10.1007/s11705-018-1709-8.

[121] X. Zhao, L. Wang, J. Li, S. Xu, W. Zhang, Y. Wei, X. Guo, P. Tian, and Z. Liu, "Investigation of methanol conversion over high-Si beta zeolites and the reaction mechanism of their high propene selectivity," *Catal. Sci. Technol.*, vol. 7, 2017. DOI: 10.1039/C7CY01804E.

[122] S.-Y. Yang, B.-X. Li, J.-W. Zheng, Y.-C. Yang, and X.-H. Gao, "Performances and Net CO_2 Emission of Light Olefin Production Based on Biomass-to-Methanol and DMTO-II Technologies with CO_2 Capture and Sequestration," *ACS Sustainable Chemistry & Engineering*, vol. 9, 2021. DOI: 10.1021/acssuschemeng.0c02334.

[123] J. Saavedra Lopez, R. A. Dagle, V. L. Dagle, C. Smith, and K. O. Albrecht, "Oligomerization of ethanol-derived propene and isobutene mixtures to transportation fuels: catalyst and process considerations," *Catal. Sci. Technol.*, vol. 9, 2019. DOI: 10.1039/C8CY02297F.

[124] L. Attanatho, S. Lao-ubol, A. Suemanotham, N. Prasongthum, P. Khowattana, T. Laosombut, N. Duangwongsa, S. Larpkiattaworn, and Y. Thanmongkhon, "Jet fuel range hydrocarbon synthesis through ethylene oligomerization over platelet Ni-AlSBA-15 catalyst," *SN Applied Sciences*, vol. 2, 2020.

[125] F. Jiao, J. Li, X. Pan, J. Xiao, H. Li, H. Ma, M. Wei, Y. Pan, Z. Zhou, M. Li, S. Miao, J. Li, Y. Zhu, D. Xiao, T. He, J. Yang, F. Qi, Q. Fu, and X. Bao, "Selective conversion of syngas to light olefins," *Science*, vol. 351, 2016. DOI: 10.1126/science.aaf1835.

[126] Y. Zhou, J. Zhang, W. Ma, X. Yin, G. Chen, Y. Liu, and J. Li, "Small pore SAPO-14-based zeolites with improved propylene selectivity in the methanol to olefins process," *Inorg. Chem. Front.*, vol. 9, 2022. DOI: 10.1039/D2QI00155A.

[127] M. Yang, D. Fan, Y. Wei, P. Tian, and Z. Liu, "Recent Progress in Methanol-to-Olefins (MTO) Catalysts," *Advanced Materials*, vol. 31, 2019. DOI: 10.1002/adma.201902181.

[128] K. H. Kuechler, S. H. Brown, H. Jaensch, G. M. Mathys, S. Luo, and J. C. Cheng, "Olefin oligomerization to produce hydrocarbon compositions useful as fuels," US Patent 7678954B2, 2010.

[129] M. Stöcker, "Methanol to Olefins (MTO) and Methanol to Gasoline (MTG)," in *Zeolites and Catalysis*. 2010, ch. 22. DOI: 10.1002/9783527630295.ch22.

[130] J. Ruokonen, H. Nieminen, A. R. Dahiru, A. Laari, T. Koiranen, P. Laaksonen, A. Vuokila, and M. Huuhtanen, "Modelling and Cost Estimation for Conversion of Green Methanol to Renewable Liquid Transport Fuels via Olefin Oligomerisation," *Processes*, vol. 9, 2021. DOI: 10.3390/pr9061046.

[131] U. Albrecht, P. Schmidt, W. Weindorf, R. Wurster, and W. Zittel, "Kraftstoffstudie: Zukünftige kraftstoffe für verbrennungsmotoren und gasturbinen - abschlussbericht," Tech. Rep., 2013.

[132] A. Avidan, "Gasoline and Distillate Fuels From Methanol," in *Methane Conversion*, ser. Studies in Surface Science and Catalysis, D. Bibby, C. Chang, R. Howe, and S. Yurchak, Eds., vol. 36, 1988. DOI: 10.1016/S0167-2991(09)60524-3.

[133] P. R. Gruber, M. W. Peters, J. M. Griffith, Y. A. O. andLeo E. Manzer, J. D. Taylor, and D. E. Henton, US Patent 8193402B2, 2012.

[134] M. Henry, M. Bulut, W. Vermandel, B. Sels, P. Jacobs, D. Minoux, N. Nesterenko, S. Van Donk, and J. Dath, "Low temperature conversion of linear C4 olefins with acid ZSM-5 zeolites of homogeneous composition," *Applied Catalysis A: General*, vol. 413-414, 2012. DOI: 10.1016/j.apcata.2011.10.043.

[135] M. E. Wright, B. G. Harvey, and R. L. Quintana, "Diesel and jet fuels based on the oligomerization of butene," US Patent 8395007B2, 2013.

[136] M. Brondani, J. S. de Oliveira, F. D. Mayer, and R. Hoffmann, "Life cycle assessment of distillation columns manufacturing," *Environment, Development and Sustainability*, vol. 22, 2020. DOI: 10.1007/s10668-019-00459-5.

[137] P. Wankat, *Separation Process Engineering*. Prentice Hall, 2007.

[138] A. C. Olesen, C. Rømer, and S. K. Kær, "A numerical study of the gas-liquid, two-phase flow maldistribution in the anode of a high pressure PEM water electrolysis cell," *International Journal of Hydrogen Energy*, vol. 41, 2016. DOI: 10.1016/j.ijhydene.2015.09.140.

[139] X. Zhang, J. Witte, T. Schildhauer, and C. Bauer, "Life cycle assessment of power-to-gas with biogas as the carbon source," *Sustainable Energy Fuels*, vol. 4, 2020. DOI: 10.1039/C9SE00986H.

[140] K. Caldeira and I. McKay, "Contrails: tweaking flight altitude could be a climate win," *Nature*, vol. 593, 2021. DOI: 10.1038/d41586-021-01339-7.

[141] C. Voigt, J. Kleine, D. Sauer, R. H. Moore, T. Bräuer, P. Le Clercq, S. Kaufmann, M. Scheibe, T. Jurkat-Witschas, M. Aigner, U. Bauder, Y. Boose, S. Borrmann, E. Crosbie, G. S. Diskin, J. DiGangi, V. Hahn, C. Heckl, F. Huber, J. B. Nowak, M. Rapp, B. Rauch, C. Robinson, T. Schripp, M. Shook, E. Winstead, L. Ziemba, H. Schlager, and B. E. Anderson, "Cleaner burning aviation fuels can reduce contrail cloudiness," *Communications Earth and Environment*, vol. 2, 2021. DOI: 10.1038/s43247-021-00174-y.

[142] R. Frischknecht, F. Wyss, S. Knöpfel, T. Lützkendorf, and M. Balouktsi, "Cumulative energy demand in LCA: the energy harvested approach," *The International Journal of Life Cycle Assessment*, vol. 20, 2015. DOI: 10.1007/s11367-015-0897-4.

[143] N. Jungbluth, M. Stucki, K. Flury, R. Frischknecht, and S. Büsser, "Life Cycle Inventories of Photovoltaics," Swiss Federal Office of Energy SFOE, Tech. Rep., 2012.

[144] A. Coppola and F. Scala, "A Preliminary Techno-Economic Analysis on the Calcium Looping Process with Simultaneous Capture of CO_2 and SO_2 from a Coal-Based Combustion Power Plant," *Energies*, vol. 13, 2020. DOI: 10.3390/en13092176.

[145] J. Na, B. Seo, J. Kim, C. Lee, H. Lee, Y. Hwang, B. Min, D. Lee, H.-S. Oh, and U. Lee, "General technoeconomic analysis for electrochemical coproduction coupling carbon dioxide reduction with organic oxidation," *Nature Communications*, vol. 10, 2019. DOI: 10.1038/s41467-019-12744-y.

[146] Charles Maxwell. (2022). "Cost Indices - Towering Skills," [Online]. Available: https://www.toweringskills.com/financial-analysis/cost-indices/.

[147] Bundesamt für Energie BFE. (2021). "Analyse des schweizerischen Energieverbrauchs 2000–2020 nach Verwendungszwecken," [Online]. Available: https://www.bfe.admin.ch/bfe/de/home/versorgung/statistik-und-geodaten/energiestatistiken/energieverbrauch-nach-verwendungszweck.html.

[148] M. J. S. Zuberi, K. Narula, S. Klinke, J. Chambers, K. N. Streicher, and M. K. Patel, "Potential and costs of decentralized heat pumps and thermal networks in Swiss residential areas," *International Journal of Energy Research*, vol. 45, 2021. DOI: 10.1002/er.6801.

[149] E. Popovski, T. Fleiter, H. Santos, V. Leal, and E. O. Fernandes, "Technical and economic feasibility of sustainable heating and cooling supply options in southern European municipalities-A case study for Matosinhos, Portugal," *Energy*, vol. 153, 2018. DOI: 10.1016/j.energy.2018.04.036.

[150] Sigma-Aldrich. (2022). "Diphenylether (W366706)," [Online]. Available: https://www.sigmaaldrich.com/CH/de/product/aldrich/w366706.

[151] S. Schüppler, P. Fleuchaus, A. Duchesne, and P. Blum, "Cooling supply costs of a university campus," *Energy*, vol. 249, 2022. DOI: 10.1016/j.energy.2022.123554.

[152] M. Fasihi, R. Weiss, J. Savolainen, and C. Breyer, "Global potential of green ammonia based on hybrid PV-wind power plants," *Applied Energy*, vol. 294, 2021. DOI: 10.1016/j.apenergy.2020.116170.

[153] IRENA (2020), "Green Hydrogen Cost Reduction: Scaling up Electrolysers to Meet the 1.5°C Climate Goal," International Renewable Energy Agency, Abu Dhabi.

[154] M. Bernt, A. Hartig-Weiß, M. F. Tovini, H. A. El-Sayed, C. Schramm, J. Schröter, C. Gebauer, and H. A. Gasteiger, "Current Challenges in Catalyst Development for PEM Water Electrolyzers," *Chemie Ingenieur Technik*, vol. 92, 2020. DOI: 10.1002/cite.201900101.

[155] I. Dincer, V. Cozzani, and A. Crivellari, "Chapter 4 - System modeling and analysis," in *Hybrid Energy Systems for Offshore Applications*, ser. Hybrid Energy Systems, I. Dincer, V. Cozzani, and A. Crivellari, Eds., Elsevier, 2021, pp. 37–54. DOI: 10.1016/B978-0-323-89823-2.00004-X.

[156] B. Pribyl-Kranewitter, A. Beard, T. Schuler, N. Diklić, and T. J. Schmidt, "Investigation and Optimisation of Operating Conditions for Low-Temperature CO_2 Reduction to CO in a Forward-Bias Bipolar-Membrane Electrolyser," *Journal of The Electrochemical Society*, vol. 168, 2021. DOI: 10.1149/1945-7111/abf063.

[157] S. Fuss, W. F. Lamb, M. W. Callaghan, J. Hilaire, F. Creutzig, T. Amann, T. Beringer, W. de Oliveira Garcia, J. Hartmann, T. Khanna, G. Luderer, G. F. Nemet, J. Rogelj, P. Smith, J. L. V. Vicente, J. Wilcox, M. del Mar Zamora Dominguez, and J. C. Minx, "Negative emissions—Part 2: Costs, potentials and side effects," *Environmental Research Letters*, vol. 13, 2018. DOI: 10.1088/1748-9326/aabf9f.

[158] J. Young, N. McQueen, C. Charalambous, S. Foteinis, O. Hawrot, M. Ojeda, H. Pilorgé, J. Andresen, P. Psarras, P. Renforth, S. García, and M. Van der Spek, "The cost of direct air capture and storage: the impact of technological learning, regional diversity, and policy.," preprint, 2022.

[159] Silviana, S., Arum Lestari, Maghfira, Jethro Sanyoto, Gelbert, Diyah Hapsari, Farida, Mutiarini, Amanah, and Eka Septiani, Indah, "Analysis and Cost Estimation of Methanol / Glycerin Distillation Unit Process System," *E3S Web Conf.*, vol. 202, 2020. DOI: 10.1051/e3sconf/202020210002.

[160] J. Witte, A. Kunz, S. M. Biollaz, and T. J. Schildhauer, "Direct catalytic methanation of biogas – Part II: Techno-economic process assessment and feasibility reflections," *Energy Conversion and Management*, vol. 178, 2018. DOI: 10.1016/j.enconman.2018.09.079.

[161] A. Grosser and E. Neczaj, "Sewage sludge and fat rich materials co-digestion - Performance and energy potential," *Journal of Cleaner Production*, vol. 198, 2018. DOI: 10.1016/j.jclepro.2018.07.124.

[162] D. M. Teferra and W. Wubu, "Biogas for Clean Energy," in *Anaerobic Digestion*, J. R. Banu, Ed., 2018, ch. 7. DOI: 10.5772/intechopen.79534.

[163] European Central Bank. (2022). "Euro foreign exchange reference rates," [Online]. Available: https://www.ecb.europa.eu/stats/policy_and_exchange_rates/euro_reference_exchange_rates/html/index.en.html.

[164] C. Agutu, F. Egli, N. Williams, T. Schmidt, and B. Steffen, "Accounting for finance in electrification models for sub-Saharan Africa," *Nature Energy*, vol. 7, 2022. DOI: 10.1038/s41560-022-01041-6.

[165] A. T. Mayyas, M. F. Ruth, B. S. Pivovar, G. Bender, and K. B. Wipke, "Manufacturing Cost Analysis for Proton Exchange Membrane Water Electrolyzers," 2019. DOI: 10.2172/1557965.

[166] C. Bauer, B. Cox, T. Heck, and X. Zhang, " Potentials, costs and environmental assessment of electricity generation technologies - An update of electricity generation costs and potentials," Paul Scherrer Institute (PSI), Villigen, Switzerland, Tech. Rep., 2019.

[167] Bundesamt für Energie BFE. (2022). "WACC – Kalkulatorischer Zinssatz," [Online]. Available: https://www.bfe.admin.ch/bfe/de/home/foerderung/erneuerbare-energien/wacc-kalkulatorischer-zinssatz.html.

[168] J. Aldersey-Williams and T. Rubert, "Levelised cost of energy – A theoretical justification and critical assessment," *Energy Policy*, vol. 124, 2019. DOI: 10.1016/j.enpol.2018.10.004.

[169] L. Tao, E. C. D. Tan, R. McCormick, M. Zhang, A. Aden, X. He, and B. T. Zigler, "Techno-economic analysis and life-cycle assessment of cellulosic isobutanol and comparison with cellulosic ethanol and n-butanol," *Biofuels, Bioproducts and Biorefining*, vol. 8, 2014. DOI: 10.1002/bbb.1431.

[170] Global Petrol Prices. (2022). "Electricity prices," [Online]. Available: https://www.globalpetrolprices.com/electricity_prices/.

[171] H. Ritchie, M. Roser, and P. Rosado, "Energy," *Our World in Data*, 2020. [Online]. Available: https://ourworldindata.org/energy.

[172] The World Bank Group. (2022). "Global Solar Atlas - Photovoltaic power potential," [Online]. Available: https://globalsolaratlas.info/download/world.

[173] ——, (2022). "Global Wind Atlas - Capacity Factor IEC1," [Online]. Available: https://globalwindatlas.info/download/gis-file.

[174] N. Nawri, G. N. Petersen, H. Bjornsson, A. N. Hahmann, K. Jónasson, C. B. Hasager, and N.-E. Clausen, "The wind energy potential of Iceland," *Renewable Energy*, vol. 69, 2014. DOI: 10.1016/j.renene.2014.03.040.

[175] M. Z. Jacobson, A.-K. von Krauland, S. J. Coughlin, E. Dukas, A. J. H. Nelson, F. C. Palmer, and K. R. Rasmussen, "Low-cost solutions to global warming, air pollution, and energy insecurity for 145 countries," *Energy Environ. Sci.*, 2022. DOI: 10.1039/D2EE00722C.

[176] I. E. Agency, "Energy prices in national currency per unit," 2016. DOI: 10.1787/data-00441-en.

[177] Â. P. Ferreira, J. Gonçalves Ramos, and P. Odete Fernandes, "A linear regression pattern for electricity price forecasting in the iberian electricity market," *Revista Facultad de Ingeniería Universidad de Antioquia*, 2019. DOI: 10.17533/udea.redin.20190522.

[178] S. Bertoli, M. Goujon, and O. Santoni, "The CERDI-seadistance database," Études et Documents, n° 7, CERDI, 2016.

[179] L. Li and X. Zhang, "Reducing CO_2 emissions through pricing, planning, and subsidizing rail freight," *Transportation Research Part D: Transport and Environment*, vol. 87, 2020. DOI: 10.1016/j.trd.2020.102483.

[180] S. van der Meulen, T. Grijspaardt, W. Mars, W. van der Geest, A. Roest-Crollius, and J. Kiel, "Cost Figures for Freight Transport – final report," Netherlands Institute for Transport Policy Analysis (KiM), Tech. Rep., 2020.

[181] R. K. Rosenbaum, M. Z. Hauschild, A.-M. Boulay, P. Fantke, A. Laurent, M. Núñez, and M. Vieira, "Life cycle impact assessment," in *Life Cycle Assessment: Theory and Practice*, M. Z. Hauschild, R. K. Rosenbaum, and S. I. Olsen, Eds. Springer International Publishing, 2018. DOI: 10.1007/978-3-319-56475-3_10.

[182] S. Mehrotra, "On the Implementation of a Primal-Dual Interior Point Method," *SIAM Journal on Optimization*, vol. 2, 1992. DOI: 10.1137/0802028.

[183] B. Cox, C. Bauer, A. Mendoza Beltran, D. P. van Vuuren, and C. L. Mutel, "Life cycle environmental and cost comparison of current and future passenger cars under different energy scenarios," *Applied Energy*, vol. 269, 2020. DOI: 10.1016/j.apenergy.2020.115021.

[184] F. Grimaldi, H. Ramirez, C. Lutz, and P. Lettieri, "Intensified production of zeolite A: Life cycle assessment of a continuous flow pilot plant and comparison with a conventional batch plant," *Journal of Industrial Ecology*, vol. 25, 2021. DOI: 10.1111/jiec.13180.

[185] Alfa Aesar - by Thermo Fisher Scientific. (2022). "Catalysts," [Online]. Available: https://www.alfa.com/en/.

[186] Luis Eduardo Correa Gallego. (2022). "PinchAnalysis - Heat Integration Analysis," [Online]. Available: https://github.com/LuisEduardoCorreaGallego/PinchAnalysis-Console.

[187] L. J. France, P. P. Edwards, V. L. Kuznetsov, and H. Almegren, "Chapter 10 - The Indirect and Direct Conversion of CO2 into Higher Carbon Fuels," in *Carbon Dioxide Utilisation*, P. Styring, E. A. Quadrelli, and K. Armstrong, Eds., Elsevier, 2015. DOI: 10.1016/B978-0-444-62746-9.00010-4.

[188] "Codes for the representation of names of countries and their subdivisions — Part 1: Country code," International Organization for Standardization, Standard, 2020.